AMERICAN UNIVERSITY OF BEIRUT

TORREFACTION OF OLIVE STONES FOR ENERGY USE

by
SARY BASSAM FAYYAD

A thesis
submitted in partial fulfillment of the requirements
for the degree of Master of Engineering
to the Baha and Walid Bassatne Department of Chemical Engineering and Advanced Energy
of the Maroun Semaan Faculty of Engineering and Architecture
at the American University of Beirut

Beirut, Lebanon
August 2020

AMERICAN UNIVERSITY OF BEIRUT

TORREFACTION OF OLIVE STONES FOR ENERGY USE

by

SARY BASSAM FAYYAD

Approved by:

Dr. Mohammad N. Ahmad, Professor — Advisor
Department of Chemical Engineering and Advanced Energy

Dr. Joseph Zeaiter, Associate Professor — Member of Committee
Department of Chemical Engineering and Advanced Energy

Dr. Cassia Boyadjian, Assistant Professor — Member of Committee
Department of Chemical Engineering and Advanced Energy

Date of the thesis defence: August 31, 2020

AMERICAN UNIVERSITY OF BEIRUT

THESIS/DISSERTATION/ PROJECT RELEASE FORM

Student Name:___Fayyad_____Sary_____Bassam_____
Last First Middle

☑ Master's Thesis ○ Master's Project ○ Doctoral Dissertation

☐ I authorize the American University of Beirut to: (a) reproduce hard or electronic copies of my thesis, dissertation, or project; (b) include such copies in the archives and digital repositories of the University; and (c) make freely available such copies to third parties for research or educational purposes.

☑ I authorize the American University of Beirut to: (a) reproduce hard or electronic copies of it; (b) include such copies in the archives and digital repositories or the University; and (c) make freely available such copies to third parties for research or educational purposes after:

One -✓- year from the date of submission of my thesis, dissertation, or project.
Two ---- years from the date of submission of my thesis, dissertation, or project.
Three ---- years from the date of submission of my thesis, dissertation, or project.

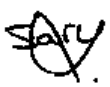

September 8, 2020

Signature Date

ACKNOWLEDGEMENTS

This work is dedicated to my family whom I am proud to be part of.

I would like to deeply thank my advisor, mentor, and friend Dr. Mohammad N Ahmad for being a huge support and help not only during my master's years, but since my first day in chemical engineering. This work couldn't have been done if it wasn't for him. Dr. Ahmad made it possible that I go on an Erasmus+ study abroad year in University of Limerick (UL) in Ireland as part of my master's program. This allowed me to expand my knowledge in so many ways beyond just academics.

I would also like to express my appreciation to Dr. Joseph Zeaiter and Dr. Cassia Boyadjian for their help and efforts.

Special thanks to our chemical engineering department members whom I consider family, especially Mrs. Souad Shaaban and Mrs. Rita Khalil.

I would like to also thank Dr. James J. Leahy and Dr. Witold Kwapinski who were very kind and knowledgeable advisors during my work as a part of their biomass team in UL.

I would like to also thank Dr. Marzena Kwapinska and Ms. Anna Turbetskaya for their guidance. And thanks to all UL staff and members who helped.

Many thanks to Mr. Hamza Ismail for his expertise in modelling (modelling part) and Mr. Daniel Hickey for being helpful with his mastery on the HPLC.

Exceptional gratitude to my friends, Mr. Marc Haber, Mr. Nicolas Aramouni, and Mr. Waddah Malaeb (convinced me not to pursue a trucker career) for their technical and intellectual help in many aspects and for their never-ending support.

Highest appreciation and gratitude to my family, friends, and girlfriend Ms. Jinan Nader, for their unconditional support and patience.

AN ABSTRACT OF THE THESIS

Sary Bassam Fayyad for Master: Master of Engineering
Major: Chemical Engineering

Title: Torrefaction of olive stones for energy use

The heavy dependency of fossil fuels has led to the detrimental effects of greenhouse gas (GHG) emissions, two-thirds being CO_2, on health, environment, and climate. The need for all kinds of renewable energy (RE) stays the centre of attention and efforts. This study targets the lignocellulosic biomass part of renewable energies by investigating the torrefaction of olive stones (OS) for energy uses. Torrefaction temperature (T), residence time (RT), and particle size (PS) were the parameters studied and the optimum operation conditions were found to be 268^{o}C, 40mins, and 2.5mm, respectively. This biomass thermochemical treatment method produces solid char as the intended product with a yield of 60.5% and a high heat content of 23.81kJ/kg putting it amongst good grade coals. Further physical properties and chemical characteristics like morphology (using SEM), thermal behaviour (using TGA), chemical species (using FTIR, proximate and ultimate analysis), and hydrophobicity were examined.

CONTENTS

ILLUSTRATIONS

Figure Page

TABLES

Table Page

NOMENCLATURE

RE	Renewable Energy
IRENA	International Renewable Energy Agency
REmap	Renewable Energy Roadmaps
EIA	U.S. Energy Information Administration
GW	Gigawatt
TWh	Terrawatt-hour
OS	Olive Stone/s
SEM	Scanning Electron Microscopy
TGA	Thermogravimetric Analysis
FTIR	Fourier Transform Infrared
MC	Moisture Content
VM	Volatile Matter
FC	Fixed Carbon
M	Million
B	Billion
GDP	Gross Domestic Product
EU	European Union
USA	United States of America
LHW	Liquid Hot Water
GHG	Green House Gases
R&D	Research and Development

OMWW	Olive Mill Wastewater
HTC	Hydrothermal Carbonization
SY	Solid Yield
LY	Liquid Yield
GY	Gas Yield
T	Temperature
RT	Residence Time
PS	Particle Size
EDR	Energy Densification Ratio
GLR	Gain Loss Ratio
CE	Cellulose
HCE	Hemicellulose
LG	Lignin
-OH	Hydroxyl Group
CO	Carbon Monoxide
VOCs	Volatile Organic Compounds
CO_2	Carbon Dioxide
N_2	Nitrogen
C=O	Carbonyl Group
ANN	Artificial Neural Network
h	Euclidian Distance
DoE	Design of experiments
α	Solid Yield(modelling)

β	Liquid Yield(modelling)
γ	Gas Yield(modelling)
ε	Particle Size(modelling)
θ	Temperature(modelling)
μ	Residence Time (modelling)

CHAPTER I
INTRODUCTION

Climate change is highly affected by how our priceless resources of water, land and energy are used which are in turn affected by climate itself. Unless a worldwide effort is dedicated to protecting these resources and bound the increase in Earth's temperature to no more than 2℃ [1], the problem will only aggravate. These efforts need to be based on reliable integrated approaches, proper resources evaluations, and effective resource utilisation and management keeping in view the big picture including sustainability and economy [2, 3]. The need to shift the world's dependence to renewable or cleaner sources of energy is becoming more and more necessary with increased air pollution, adding all related health effects, and global climate disruption being the major provokers. More than 60% of worldwide greenhouse gas emissions, mainly CO_2, result from the use of fossil fuels for energy purposes [3, 4]. Based on IRENA's Remap analysis[5], more than 80% reduction in CO_2 emissions must be seen by 2050 given that energy efficiencies and renewables (assigned an average of 47% of total reduction) involvement increase.

Wind, solar, hydro, and biomass are promising technologies as energy source alternatives whereby they have low to no emissions, are environmentally friendly, sustainable, and are naturally occurring. This, along with the many issues accompanied with the heavy dependence on fossil fuels, is alarming the time to start focusing on renewable energy (RE) and for allocating a lot of effort and money for its enhancement on all levels. Changes in economics, technologies, and easier admittance to energy services and resources, initiated and stirred by new businesses and self-motivations are the factors that triggered preceding transformations in energy [6-8]. However, following

practices, successes, and failures from several countries showed that such alterations can take up to 50 years to be well established in market and practice [9].

A fertile base must be established to handle such changes as they become larger in scale, mass, and reach. Infrastructure readiness is of utmost importance to incorporate the technologies, facilities, and networks of the renewables energy systems whether intracity or peripheral, and interlinked or specialized. Several of the main aspects are upgraded and added transmission links for proper power distribution, coordination of long distance and shared electricity connections, well planned electric vehicles recharging stations and units, and effective biomass organization plans from source to use. All this, nevertheless, with suitable energy policies and meticulous work structures, fully considered properties of energy systems, and thoroughly studied energy requirements and availability, success chances can dramatically increase [3, 10].

The main shift in energy away from fossil fuels and into renewables which are increasingly efficient and practical especially solar powered photovoltaics but are still not enough. Since 2010 and throughout 2015, energy supplied by renewables parted 19% of total and more than 50% of new power facilities, and although 25% of the global electric power was provided by renewables in 2017, CO_2 representing 65% of the greenhouse gases, increased by 1.4% in emissions [4, 10-14]. Notably, supplying RE as electricity is the preferable choice due to electricity's efficient form besides it parting 20% of total world energy consumption. Nevertheless, 2017 marked one of the best years for renewables contribution in power whereby new 167 GW were introduced, with particularly solar energy being in the lead [3, 11]. Reductions in technology prices of renewables was at the core of its boost whereby global investments in RE facilities was 2-fold that of fossil fuels from 2012 till 2017, and almost $242 B in 2016 [3, 10]. In terms

of costs, over a span of 7 years till 2017, that of electricity has astonishingly decreased by almost three quarters for PV, and almost a quarter for wind reaching 2.5 cents U.S. average for each kWh. Yet, these rates are still higher than those of conventional energy source and based on IRENA's REmap it is required to have two thirds of power generation from RE alone in the coming 10 years while experiencing 1.4% yearly development rate [15].

In another sector, transportation energy is split half between cars on one side and ships, trains, planes, and heavy wheelers on the other, contributing by around 14% of polluting emissions [5, 16]. Nonetheless, quick growth of alternate energy was witnessed in transportation where the number of electric bikes and trikes reached 300 million and that of electric cars 2 million in service and more than 1% of total vehicles sold in 2016 [17, 18].

Motivation for RE objectives are constantly raised in many countries and some are already using or are on their way to use renewable sources of energy especially European countries.

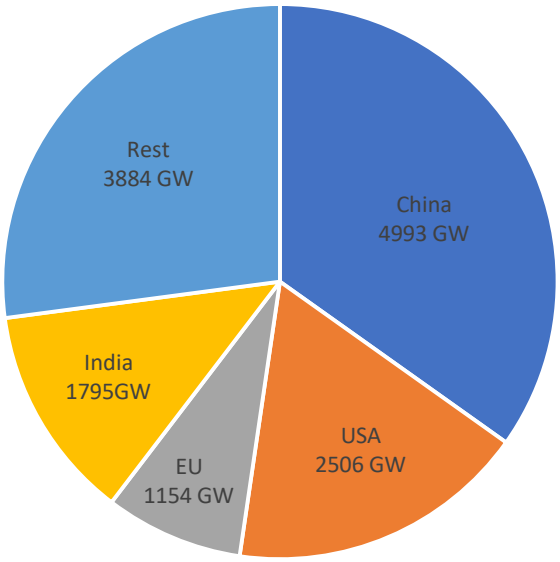

Figure 1 RE Addition Contribution from 2018 till 2050 [3, 15]

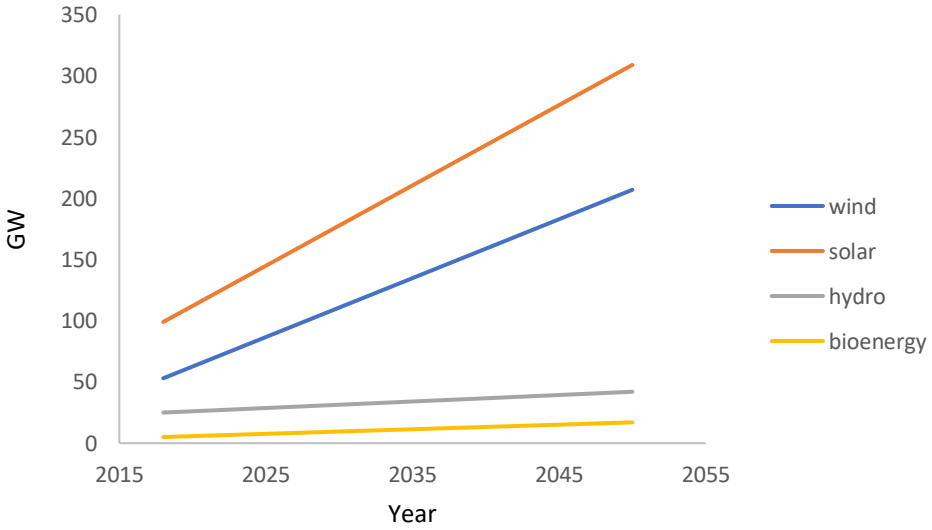

Figure 2 Addition of GW RE by Type from 2018 till 2050 [3, 15]

The required 27% RE target set by the EU for 2030 was modified to reach 30% in summer of 2018, and considerations on increasing it are planned in 2023 [19].

'Energy transition' in German means *'Energiewende'* which is a strong progression by Germany towards relying largely on the main renewables, wind, solar, and hydro, for energy supply by 2050 bringing down all coal-based energy generation and reducing greenhouse gases by almost 90% from all sectors [3, 20-22].

In Denmark, a governmental objective was set in 2012 to rely totally on renewables for energy by 2050[23]. Some set numbers are jumps to 80, 6.4, and 0 TWh of wind, solar, and fossil fuel energy by 2050, from 11.6, 0.6, and 155 TWh, respectively [3, 23, 24]. This, along with the full agreement on climate goals integrated with policies reinforcing industries supplying renewables, and a national determination promoting renewables tax incentives, hugely helps such energy achievements [25].

For non-European countries such as India and USA, work on renewables is also promising. A goal of 175 GW, split almost 57% solar and 34% wind, was set by India for 2022 and was later increased by nearly 30% projected to 2027 [3, 26]. The USA is doing a very good job with conversions to RE even with its highly diverse energy districts and their differences, regulations, numerous utilities, and locations across the continent. RE supplied 11.4% of the total energy requirements and 56% of all electricity demand in 2019 is supplied from RE resources as stated by the U.S. Energy Information Administration (EIA), making it three folds greater than what it was in year 2000 [3, 27]. The range of U.S. energy programs extends to the transportation field supported by following proper planning, timelines, and enhancements [3, 28].

After the oil crisis that hit Brazil in 1973, the government favoured the use of sugar cane-derived ethanol for automobiles instead of gasoline in a movement called the

'*Programa Nacional do Álcool'* or the '*Pró-Álcool',* pushing the demand for this sugar cane fuel [3, 29].

Back in 2017, China, the main user and maker of energy, had alone 50% of solar energy worldwide adding up to 94 GW, which was met in 2018 by governmental support to the PV sector through cost reductions [3, 30]. These efforts are setting up China's future view of reducing air pollution by around 63% per GDP and increasing renewables portion in energy requirements to reach almost 20% for year 2030 [3, 31].

Russia is a major fossil fuel producer and consumer ranking in the top three countries possessing fossil fuel resources [3, 32]. Yet, it's quite important for such large countries to rely on RE as much as possible as they are also the major consumers, hence having the major weight of pollution. In 2013, Russia has succeeded in providing 5 GW of RE through wind and solar signifying its ability to easily reach the set target of almost 6 GW before 2030 [3, 32, 33]. To do so, among several other measures, the nation is encouraging bid sales in wind and solar sector benefitting even the remote inhabitants in terms of employments and energy availability [3, 32]. It is important to point out here that investing in clean energy facilities, industries, and technologies, backed up by governmental policies, help promote employment, stimulate the economy, and increase GDP.

In efforts to increase its dependence on renewables, reduce pollution, and decrease imported energy costs, Turkey is seeking ways to employ wind and solar based energies as its economy continuously evolves. Some challenges, however, present themselves for the long run as preparations and plans remain unclear given the sizable growth in big scale renewables industries, which are short on funding and impact small such contributors [34]. Nevertheless, a capacity of 5GW PV power was reached in 2018

encouraged by “feed-in tariff” mechanisms, indicating high success in attaining Turkey’s 2023 energy vision [3].

Despite the continuously spreading use of biomass as a source of energy, it is incomparable to the use of fossil fuels which still dominates the energy realm. This all boils down to the properties of the different energy sources. Fossil fuels are cheaper, higher in energy density, versatile, and compatible with pre-existing facilities and equipment. Yet, it is expected that energy from biomass will increase by 2 times from 16,000 TWh to around 32,000 TWh in 2050 of which 65% would be used upfront and 35% transformed to liquid fuels. However, operating with biomass fed energy in other sectors like heavy sea, air, and land transportation, or power demanding industries, remains difficult [35-39]. The reliability and affordability of biomass raw material present sizable problems; for instance, heavy industries alone require approximately 1 billion tonnes of biomass equating to its overall requirements in all sectors globally. USA is one country with such raw material capabilities being at most a quarter of the world’s potential [40]. But, although a lot of development is needed to make a transition in these sectors, biomass or biofuel could have a good potential for some productions and transport as it is characterized by high carbon content and decent capacity of energy storage density [3, 41-43].

The Mediterranean region is an attractive bioenergy centre as several organic wastes including residues of greenhouse crops and olive oil production are found in abundance [44, 45]. Nonetheless, biowaste is not limited to the Mediterranean region as the bioenergy has been given such importance in Europe to the point of having specific agricultural decrees. The problem with this kind of waste is not only in the large volumes produce, but also in its diversity, low density, high moisture, and high cost of storage and

transport, so using it directly is highly inefficient. Another problem emerges when plastics are a portion of the biomass waste which makes it even more difficult to deal with. Now, of course, one of the approaches applied is composting after screening out the plastics which is in turn unused [3, 46]. Although compost has a great end use, but it's not enough as a solution and is rather time consuming. Thermal processes, meanwhile, like torrefaction, pyrolysis, gasification, and hydrothermal carbonization present better solutions. Such efficient pre-treatment methods render biomass more "fuel" like along with readily taking plastics residues effects into consideration. Although energy is put into thermally treating biomass, but the outcome significantly pays off.

Considering olive oil industries, in particular, and the masses of waste it produces globally and that the solid part of which (mainly olive stones) is recoverable, there is a decent potential in harvesting bioenergy [47, 48]. Production of biogas via anaerobic digestion and activated carbon from olive oil process leftovers might be employed as energy recovery paths [48-57]. Nevertheless, the wet waste produced is rich in organic polluting compounds and is difficult to decompose without other proper technological interventions [58]. However, the solid residue, mainly olive stones (OS), can be used for fire, heat, and power either raw or after thermal treatments like torrefaction, pyrolysis, and gasification which also produce useful combustible gas [48, 59-63].

Not only do the benefits of the shift in energy pour in favour of the environment and material, but also touch on the economy of several energy field subsectors. If energy transformation plans go well globally, it is estimated by IRENA's 2020 Global Renewables Outlook that jobs in the electric grid networks would double by year 2050 reaching 14.5 M, and more than double in power efficiency reaching slightly over 21 M jobs [5]. Around 42 M jobs are estimated to emerge in RE alone by 2050 outweighing

conventional energy job count at the time as well as fossil fuel inevitable job losses; refer to Figure 3. Other indirect jobs will also be created as in contracting, construction, staff, management and others; adding these to the count could push up the energy jobs to almost 100 M by 2050 [5]. It is worth mentioning that employment rates will vary according to each country's current energy practices, its shift desire, and business and political relations. Furthermore, the GDP of countries would increase due to the incoming jobs and investments throughout the next 30 years of energy transition. The global average per capita GDP yearly increase is almost 370$ with as low as 14% of the value in investment requirements [5].

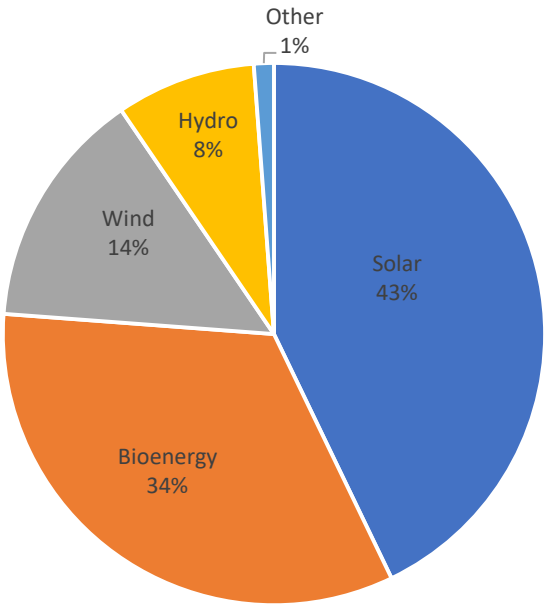

Figure 3 RE Job Distribution by Type in 2050 [5]

Numerous energy solutions are still on the lab bench or in trial sizes and engineering endeavours for end use solutions still active, but unless governments pitch in with incentives and funding, upsizing these to make them strong and feasible, economically and practically, will remain widely challenging. Since 2012 funding and investments in the R&D of clean energy engineering, technology, and design has been on standby; not the case for renewables. While investments for clean energy were a shy $10 B per year, those for renewable energy were 30 times more and amounted to almost $300 B per year [3]. These numbers focus mainly on solar and wind power and should give some attention to downstream necessities especially when it comes to bioenergy.

It is understandable that progressions in wind and solar is swifter because the concepts and mechanisms involved are simpler, but biomass can also be quite an alternative energy source. Its high diversity in source, type, treatment, and use obviously requires more studies, experimentation, and time, but progressing it as much as other alternatives gifts versatility in end use. Several studies exist covering many biomass types but there wasn't a major focus on olive stones (OS) which is a significant bio-waste in many countries especially European.

The aim of this work is to study the potential of olive stone torrefaction for the end use of firing and co-firing, and to analyse the characteristic of its solid products particularly. The study being conducted on a lab scale representing industrial sized torrefaction plants which produce OS briquettes for woodstoves and room-heaters as a stand-alone or co-firing fuel. Here comes the practicality of the project as the conditions of the process heavily affect the produced torrefied OS and finding the optimal conditions in terms of quality while producing a cleaner fuel is the challenge.

CHAPTER II
BACKGROUND

A. Lignocellulosic Biomass

What is biomass exactly? According to the U.S. Energy Information Administration, biomass is a renewable energy source consisting of any organic material remaining from animals and plants. The reason it contains energy is because of a process called photosynthesis, storing the sun's energy in the form of chemical potential then releasing it as heat energy when burned. Examples are wood and its processing waste, forest slashes, agricultural residues, crop wastes, grass cuttings, kitchen leftovers, and manure as shown in Figure 4 and Figure 5 [64].

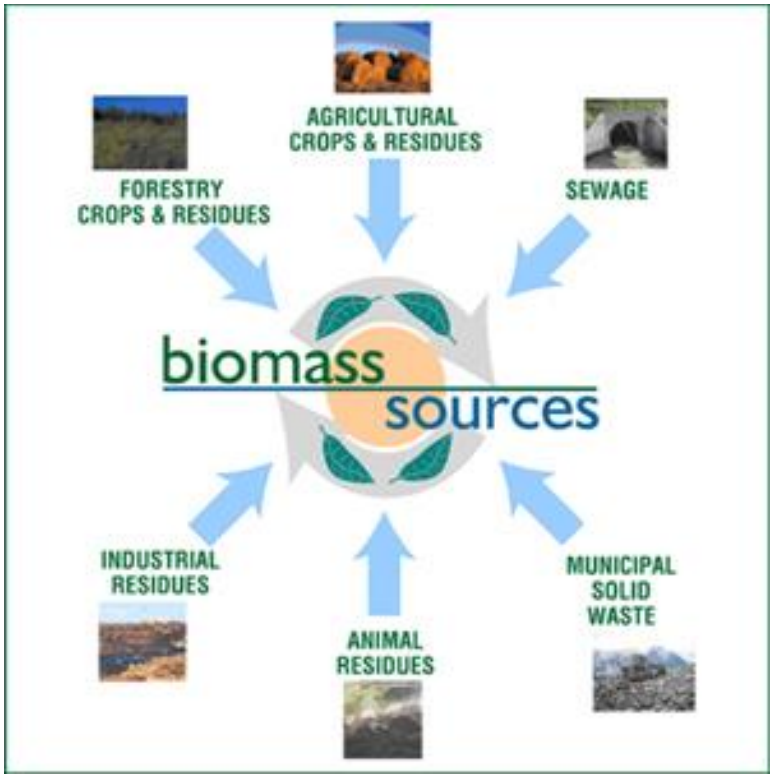

Figure 4 Different Biomass Sources [65]

Figure 5 Different Agricultural Waste [66]

Interest here, in particular, is lignocellulosic biomass which is the most abundant organic material on Earth. The secondary wall of plants is very rich in lignocellulose consisting of 40-80% cellulose (CE), 10-40% hemicellulose (HCE), and 5-25% lignin (LG) [67]. Cellulose (Figure 7) is primarily made of glucose molecules and it gives the plant structure, stability, and storage ability. Hemicellulose (Figure 8) is a mixture of linear and branched polysaccharides (pentose, xylose, hexose) and is a constituent of the cell wall. Finally, lignin (Figure 9) which is a non-polysaccharide formed by heteropolymers aiding the plant cell in stressful and pathogenic situations [67, 68]. Figure 6 shows a well-defined schematic of a plant cell lignocellulosic structure and components.

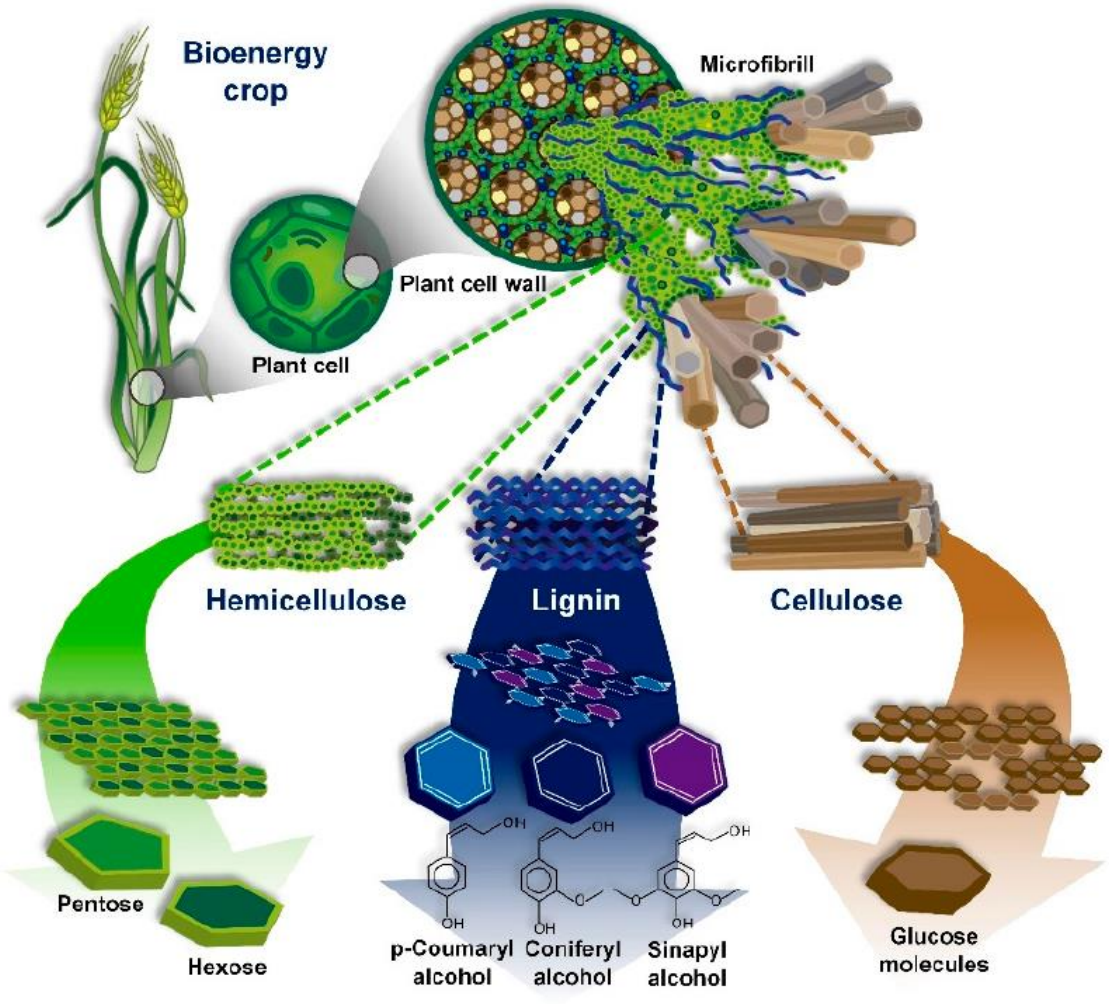

Figure 6 Schematic of Lignocellulose Components [67]

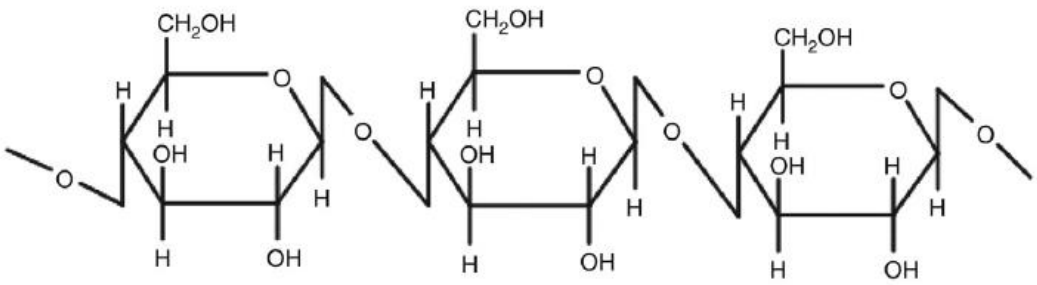

Figure 7 Cellulose [68]

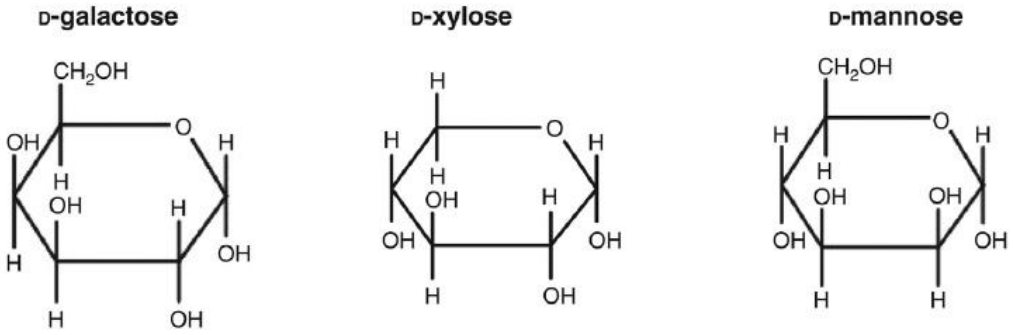

Figure 8 Hemicellulose [68]

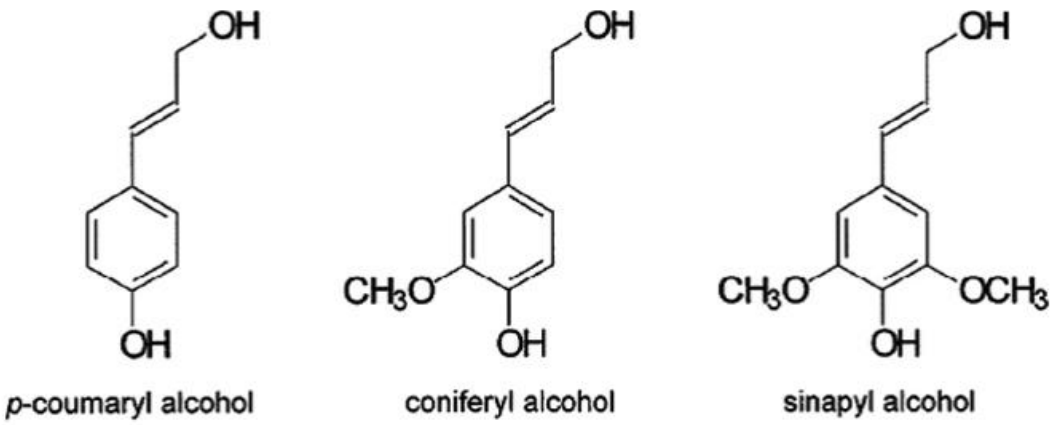

Figure 9 Lignin [69]

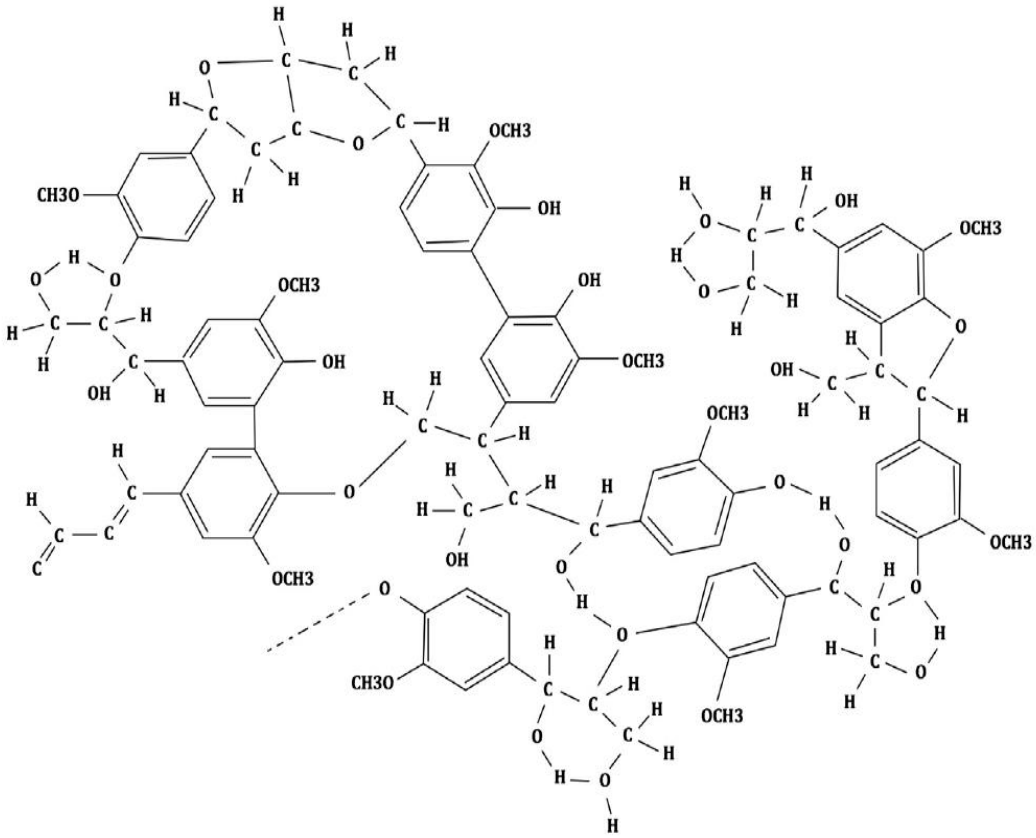

Figure 10 Lignin Structure

There are a lot of sources for biomass energy such as crops, organic waste and organic residues and the Mediterranean region is a perfect place for such resources especially from the olive production sector [44, 70]. The primary source of olive stones is the olive oil industry spread about the Mediterranean region and Europe. Table olive and olive oil is a very active production process there, which is the source of 95% of olives worldwide [71-73] . Rodriguez et al. reported that by the end of the olive season in year 2006, the olive industry worldwide produced 4.31 million tons of table olive and olive oil, whereby Spain alone produced 0.43 million tons of stone from table olive and olive oil production [74, 75]. This results in both solid and liquid waste including pulp, skin, seed, and stone, all constituents of the olive cake (pomace) and olive mill waste [76],

holding negative effects on the environment. These tons of waste are not very useful, and can be problematic if left untreated as they have high polyphenolic compounds which are polluting organics [77, 78]. It was reported that one of the main pollutants of ground and surface waters is olive oil mill waste as it is rich in toxic phenols and organic and colored organic matter which can also affect sprouting and vegetables [73, 79-82].

However, other studies have mentioned that given the hemicellulose, lignin and cellulose content of the olive by-products its value increases. Despite the fact that olive stones has potential in calorific values which promotes it to be used as a source of biofuel [71], these compounds can be separated, and along with the polysaccharides found, can have health and nutritional benefits in some applications [83]. Risk of cardiovascular diseases can be decreased due to the ability of soluble and insoluble fibers to regulate cholesterol by promoting it into bile acid hence increasing its excretion and inhibiting its recapture [84-86]. These fibrous compounds were also found to help in regulating blood glucose levels that might effective against diabetes, and cleanse metabolic substances preventing some cancers in the digestive tract [87, 88]. Moreover, the physiochemistry of the components that make up the polysaccharide structure of the by-products could possibly be used to reduce oxidation reactions, promote suspensions, and improve oil and water preservation enhancing the characteristics of food produce [89]. Table 1 **Error! Reference source not found.**shows the cellulose, hemicellulose, and lignin content of the stone, skin, and olive mill wastewater (OMWW) of the residual cake of olive oil production.

Table 1 Olive oil by-products Lignocellulose Chemical Composition

Olive Oil waste residue	Cellulose	Hemicellulose	Lignin	Reference
Stone	18.6 %	25.1%	39.3%	[90]
	25.4%	25.6%	30.5%	[91]
	31.9%	21.9%	26.5%	[75, 92]
Skin	12.1%	12.2%	43.3	[90]
OMWW	0.6%	0.6%	51.3%	[90]

Furthermore, the physical makeup of the olive can be separated into three parts as in Figure 11.

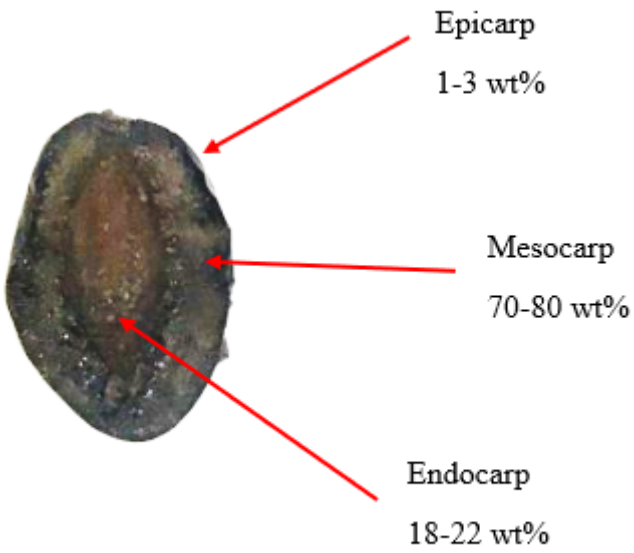

Figure 11 Olive Fruits Parts

Epicarp: this is the skin of the olive fruit, the very most outer layer, and it makes up 1-3 wt% of the whole olive. Contains chlorophyll (green), carotenoids (yellow, orange, red), and anthocyanins (red, purple, blue) which determine its colour [75].

Mesocarp: this part is the pulp/flesh, the edible part between the skin and the stone. It is 70-80 wt% of the olive, the main part where all the fruit components are found [75].

Endocarp: this is the olive stone, the woody centre of the olive, making up 18-22 wt% of the whole fruit and contains the seed inside [75, 93].

But how is the pit/stone separated?

The pit is considered as fuel in some mills where they use it for heating water in the process, sold as wood pellets substitute, or used to produce syngas, sugars, hemicellulose, and cellulose [94-97]. The pit extracted from the roller method make up around 16% of the olives in but their properties are affected due to the separation mechanism and the use of additives. Unlike the roller method, the centrifugation method adopted by the 2- and 3- phase systems preserve the pit integrity. However, pit yield here is roughly half that of the roller method with 8% of olives which count to an average of 16 kg carrying around 20% moisture [98]. The pits are then dried up and the pomace leftover ends up for other uses. When it comes to the pomace, using it for heating and combustion presents similar troubles but it costs half as much. In addition, the value of pomace is highly affected by whether water was used for pit extraction or not whereby the more moisture it contained the lower its value and demand [98]. However, dehydrating residual pomace proves to be useful in areas other than heating, namely compost, fertilizers, soil enhancement, extractions, and livestock fodders [99-101]. For

the past decade, the use of the 2- and 3-phase extraction systems caused the oil content of pomace to decline with an increase in its moisture content, hence pomace processing sites weren't as interested as before. These mills, which now pay only 1.75 euro/100 kg, used to buy pomace for around 3.5 euro/100 kg for the benefit of extracting pomace olive oil, meanwhile pomace sellers used the revenue for maintenance and disposal costs [98]. There are several ways to recover olive pits the simplest of which is direct depitting through table olives processing. Other ways depend on the stage of oil production at which the pit is removed either from pulp, pomace, or spent pomace.

From Pulp: Olives are grinded, and it's at this stage where the pits are removed, then malaxated to commence to oil extraction and pomace with no pits as a by-product; Figure 12.

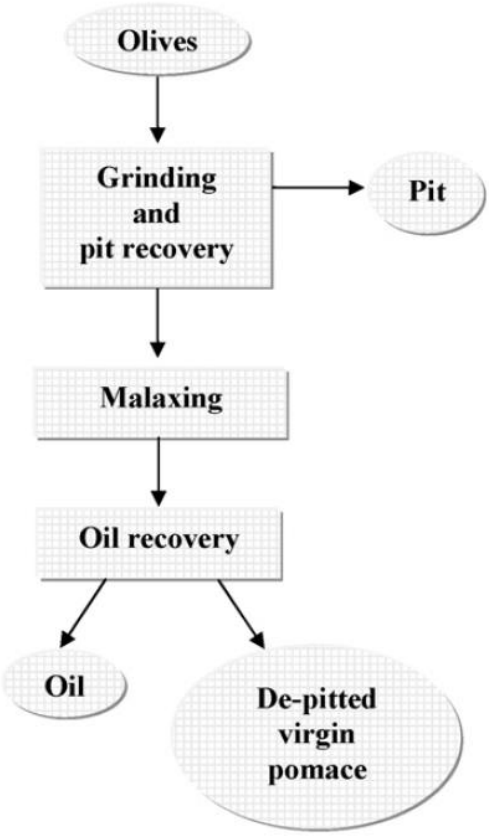

Figure 12 Pit from Pulp [98]

From Pomace: Olives are crushed, malaxated, and oil is recovered along with pomace as by-product. It is only at this stage where pomace is de-pitted, using centrifugation, to end up with pits and clean pomace; Figure 13.

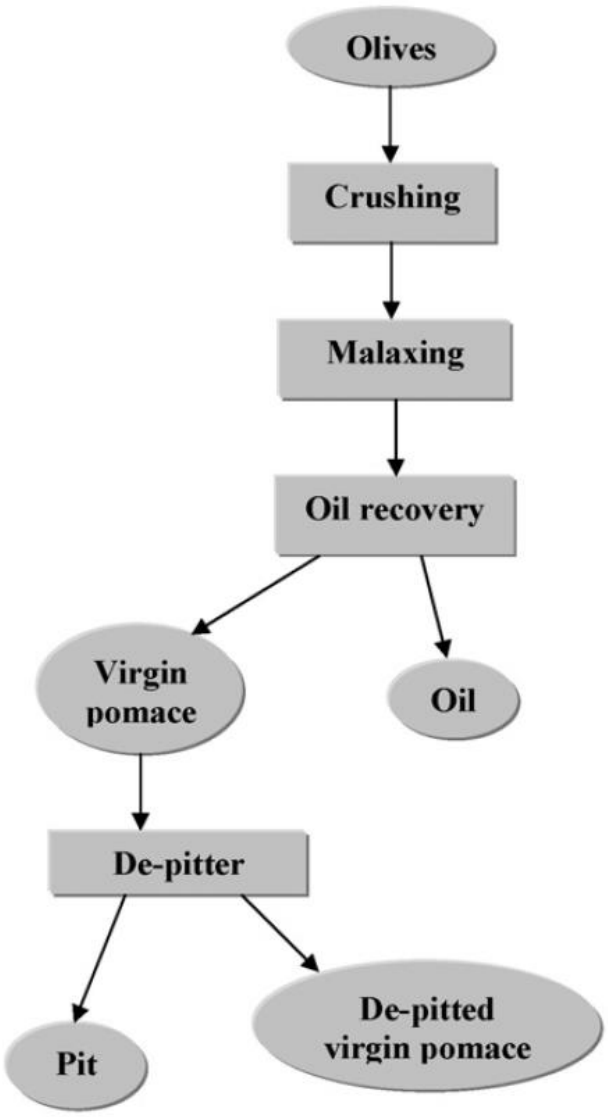

Figure 13 Pit from Pomace [98]

From Spent Pomace: Initial steps are the same except that here the pomace is processed to extract olive pomace oil, and the exhausted pomace is de-pitted for pit recovery using the same roller machine; Figure 14.

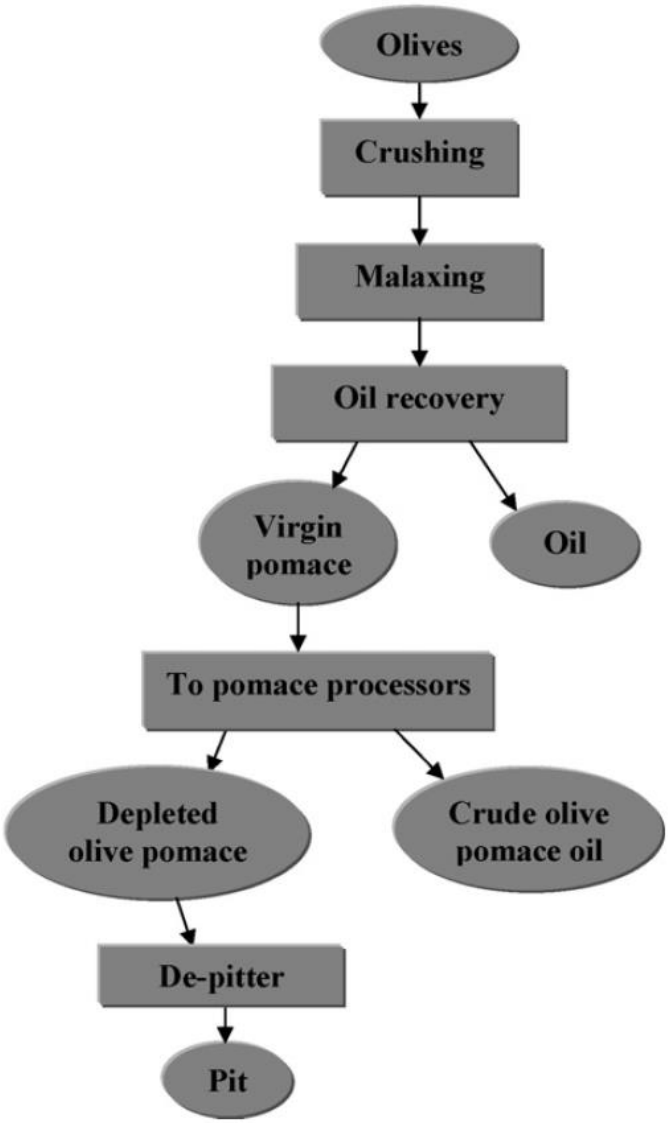

Figure 14 Pit from Spent Pomace [98]

Regardless of the extraction technique, the pits are used for heating and combustion in small and large applications. Unlike several biomass, olive pits are clean off leaves, skins, dusts, and flesh and are available during winter which gives them an advantage as they produce less fumes and ash. The heating value is also acceptable, comparable to other substitutes but better than household pellets except for the ash, with an average of 18 MJ/kg stretching to 20 MJ/kg depending on the moisture content [38-40]. Nevertheless, pomace-extracted pits contain additives posing some problems when it comes to fumes, ash, smell, and dirt collection in small scale applications but are diminished in bigger factories.

B. Pre-treatment Methods

There is a huge range of biomass pre-treatment methods differing in the type of treatment/separation and in the end use of the products. It is noteworthy to mention the diverse end uses of olive stones tackled by several authors. Montane et al. (2001) discussed the production of Furfural, which is a solvent used in industries, from olive stone [75, 102]. And Tejeda-Ricardez et al. (2003) studied the production of phenol-formaldehydes from olive stone extracted phenols [103]. The formulation of plastic filters from olive stones and polypropylene integration was addressed by Siracusa et al. (2001) and the use of olive stones as an abrasive was studied by Dawson (2006) [104, 105]. Olive stone grains in cosmetics has been reported by Mohammadi et al. (2005) mixed with hydrating agents due to its exfoliation abilities [106]. Investigations of olive stones used as metal and metallic ions adsorbents were conducted by Blazquez et al. (2005), Calero et al. (2006), and Fiol et al. (2006) [107-109].

Carrying on, not to drift the section too much off topic with going into the details of all treatment processes, only several lignocellulosic pre-treatment methods will be briefly mentioned. Acid pre-treatment includes the use of sulfuric acid to hydrolyse almost all of the hemicellulose and cellulose, but this process, although efficient, is cost intensive due to further steps like neutralization, corrosion, and equipment. Another pre-treatment method is Liquid hot water (LHW) in which water at high temperature, pressure, and low pH is used to hydrolyse cellulose, hemicellulose, and to alter lignin integrity. Steam explosion is a similar method except that pressure is rapidly released and sometimes employs catalysts and chemical additives. On the other hand, a very simple method is the use of mechanical means to decrease biomass particle size for the purpose of increasing its surface area, increasing substance accessibility, and preparation for thermal or chemical treatments. The use of ionic liquids for pre-treatment aims at transforming the cell walls of the plant solubilizing its components. This eases the performance of next stages whether enzymatic or hydrolytic processes but is expensive. Alkaline pre-treatment is another method in which an alkaline solution is used over hours even days to degrade the lignin making the cell wall easily penetrable by next step agents [110].

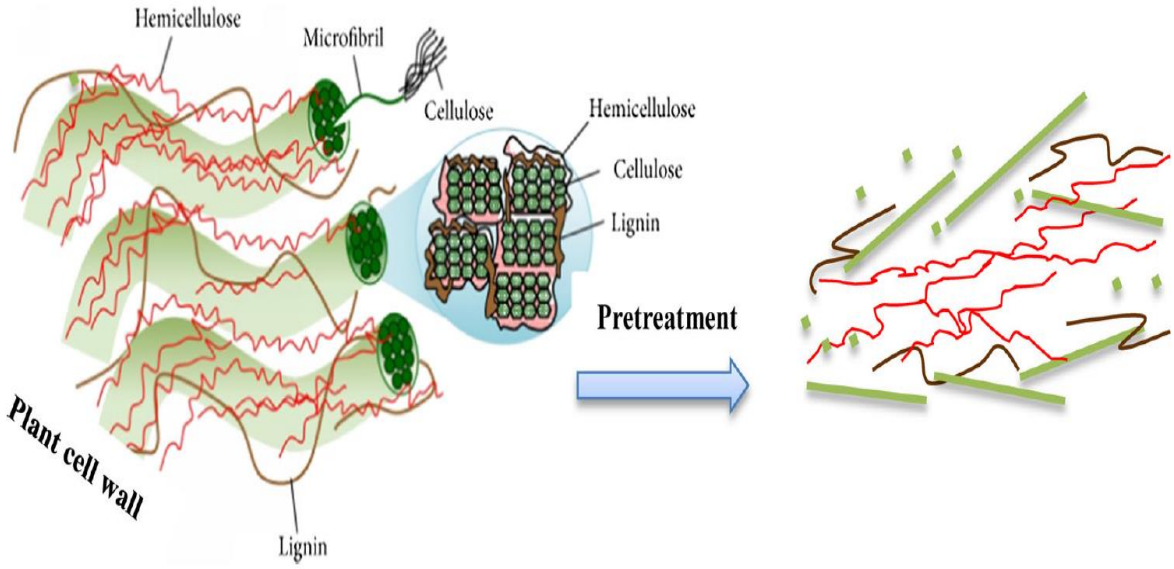

Figure 15 Lignocellulosic Breakdown Upon Treatment

To narrow down on the scope of this study, several thermal treatment methods will be reviewed next. Those are used to enhance fuel properties of biomass, whether solid, liquid, or gas, and reduce their pollutants such as volatile organic compounds (VOCs) and CO even though burning biomass releases less GHGs. Benavente and Fullana et al. reported that the use of biomass as energy sources has increased to reach 10% of energy supply worldwide, and this number is expected to further increase to reach at least 25% by 2050 [44]. Pyrolysis, gasification, hydrothermal carbonization, and torrefaction. Bridgwater (2012) studied fast pyrolysis which is a process typically at 300-650℃ whereby condensable are the target used later for chemicals and energy [76]. Slow pyrolysis in a rotary kiln was investigated by Sangines et al. (2015) using temperatures in the range of 150-900℃ [76]. Meanwhile, gasification is operated at 800-1000℃ to maximize the gas fraction which can be immediately burned for energy or used later for chemicals as reported by Basu (2013)[111] and Knoef (2005)[112]. Hydrothermal

carbonization (HTC) is yet another thermal treatment method operated at 180-250℃ in the presence of water to produce hydrochar used for energy, soil enhancement, and adsorbent according to Atallah et al. (2020) [113]. Bergman et al. (2005) investigated biomass torrefaction, which is a thermal treatment method in the range of 200-300°C, and found that the products had good combustibility properties [114].

Table 2 Biomass Thermal Treatment Methods

Method	**Temperature Range**	**Main Product**	**Use**
Gasification	800-1000℃	syngas/gas	energy and chemicals
Pyrolysis	300-650℃	condensables/liquid	Energy and chemicals
Torrefaction	200-300°C	char/solid	energy
Hydrothermal carbonization	180-250℃	hydrochar/solid	used for energy, soil enhancement, and adsorbent

Cliffe and Patumsawad (2001), Pattara et al. (2010), and Rodriguez et al. (2008) studied development of olive stone energy aspect by direct firing and co-firing at a lab scale and an industrial scale [76]. Olive pit was found to be a good alternative to fossil fuels, with high heat of combustion and easy management, and its recovery is economically feasible on small and big scales [75, 98]. The kinetic parameters of thermal decomposition of olive stone was investigated by Caballero et al. (1997) and Jauhiainen

et al. (2004). Application of fast pyrolysis and gasification on olive residues to produce liquid and gas yields was conducted by Zabaniotou et al. (2000). It was found that maximum liquid and gas yields were obtained at higher treatment temperatures [115]. A study conducted by Alaya et al. (2000) and Martinez et al. (2006) aimed at the conversion of olive stones into activated char with a high surface area. Olive stones are a cheap support when producing activated carbon and KOH activated olive pits had the highest iodine adsorption performance [116, 117]. Biochar with enhanced fuel properties produced from fixed bed reactor olive stone carbonization was reported by Lopez et al. (2002) [76, 118]. Costa et al. (2014) studied raw and torrefied pine shells and olive stones in a drop tube furnace in terms of combustion kinetics, particle break-up, gas characteristics, and particulate matter to assess the effect of torrefaction. The biomass of 1mm size was torrefied at around 290℃ and all the samples were passed through the furnace along a temperature range of 900-1100℃ at 50℃ increments. It was found that torrefied biomass had enhanced heat content by 18% and had faster combustion rate [119].

C. Understanding Torrefaction

Historically, France was the first place for torrefaction to be used in the time range between late 1930s to 1945 as means of gaining a substitute petroleum when possible. When energy sources regained prosperity in distribution and availability after 1945, alternative approaches were neglected until the 1970. Another fossil fuel crisis began and encouraged again the development and utilization of RE, whereby torrefaction in France

re-emerged stronger this time in which commercial scale plans were initiated in the 1980 [120, 121].

Basu (2013) mentioned that there can be several definitions for torrefaction, and it can be described as

"a thermochemical process in an inert or limited oxygen environment where biomass is slowly heated to within a specified temperature range and retained there for a stipulated time such that it results in near complete degradation of its hemicellulose content while maximizing mass and energy yield of solid product" [111].

To define torrefaction, it is a thermochemical treatment method under oxygen deprived or inert (N_2 gas) conditions at atmospheric pressure in which temperatures of 200 to 300°C are used to pyrolyze the biomass for times extending from a couple of minutes to a couple of hours; it can be thought of a case of mild pyrolysis [114, 122]. At temperatures less than 240°C, it is categorized as light torrefaction, while 270°C and above it is categorized as severe [123]. It aims at upgrading/converting lignocellulosic biomass to greater quality biofuel also called biocoal and the solid product, which is the motive for torrefaction, is used mainly for gasification or co-firing [122, 124]. Low heating rates is important during the torrefaction process, typically below 50°C/min, since it preserves the homogeneity of the produced char [123].

During torrefaction, changes occur to structures of cellulose, hemicellulose, and lignin in all woody and herbaceous biomass; this thermal treatment destructs this fibrous structure and its tenacity. As the temperature goes up reaching 100 ℃, hemicellulose, lignin, and cellulose undergo drying as water is evaporated. Exceeding this temperature and going up to 150 ℃, lignin will start to enter a transition phase known as softening. In the range of 150-200 ℃, all the components start changing as the polymeric structures

break in a phase called depolymerisation. When temperatures are in the range of 250-300 ℃, the biomass enters the carbonisation phase whereby the components start to carbonise after the loss of oxygen and hydrogen, which increases the carbon content [114, 125]. It is noteworthy to mention that the temperatures at which changes occur are different depending on the biomass used as each has its own properties and chemical and physical behaviour upon torrefaction. The heating stages of the torrefaction process of biomass can be seen in Figure 16.

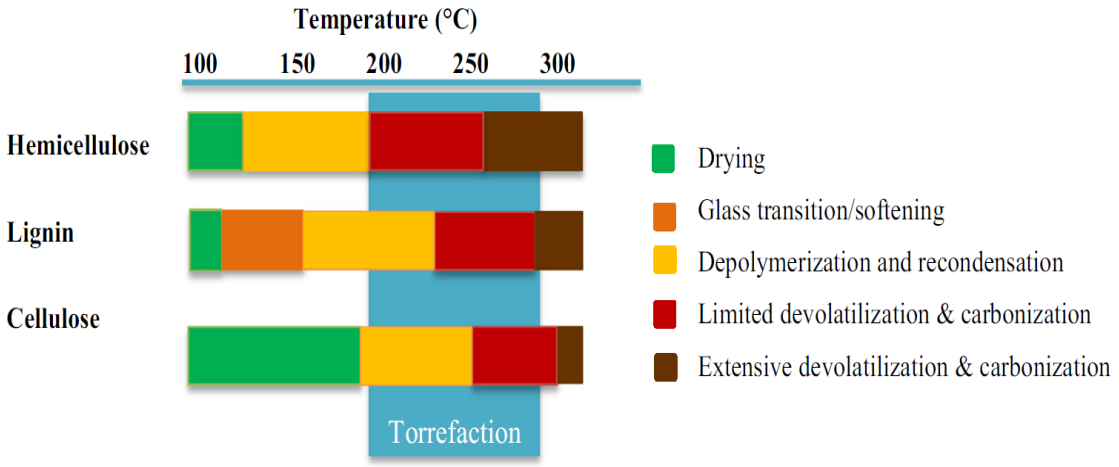

Figure 16 Torrefaction Stages with Temperature [122]

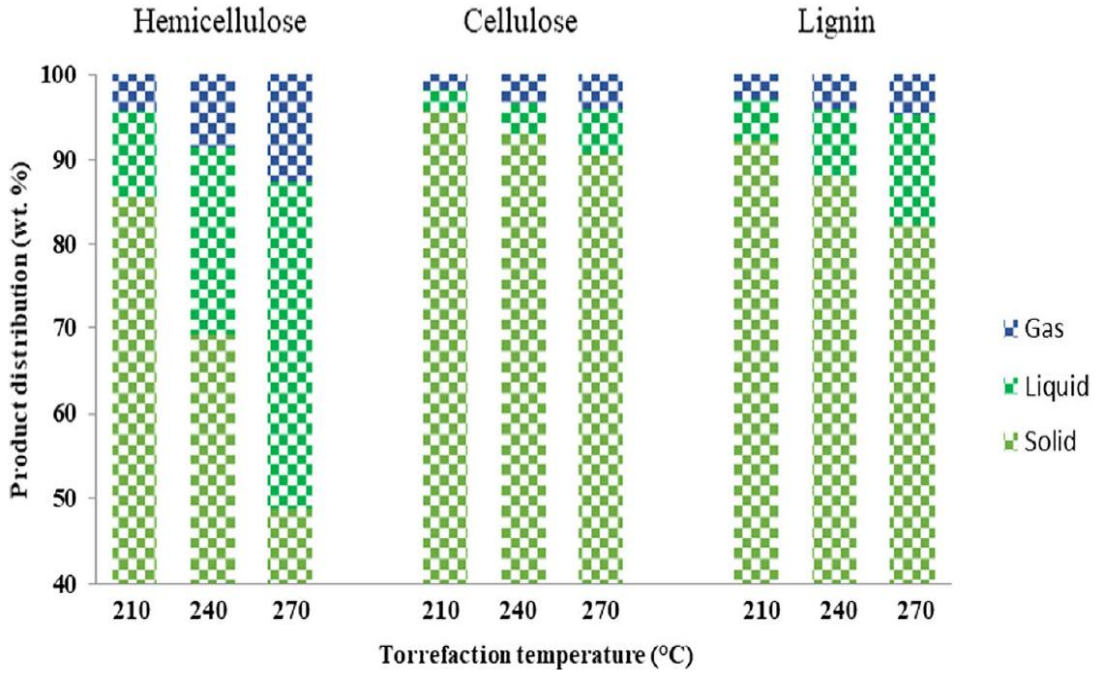

Figure 17 Distribution of Torrefaction Products on Lignocellulosic Components

Generally, upon torrefaction of biomass, 30% of the initial mass escape as volatiles and 70% remain as solid products, with 10% and 90% of the energy of the original biomass in each, respectively [114]. And as such, the products split into 3 streams: solids, liquid, and gas.

Solids: This consists of the remaining torrefied biomass, also known as char, with modifications in the sugar and polymeric structures, along with some ash [114]

Liquid: This stream consists of water, some organics like furans, alcohols, and acids (formic, acetic, lactic), in addition to some lipids like phenols, ketones, fatty acids, and tanins [114, 122, 124]

Gas: This consists of hydrogen, carbon monoxide, carbon dioxide, and methane [114]

A simple illustration of the torrefaction process is shown in Figure 18.

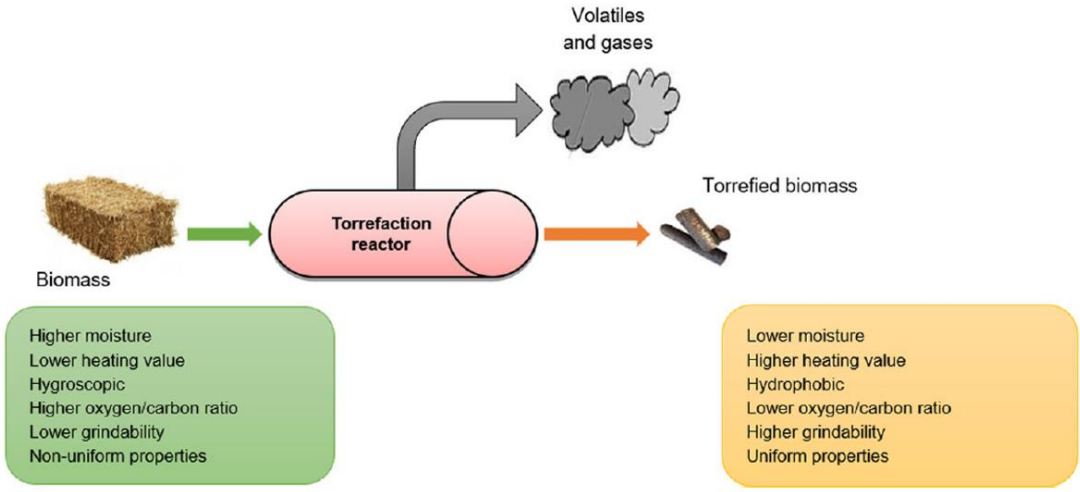

Figure 18 Changes of Biomass Upon Torrefaction [122]

It is expected that upon torrefaction the O/C and the H/C ratios decrease as the biomass loses hydrogen and oxygen resulting in a carbon rich composition. According to Bergman et al. 2005, no matter what biomass is used, its elemental composition will decrease in hydrogen and oxygen and increase in carbon, with a greater extent as the temperature of torrefaction increases [114]. This can be well represented in a Van Krevelen diagram which is a plot of the O/C versus the H/C ratios, and as these ratios decrease the biomass is closer in properties to coal. All this leads to a critical conclusion which is the increase in the energy content and density of the torrefied biomass; improving firing properties, handling and transportation [126]. The lower heating value of torrefied biomass can reach to calorific values of 20 – 24 MJ/Kg which is significantly higher than raw biomass. Moreover, the loss of water, some organic volatiles, and -OH structures from the biomass during torrefaction, limits the bonding of water after the process, topping that with the formation of non-polar structures increases the

hydrophobicity [114]. Further advantage of torrefaction is that devolatilization diminishes the emissions of SO_2, NO_x, CO_2, PAHs and dioxins, especially in OS due to its low N and S content, and it has been proven that the particulates produced upon its combustions are 40% less than what would result from burning raw biomass [75, 127, 128].

CHAPTER III
MATERIALS AND METHODS

A. Experimental

1. Materials

The materials to be used are crushed olive dried stones which are originally imported from Spain. A full 20 Kg bag of crushed OS was received containing a wide range of OS size distribution.

Half of the bag which accounted to roughly 10 Kg of crushed OS was sieved using 3 main sizes: 2-3 mm, 0.425-1 mm, and 0.18-0.425 mm. This size-categorizing fairly represented the material in which the 2-3 mm size was considered the “large grain size”, the 0.425-1 mm size was considered the “medium grain size”, and the 0.18-0.425 mm was considered the “small grain size”.

Figure 19 Raw Olive Pits

Figure 20 Crushed Olive Stones

2. Design of Experiments

There are three main conditions that the experiments were designed upon, which are: temperature (T), residence time (RT), and particle size (PS) shown in Table 3 with values. However, progressing through the characterization of the different samples, as will be discusses in coming chapter sections, some were screened out and others were expanded due to reasons explained when the results are presented. However, to be comprehensive for the modelling (Chapter V), all experiments were used, also discussed later.

Table 3 Experimental Parameters

Parameter	Values
Grain size (mm)	2-3
	0.425-1
	0.18-0.425
Temperature (℃)	200
	250
	300
Residence Time (mins)	30
	60
	120

Each grain size is to be run with every temperature under every residence time and repeating each experiment 5 times plus 1 gas run would add up to a total of 162 experiments.

The first 5 runs of each experiment were replicates i.e. using the same grain size, at the same temperature, and under the same residence time, the experiments were run 5 times. Then, performing an overall mass balance on the system and doing the necessary calculations gave the solid, liquid, and gas yield. As for the gas run, only 1 run was performed for each experiment with the purpose of collecting the released gas for later analysis when necessary.

3. Equipment and Setup

The equipment used for the lab scale torrefaction setup included the following:

- An open-ended ceramic-wall electric Carbolite furnace with a temperature range of 200 to 1300 ℃
- A 70 cm quartz tube with a diameter of 5 cm
- A 10 liter LAUDA ALPHA RA 8 ethylene glycol cooling system
- A 40 cm condenser
- An elbow fitting
- A tip fitting
- A 300 ml round bottom flask
- 2 hand-made baskets from metal sheets to accommodate all the grain sizes of the OS
- A clamp stand
- A filter and a cork
- A cooling fan
- Finally, the necessary hoses for the connections

The setup was built inside a fume hood as a measure of safety as there are high temperatures, production of gases, and the hazard of fire. The condenser was placed outside the fume hood for the ease of access and maintenance.

The setup can be seen in the photo as in Figure 21 and Figure 22.

Figure 21 Torrefaction Setup

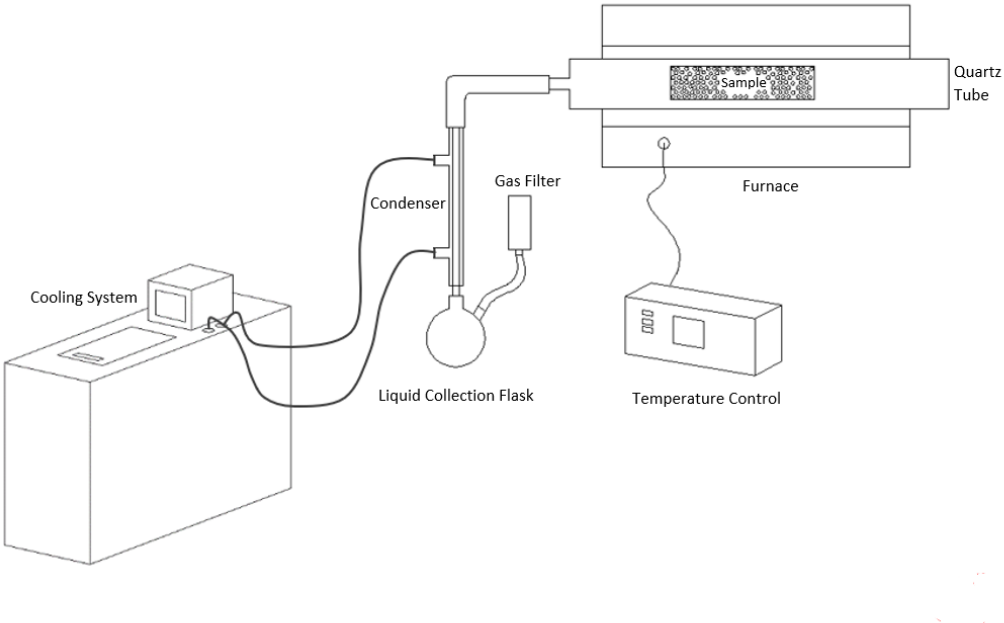

Figure 22 Experimental Setup Sketch

As mentioned earlier, the setup is inside a fume hood except for the cooling system, and the furnace can be seen tilted to guide any early condensates to the condenser and hence to the collection round bottom flask. The quartz tube (not visible) is inside the furnace with access to both of its ends whereby the tip is fitted into an elbow which leads to the condenser while the rear is open to the other side for the introduction of biomass feed. The cooling liquid (ethylene glycol) is circulated in the condenser via two 1 m rubber hoses, and the temperature of cooling is maintained at 0 ℃ at all times. The clamp stand can be seen holding the glassware all the way out from the furnace to the condenser for extra security and sturdiness. The round bottom flask has another opening where a gas line is connected to a filter to seize any particulates that may result.

The most important part of the whole setup must be the furnace. It has a small digital control unit to specify the temperature set point and to monitor the actual temperature reading. Moreover, the furnace is characterized by a hot zone which is the middle third part of the furnace length which was determined by taking several temperature measurements at different depths of the furnace. The furnace zones are illustrated in Figure 23.

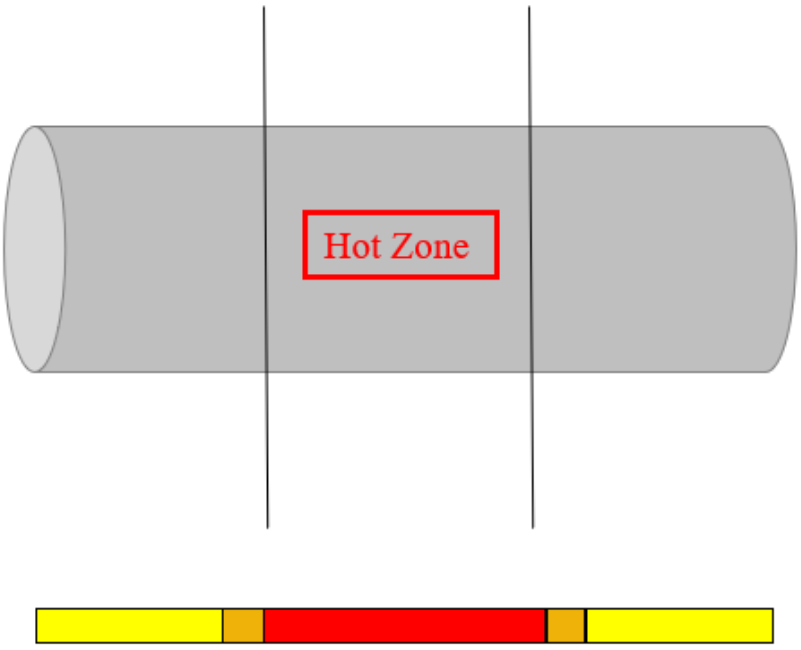

Figure 23 Illustration of Furnace Heating Zones

The hot zone is where the temperature is exactly as displayed by the controller and where the main part of the heating takes place and is represented by the red range. Moving further away from the hot zone and into the orange range, the temperature is 5-10℃ lower than the set temperature. Moving further away to the yellow zone, the temperature is 20-25℃ less than the set temperature. It is very important therefore to carefully place the biomass right in the hot zone as to ensure proper heating and accurate results.

4. Procedure

Before the start of any experiment, all the glassware is weighed; the quartz reactor, the tip, the elbow fitting, the condenser, and the round bottom flask. Then after setting up the necessary electrical, cooling, and gas connections, the cooling system is turned on to reach 0 ℃. Everything now is ready for the experiments to commence and with each weighing and assembly only experiments of the same conditions can be run, whenever a condition is changed the setup is disassembled, weighed again, and reassembled again.

To run an experiment, the first step would be weighing the metal mesh basket (OS holder), then weighing 50 g of OS and adding them to the basket. Then the basket and the OS inside it are weighed together as “weight before torrefaction”. The basket is then inserted into the quartz tube with the aid of a carefully measured metal rod to reach the hot zone.

Now that the basket containing the biomass is in its place, the cork used to seal the tube from the back is measured for weight as “cork weight before torrefaction”. The cork is the securely pushed into place to close the quartz tube.

Now the electrical heating of the furnace can be turned on after which the temperature increases gradually from room temperature to reach the set torrefaction temperature. The process is kept running for as long as the designated residence time of the experiment being conducted. When the time is over, a cooling fan is set in place from the back end of the quartz tube to actively cool the tube; the use of active cooling here is critical as after cutting the electrical heating, the furnace takes way too long to passively cool down which will affect the results as the biomass is being exposed to higher temperatures for longer times.

After an acceptable temperature is reached (low enough to handle), the cork is removed and weighed as “cork weight after torrefaction”. The basket is then pulled out and immediately weighed as “weight after torrefaction”. The gas filter and lines are also weight before and after the torrefaction, but the differences are insignificant to none to consider.

Subtracting the weights of the basket and biomass before and after torrefaction gives us the total weight loss during torrefaction. Then the difference between the weights of all the other equipment before and after torrefaction gives us the weight loss of the liquid. Finally, the gas weight lost remains the only one left and is calculated by difference.

To collect gas samples for further analysis, the same exact setup and procedure is used, except this time, a gas sampling Tedlar bag is attached to the gas vent of the round bottom flask via a properly sealed rubber line.

B. Characterization

1. Scanning Electron Microscopy (SEM)

SEM images were captured using a Tescan MIRA3 electron microscope at 10,000 V using an in-beam secondary electron (SE) detector. All the samples were sputtered with 10mm gold coat to minimize charging.

2. ThermoGravimetric Analysis (TGA)

TGA of the raw and torrefied samples was acquired using a TA Q500 instrument and a heating rate of 15°C/min was used from room temperature to 950°C in air. All samples were in powder form and only 5mg to 10mg was required.

TGA in N_2 of the samples was conducted using a NETZSCH TG 209 F1 LIBRA instrument. A heat ramp rate of 10°C/min was used from room temperature to 950°C. Only 5mg of each sample was used in powder form and placed in ceramic crucibles on a sequential auto-sampling tray.

3. Fourier Transform InfraRed (FTIR)

Adding on the TGA in N_2, the gases exiting the samples were directed from the NETZSCH instrument to the BRUKER TGA-IR TENSOR 27 for gaseous spectroscopic analysis.

FTIR of the raw and torrefied solid samples analysis was performed using a benchtop Agilent Cary 630 FTIR Spectrometer. Samples used were in powder form and a generous amount was placed on the lens to ensure it was completely covered. The lens was thoroughly wiped after each test with methanol.

4. Bomb Calorimetry

Heating values of all the sample, raw and torrefied, were obtained using an IKA C200 bomb calorimeter with a 25℃ maximum operating temperature.

The bomb was prepared using 0.5g to 1g of each sample and 5ml of distilled water was added before tightening and oxygen priming to 30 bars.

Prior to each run, 1 litre of chilled water and 1 litre of tap water were poured into the instrument water reservoir.

5. Proximate and Ultimate Analysis

Proximate and ultimate analyses for all samples were conducted using standard methods. Samples used were in powder form.

Moisture content procedure [129]:

- Pre-drying empty crucibles, cooling and weighing them
- 1g of sample was then added to the crucible and weighed
- Next place crucible in preheated oven between 104 to 110℃ for 1 hour

Moisture content calculation [129]:

$$MC\ \% = \left[\frac{sample\ weight\ - sample\ weight\ after\ heating}{sample\ weight}\right] \times 100$$

Volatile matter procedure [130]:

- Weight an empty crucible
- Add 1g of sample to the crucible and weigh again
- Place crucible in preheated furnace at 950℃ for exactly 7 minutes
- Leave to cool then record weight

Volatile matter calculation [130]:

$$VM\ \% = D - MC$$

Where,

$$D = \left[\frac{(weight\ of\ crucible\ before\ heating - weight\ of\ crucible\ after\ heating)}{(weight\ of\ crucible\ before\ heating - weight\ of\ empty\ crucible)}\right] \times 100$$

Ash content procedure [131]:

- Weigh an empty crucible
- Add 1g of sample to the crucible and weigh again
- Place crucible in cold furnace and heat up to 500℃ over a span of 1 hour
- Continue heating up to 750℃ and hold for 2 hours
- Leave to cool then record weigh

Ash content calculation [131]:

$$Ash\ \% = \left[\frac{crucible\ weight\ with\ ash\ - empty\ crucible\ weight}{sample\ weight}\right] \times 100$$

Fixed carbon calculation:

$$FC\ \% = 100 - Ash\% - VM\% - MC\%$$

Ultimate analysis was conducted using a LECO CHNS Ultimate Analyzer. Sample weights of 0.35g were used.

As there is no standard procedure for oxygen % determination, it is determined by difference [132]:

$$O\ \% = 100 - C\% - H\% - \ N\% - S\% - Ash\%$$

6. Chlorine Content

Washings from the bomb calorimeter for all samples were stored in vials for chlorine content testing. The tests were conducted using an Agilent 1290 Infinity II HPLC system.

7. Hydrophobicity

To determine the level of hydrophobicity of each sample, a simple drying technique was used.

Glass vials used were weighed before and after the addition of some sample mass. The vials were then dried over 48 hours at 80℃ and -0.5bar and weighed immediately after to get the water weight and percentage adsorbed.

The weighing process and percentage calculation was repeated after 1 hour, 2 hours, 4 hours, 6 hours, 24 hours, 2 days, and 5 days.

To make sure glass adsorption of water was not significant, the procedure was performed on five empty glass vials with very negligible difference.

CHAPTER IV
RESULTS AND DISCUSSION

A. Mass Balance

Simple mass balance calculations, in grams, were conducted on every run of every experiment as there are several replicates for each. The solid, liquid, and gas yields (SY, LY, GY) were then calculated based on the obtained mass balance. The results for all torrefaction conditions are presented in Table 4, and note that for ease of discussion, the particle size was taken as an average rather than range.

Table 4 Solid, Liquid, and Gas Yields for Torrefaction Conditions

Avg. particle size (mm)	**Temp. (^{o}C)**	**Res. time (min)**	**Solid yield (wt%)**	**Liquid yield (wt%)**	**Gas yield (wt%)**
2.5	200	30	87.9	8.2	3.9
2.5	200	60	87.2	12.5	0.3
2.5	200	120	86.2	13.4	0.3
2.5	250	30	85.1	13.3	1.6
2.5	250	60	80.3	17.7	1.98
2.5	250	120	62.9	16.03	21.1
2.5	300	30	47.2	41.6	11.2
2.5	300	60	40.2	49.1	10.7
2.5	300	120	38.8	50.03	11.1

0.71	200	30	89.5	7.1	3.4
0.71	200	60	86.8	12.1	1.1
0.71	200	120	85.9	13.7	0.42
0.71	250	30	88.7	10.4	0.84
0.71	250	60	79.4	18.75	1.8
0.71	250	120	70.8	25.1	4.05
0.71	300	30	74.1	21.7	4.2
0.71	300	60	37.1	50.9	12.02
0.71	300	120	37.2	50.5	12.3
0.3	200	30	91.1	8.5	0.37
0.3	200	60	87.7	12.1	0.16
0.3	200	120	86.5	12.6	0.96
0.3	250	30	86.7	11.5	1.8
0.3	250	60	81.4	16.9	1.7
0.3	250	120	68.2	26.6	5.2
0.3	300	30	70.3	24.8	4.8
0.3	300	60	39.4	48.6	11.9
0.3	300	120	38.4	50.4	11.2

By simply observing the yield values, a distinct region of conditions can be highlighted with special interest in the solid yields. Looking at the solid yields for the range of conditions from 250ºC and 120mins to 300 ºC and 120 mins for all three sizes, with everything in between, shows that those for the 2.5mm size torrefaction was most intense. Not much can be said about the similar solid yields for the conditions 300 ºC for 60 and 120mins for all the 2.5, 0.71, and 0.3mm sizes; being 40.2% and 38.8, 37.1% and 37.2, 39.4% and 38.4%, respectively. However, the gap between the difference increases for 250 ºC for 120mins and 300 ºC for 30mins where the solid yields are 62.9% and 47.2% for the 2.5mm size, respectively, 70.8% and 74.1% for the 0.71mm size, and 68.2% and 70.3% for the 0.3mm.

The observation is clearly symbolised in Figure 24 with the number 1, 2, 3, and 4 representing different conditions. Focusing on the area designated by the red circle, the solid yield of size 2.5mm is lowest for condition sets 1 and 2.

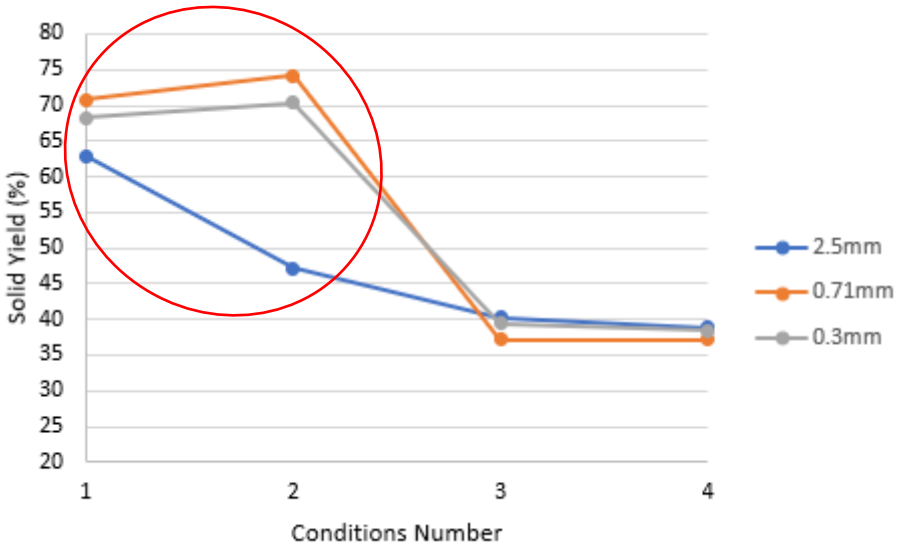

Figure 24 Solid Yields Representation for the Special Conditions Region (1: 250 °C and 120mins, 2: 300 °C and 30mins, 3: 300 °C and 60mins, 4: 300 °C and 120mins)

It was worth investigating this conditions region more as it showed a distinct and better response. To continue with, the conditions under focused study became as represented in Table 5. Four new condition sets were added for the 2.5mm size with the introduction of a temperature of 270 °C at 30min, 45mins, 60mins, and 120mins. For sizes 0.71mm and 0.3mm, only one condition set was added: 270 °C at 30min.

Table 5 Solid, Liquid, and Gas Yields for Selected Torrefaction Conditions

Avg. particle size (mm)	Temp. (°C)	Res. time (min)	Solid yield (wt%)	Liquid yield (wt%)	Gas yield (wt%)
2.5	200	30	87.9	8.2	3.9
2.5	250	30	85.1	13.3	1.6
2.5	250	120	62.9	16.03	21.1
2.5	270	30	82.3	14.9	2.69
2.5	270	45	60.5	32.78	6.72
2.5	270	60	47.66	40.44	11.89
2.5	270	120	48.54	24.07	27.39
2.5	300	30	47.2	41.6	11.2
0.71	200	30	89.5	7.1	3.4
0.71	250	30	88.7	10.4	0.84
0.71	270	30	84.19	12.84	2.18
0.71	300	30	74.1	21.7	4.2
0.3	200	30	87.7	12.1	0.16
0.3	250	30	86.7	11.5	1.8
0.3	270	30	81.83	16.44	1.722

0.3	300	30	70.3	24.8	4.8

B. Visual Observation

Upon different torrefaction conditions, the resulting solid residue (char) varies in colour. Figure 25, Figure 26, and Figure 27 illustrate the different appearances of raw and torrefied OS of all conditions. Also, for comparison, Figure 28 shows normal wood and coal.

Table 6 will serve as a guide for Figure 25, Table 7 will serve as a guide for Figure 26, and Table 8 will serve as a guide for Figure 27.

To start with, Table 6 shows the 2.5mm particle size and the torrefaction conditions performed. Going from top left of Figure 25 to top right, the OS start raw and then the temperature increases through 200 ^{o}C, 250 ^{o}C, 270 ^{o}C, till 300^{o}C. With this increase, the colour of the OS becomes darker going from light brown from raw to dark black at the highest temperature. Likewise, going from top of the figure to the bottom of each column shows an increase in residence time through 30 mins, 45 mins, 60 mins, and 120mins. With this increase, the colour of OS also becomes darker than whatever initial colour of the corresponding temperature.

Table 6 Guide of the Torrefaction Conditions for the 2.5mm Particle Size

Temperature / Time	Raw	200 °C	250 °C	270 °C	300 °C
30mins	X	X	X	X	X
45mins				X	
60mins				X	
120 mins			X	X	

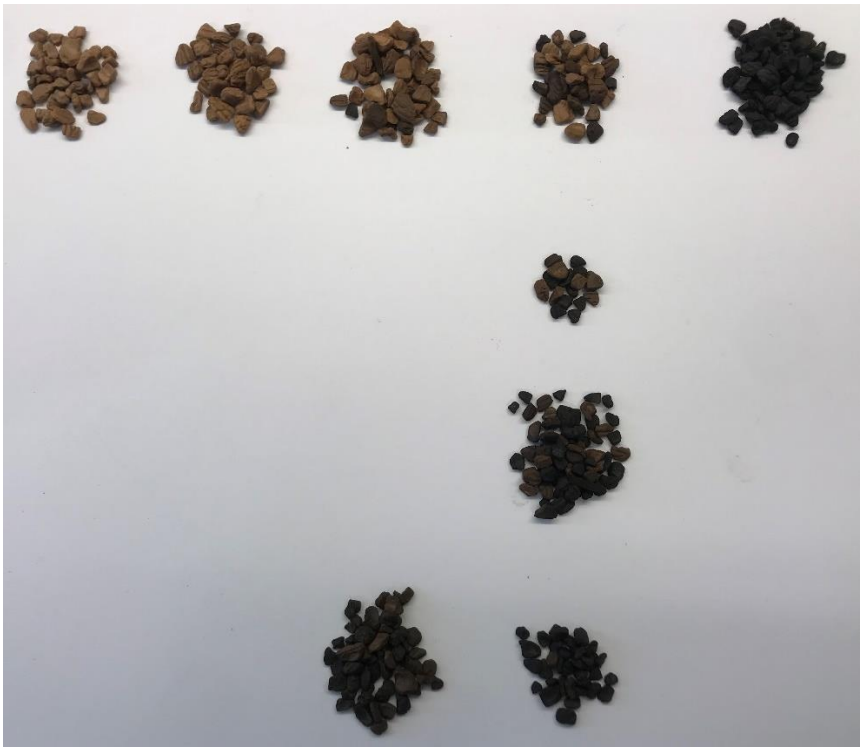

Figure 25 OS of Particle Size 2.5mm Under Different Torrefaction Conditions

Table 7 shows the 0.71mm particle size and the torrefaction conditions performed. Going from top left of Figure 26 to top right, the OS start raw and then the temperature increases through 200 °C, 250 °C, 270 °C, till 300 °C. With this increase, the colour of the OS also becomes darker going from light brown from raw to dark black at the highest temperature. However, only 30mins was used as the residence time in this size group, and notice that at 250 °C and 270 °C the OS colour is slightly lighter than what is in the 2.5mm group counterpart.

Table 7 Guide of the Torrefaction Conditions for the 0.71mm Particle Size

Temperature / Time	**Raw**	**200 °C**	**250 °C**	**270 °C**	**300 °C**
30mins	X	X	X	X	X
45mins					
60mins					
120 mins					

Figure 26 OS of Particle Size 0.71mm Under Different Torrefaction Conditions

Table 8 shows the 0.3mm particle size and the torrefaction conditions performed. Going from top left of Figure 27 to top right, the OS start raw and then the temperature increases through 200 ^{o}C, 250 ^{o}C, 270 ^{o}C, till 300 ^{o}C. With this increase, the colour of the OS also becomes darker going from light brown from raw to dark black at the highest temperature. Here again, only 30mins was used as the residence time in this size group, and the same can be noticed whereby at 250 ^{o}C and 270 ^{o}C the OS colour is slightly lighter than what is in the 2.5mm group counterpart.

Table 8 Guide of the Torrefaction Conditions for the 0.3mm Particle Size

Temperature / Time	Raw	200 °C	250 °C	270 °C	300 °C
30mins	X	X	X	X	X
45mins					
60mins					
120 mins					

Figure 27 OS of Particle Size 0.3mm Under Different Torrefaction Conditions

Figure 28 shows normal wood which is lighter than all the treated OS and coal which is darker.

Figure 28 Normal Wood (Left) and Coal (Right)

C. Effect of Temperature and Time on Yields

From the experimental results it is observed that as temperature increases, the solid yield decreases while the liquid and gas yields increases due to some mass of the solid feed being volatized into liquid and gas [70, 133-135]. By observing Figure 29(a), increasing the temperature from 200 to 250, 270 and to 300^{o}C for 2.5 mm size and 30 mins, increased the liquid yield from 8.2% to 41.6% and gas yield from 3.92% to 11.21%, and decreased the solid yield from 87.9% to 47.2%. An important point to make here is that these values were very distinct because the corresponding changes in solid, liquid, and gas yields for the smaller particle sizes over the same temperatures were smaller. For 0.71mm and 30mins, as in Figure 29(b), increasing the temperature from 200 to 250, 270 and to 300^{o}C increased liquid ad gas yields from 7.1% and 3.4% to 21.7% and 4.2%, respectively, and decreased the solid yield from 89.5% to only 74.1%. Almost a similar trend and change intensity can be seen from Figure 29(c) for the 0.3mm and 30mins conditions, with yields changes: for solid from 87.7% to only 70.3%, for liquid from 12.1% to 24.8%, and for gas from 0.16% to 4.8%. In all cases, this decrease in SY and increase in LY and GY is in agreement with remarks of Negi et al. (2020) and Nhuchhen et al. (2014) due to the extensive devolatilization of hemicellulose and some cellulose that occurs with increase in temperature, especially at 250^{o}C and 270^{o}C, releasing more H_2O, CO_2, and acids [122, 136].

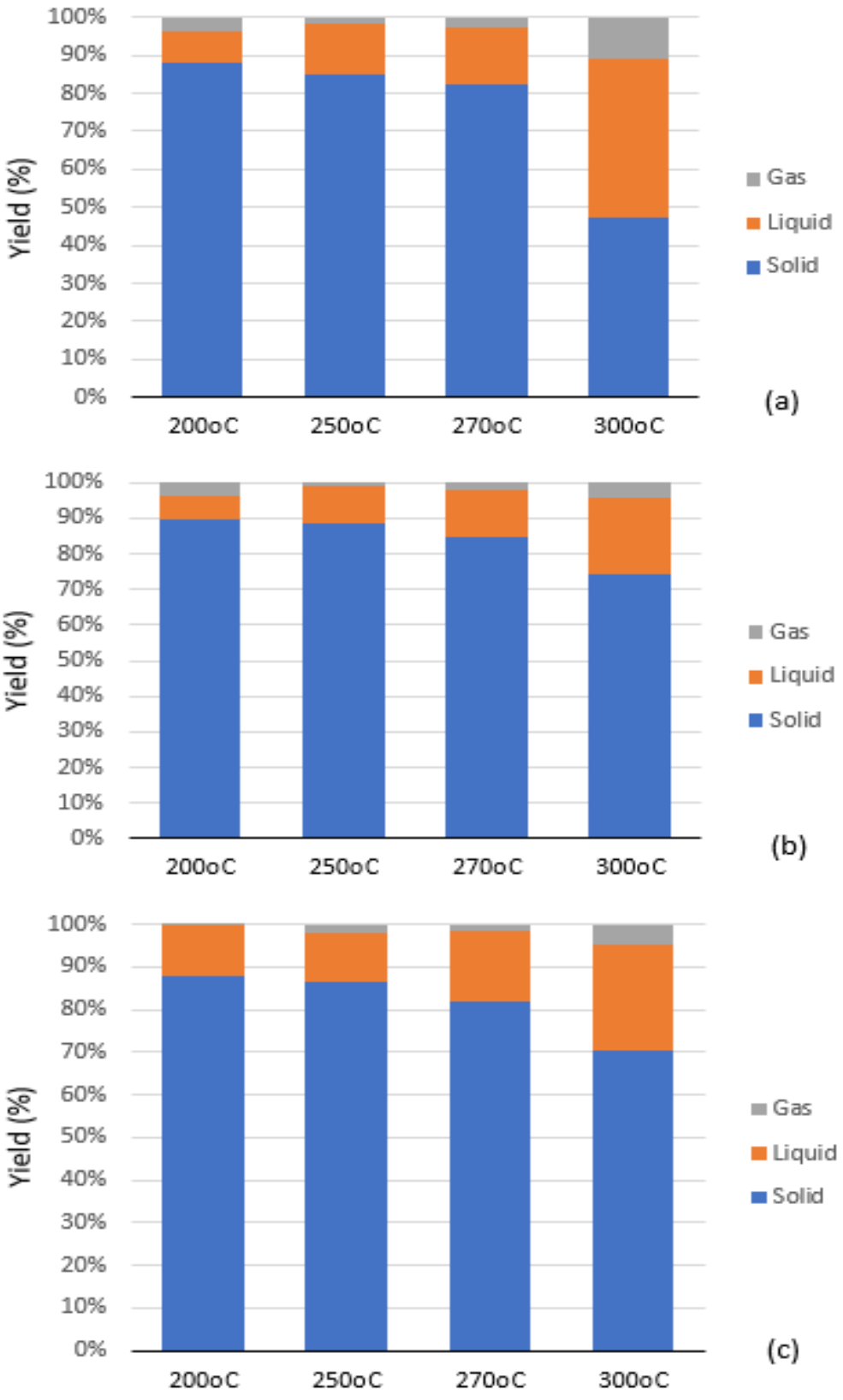

Figure 29 Solid, Liquid, and Gas Yields as a Function of Temperature for (a) 2.5mm and 30mins (b) 0.71mm and 30mins (c) 0.3mm and 30mins

As for residence time, increasing it from 30, 60, and to 120 mins for 0.71 mm and 250ºC, increased the liquid and gas yields from 10.4% to 25.1% and from 0.84% to 4.05%, respectively, but decreased the solid yield from 88.7% to 70.8% as shown in Figure 30(a). Similar trends of decrease in solid yield and increase in liquid and gas yields can be seen in Figure 30(b) and (c).

It is noteworthy to mention that the effect of temperature is intensified with increase in time, and the effect of time is intensified with increase in temperature. The same was found to be true for greenhouse crop residues, whereby the time had a more considerable effect as the temperature increased [70], and is also with agreement with works on tomato peels [137] and cotton stalk [138]. Then it is clear that the most important parameters for the process are the temperature and the residence time [127, 139].

Time also had a major effect on the yields since increasing the residence time decreases the solid yield, which is in accordance with what was reported for greenhouse crop residues [70], but increases the liquid and gas yields, generally, due to increase in devolatilization extent [136]. It is noteworthy to mention that torrefaction residence time is effective within the range of 10-60 mins, anything below that does not really have an effect, and the effectiveness of anything above starts to decline [122, 136].

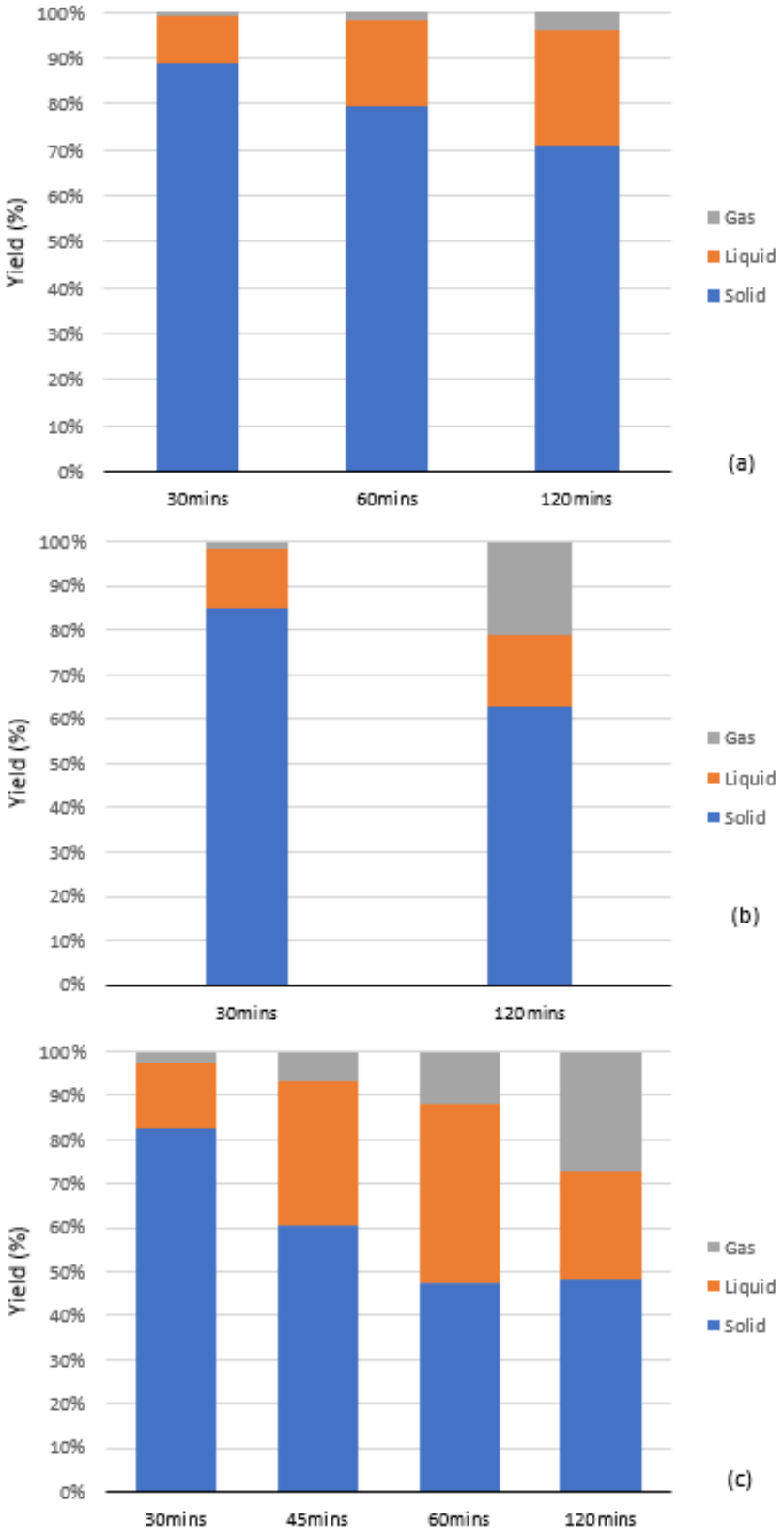

Figure 30 Solid, Liquid, and Gas Yields as a Function of Residence Time for (a) 0.71mm and 250℃ (b) 2.5mm and 250℃ (c) 2.5mm and 270℃

Temperature and time are the parameters that majorly effect the yields with temperature being the most effective and this conclusion is in total agreement with literature as reported by Nhuchhen et al. (2014), Bergman et al. (2005), and Negi et al. (2020) [114, 122, 136]. As the temperature increases, no matter the particles size or residence time, more of the solid feed mass is being lost as more volatiles are being released, hence decreasing the solid mass yield, and increasing the liquid and gas yields. This is mainly due to the softening of the present hemicellulose which is then dehydrated, deacetylated, and depolymerized, even more severely at higher temperatures [126, 140]. Moreover, as the temperature rises to the 270-300^{o}C range and above, cellulose starts to breakdown which contributes to more mass loss at those elevated temperatures [140-142] Similarly, when the solid feed resides in the reactor for a longer duration, it gives more time for more volatiles to be released thus decreasing solid mass and yield and increasing liquid and gas yields. It was also found that the residence time is more effective at higher temperatures.

D. Effect of Particle Size on Yields

The effect of particle size was less significant since as the average particle size increases the solid residue yield decreases slightly, except for harsher torrefaction conditions where the changes become more noticeable. But as an example of most cases, changing the particle size from 0.3 to 2.5mm at a constant 200°C and 30 mins change the solid yield from 91.1%. to only 87.8% as in the bar graph of Figure 31(a).

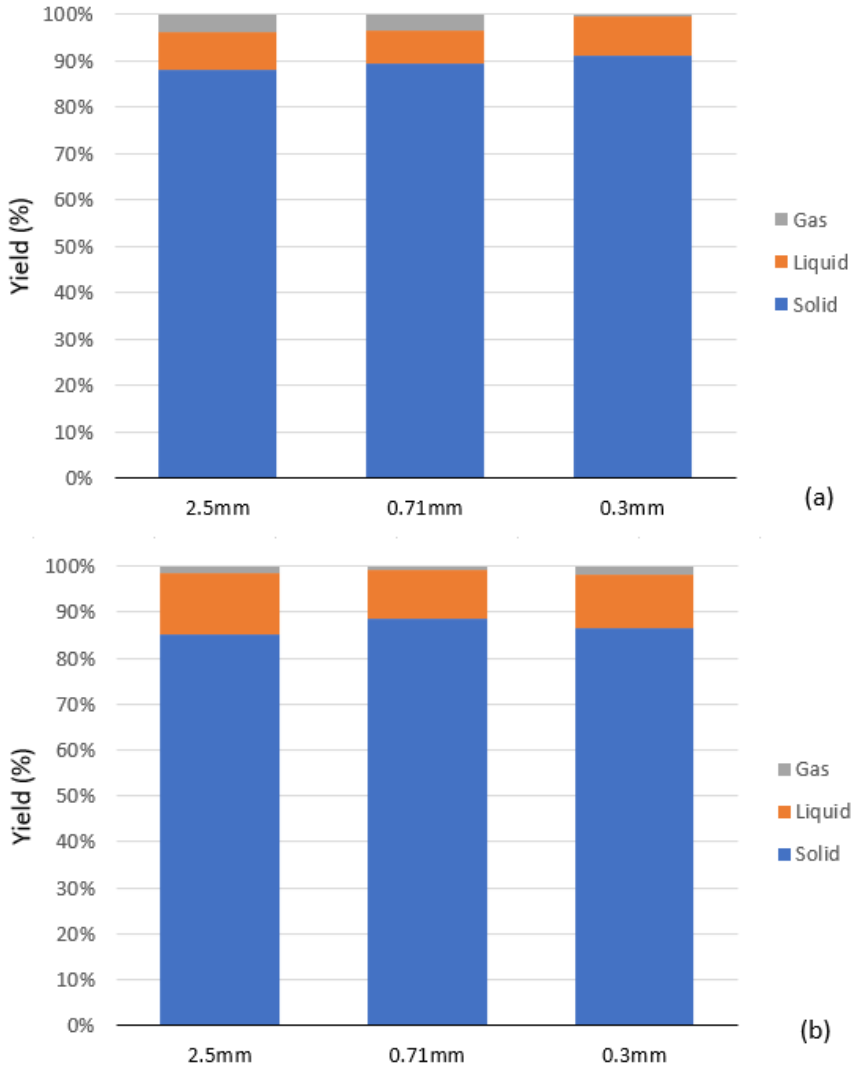

Figure 31 Solid, Liquid, and Gas Yields as a Function of Particle Size for (a) 200℃ and 30mins (b) 250℃ and 30mins

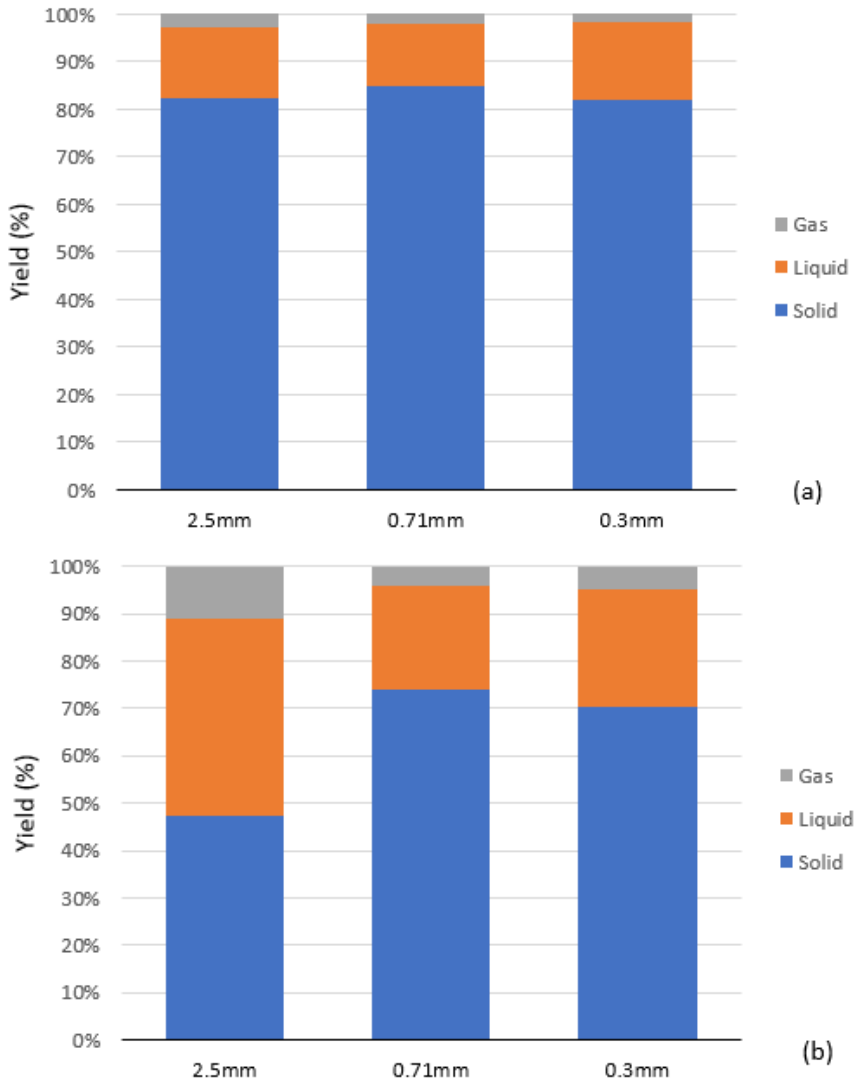

Figure 32 Solid, Liquid, and Gas Yields as a Function of Particle Size for (a) 270°C and 30mins (b) 300°C and 30mins

When it comes to the liquid and gas yields, it is quite a bit difficult for a conclusive pattern to be held as a function of particle size if analysed as is since they do not present clear trends. However, if the products were categorized as volatized products (gas and liquid) and solid, the trend becomes clearer. Adding up the liquid and gas yields makes it easier to spot a trend for the "volatized" fraction of the products. For instance, at 250°C and 30 mins, as the particle size increases from 0.3 mm to 2.5 mm the "volatized" yield

increases from 13.3% to 14.9%. Only when torrefaction conditions become harsh a change in “volatized” fraction is more significant as seen in Figure 32(b) with 300℃ and 30mins. And notice how at 2.5mm size it is even more intense relating to what was pointed out earlier in the mass balance section (Chapter IV - Part A) concerning the interesting red circle region. Add to that, it can be observed that the medium particle size, i.e. 0.71mm average, doesn’t have a pattern, dipping in value in some cases and peaking in others.

So, it can be said that, for most cases, the trends for solid, liquid, and gas yields are not very clear in behaviour as a function of particle size, with a shy tendencies of decrease in the solid yield and increase in the liquid and gas yields as the particle size increases. However, when OS are subject to intense torrefaction conditions going up to 300℃, yields become more distinct for all sizes but especially affective for the 2.5mm size. This disagreed with Peng et al. (2012), as he found that increased particle size of pine sawdust actually increased its SY [143].

Nevertheless, this behaviour can still be explained by, first of all, sawdust is very different than OS and was torrefied in another setup design. Secondly, it can be said that although smaller particle sizes of the same material tend to have a higher surface area, but because of the setup limitations (using the same feed mass and feed holder) smaller particles tend to pack much closer deeming the increased surface area less important. This in turn essentially reduces the exposed surface area of the feed particles to the hot atmosphere of the reactor, hence reducing devolatilization/vaporization. The particles are highly irregular in shape and random in packing so larger particles cannot pack as closely so more of their surfaces are exposed to the heat which allows for more vaporization to take place.

Looking at the inside of the bed, when larger particles are present the pore diameter increases which decreases the pressure drop, and the opposite happens for smaller particle sizes. This affects the heat diffusion to the inside of the sample bed and the mass diffusion towards the peripheries of the bed. As the particle size decreases, the pressure drop increases making heat diffusion in and volatilization out more difficult. On the other hand, when it comes to interparticular heat and mass transfer, i.e. inside the biomass particle, Peng et al. (2012) argued that these actually influence the torrefaction rate of bigger particles [143]. Comparing the two different torrefaction cases, there is a competition between interparticular and intraparticular heat and mass transfer on one hand, and between temperature and mass gradients and particle packing on the other hand.

Figure 33 shows a model-based representation of the effect of the torrefaction parameters on the SY, LY, and GY. The relation curves from the model show very good agreement with the experimental analysis with the largest slopes attributed to temperature changes, followed by residence time, and minimal for particle size. More details on the model will be discussed in Chapter V.

It is important to shed light on the difference between the solid and liquid yield trends and the gas yield trends from the predictive model. The solid and liquid yields trends are linear while the gas yield trends are non-linear as a function of all the parameters although the yields should all have a similar profile based on the mass balance. But due to measurement errors the relative errors for the solid and liquid yields are smaller than the ones for the gas yields thus to capture the whole range of the gas yield a nonlinear equation is more suitable.

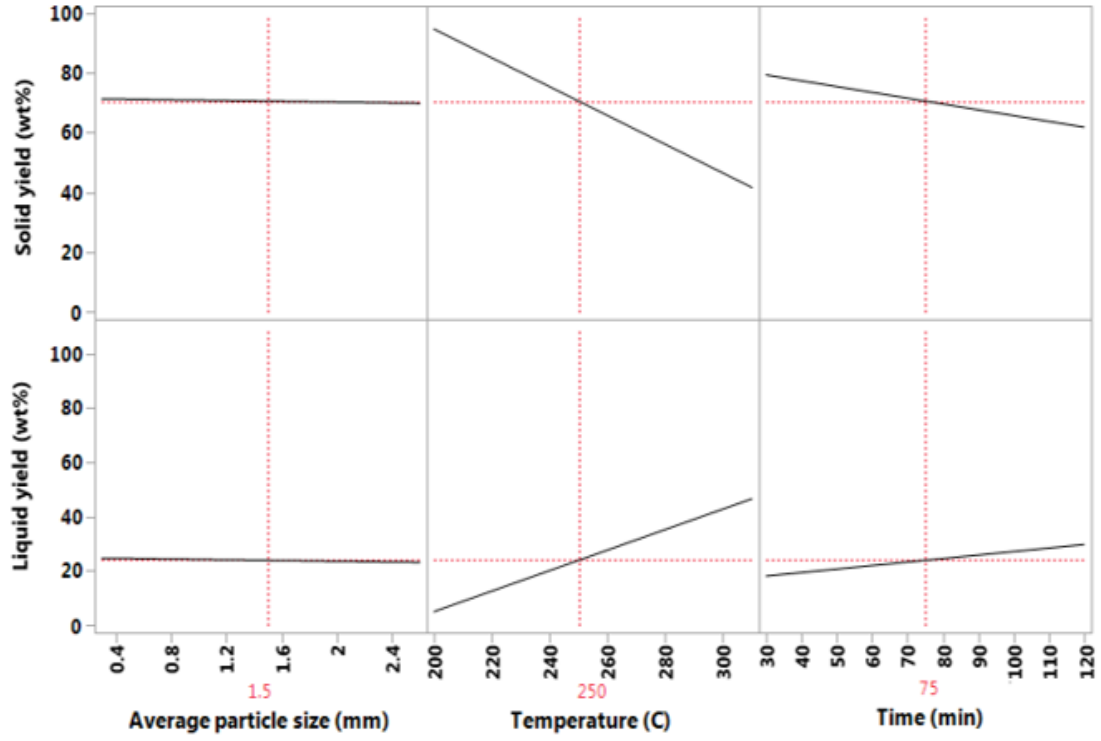

(a)

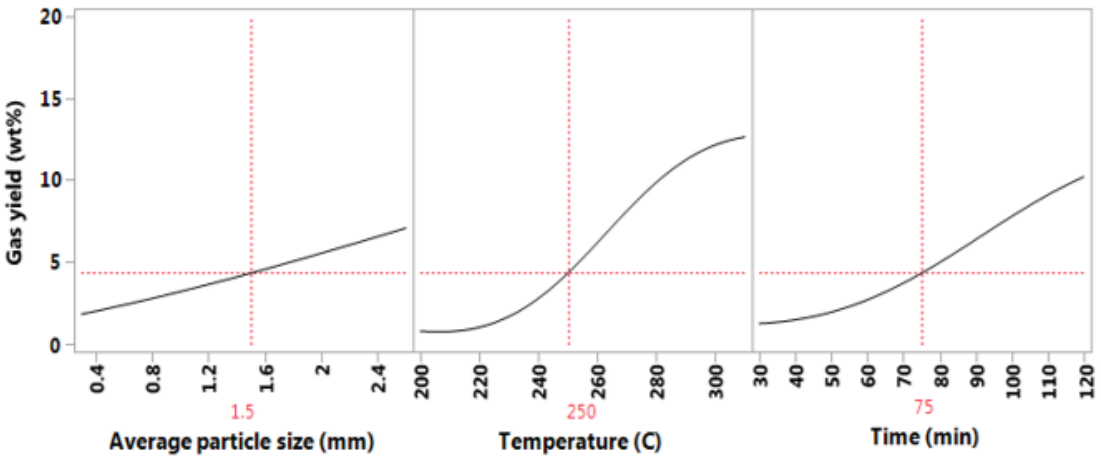

(b)

Figure 33 Model Based Torrefaction Conditions vs. Yields; (a) Solid and Liquid Yields (b) Gas Yield

E. Heat Content and Optimal Conditions

The most important property to tackle in this study is the heat content (calorific value) of the produced OS after torrefaction as, ultimately, the end use of it is for energy. Using bomb calorimetry, the heat content for the samples of the selected torrefaction condition sets was acquired. Table 9 shows different heat content results for the selected samples and, relevantly, the last two columns contain the calculated energy yields and energy densification ratio.

To calculate the solid yield (%), the following equation was used [70]:

$$SY(\%) = \frac{mass\ of\ torrefied\ OS}{mass\ of\ raw\ OS} \times 100$$

To calculate the energy yield (%), the following equation was used [45]:

$$EY(\%) = \frac{heat\ Content\ of\ torrefied\ OS}{heat\ content\ of\ raw\ OS} \times 100$$

To calculate the energy densification ratio (%), the following equation was used [144]:

$$EDR\ (\%) = \frac{SY(\%) \times EY(\%)}{100}$$

Table 9 Heat Content, Energy Yields, and EDR for Selected Samples

Avg. particle size (mm)	Temp. (^{o}C)	Res. time (min)	Solid yield (wt%)	Heat Content (kJ/g)	Raw OS Heat Content (kJ/g)	Energy Yield (%)	EDR (%)
2.5	200	30	87.9	18.697	18.528	100.9	88.70176
2.5	250	30	85.1	19.113	18.528	103.2	87.78693
2.5	250	120	62.9	21.2	18.528	114.42	71.97107
2.5	270	30	82.3	20.266	18.528	109.4	90.02007
2.5	270	45	60.5	23.81	18.528	128.5	77.74746
2.5	270	60	47.66	22.426	18.528	121.03	57.68691
2.5	270	120	48.54	23.6448	18.528	127.6	61.94509
2.5	300	30	47.2	22.965	18.528	123.9	58.50324
0.71	200	30	89.5	18.538	18.528		
0.71	250	30	88.7	18.761	18.528		
0.71	270	30	84.19	19.131	18.528		
0.71	300	30	74.1	20.892	18.528		
0.3	200	30	87.7	18.653	18.528		
0.3	250	30	86.7	18.9	18.528		
0.3	270	30	81.83	19.68	18.528		
0.3	300	30	70.3	21.87	18.528		

According to the heat content values in Table 9, the highest were recorded by the largest particle size, 2.5mm, with 18.7kJ/g, 19.1kJ/g, 20.3kJ/g, and 23kJ/g for 200 °C, 250 °C, 270 °C, and 300 °C, all for 30mins, respectively. In comparison, the 0.71mm size recorded 18.5 kJ/g, 18.8 kJ/g, 19.1 kJ/g, and 20.9 kJ/g, and the 0.3mm size recorded 18.7 kJ/g, 18.9 kJ/g, 19.7 kJ/g, and 21.9 kJ/g for 200 °C, 250 °C, 270 °C, and 300 °C, respectively. This analysis is aided by the graph in Figure 34 in which the curve of the 2.5mm particle size is shifted up the heat content axis.

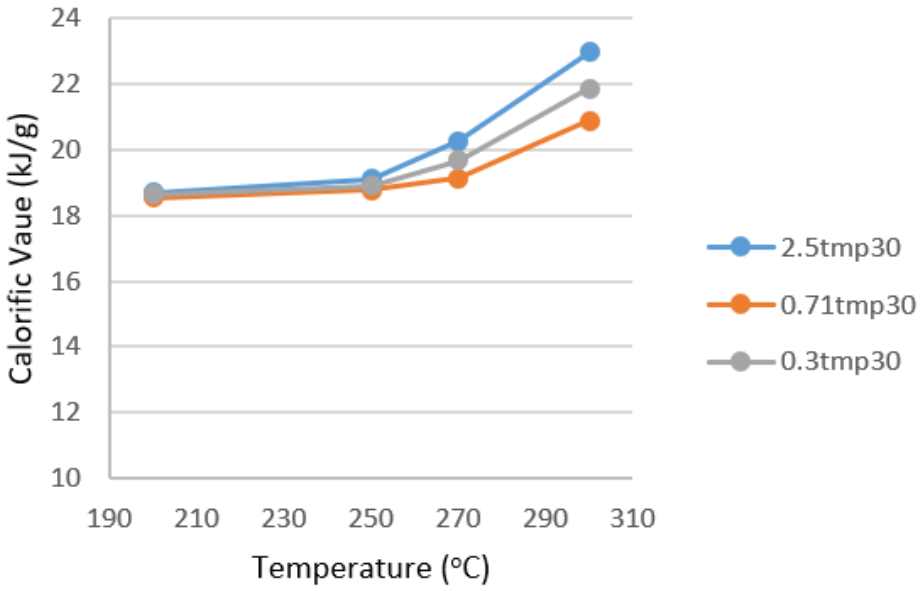

Figure 34 Heat Content as a Function of Temperature for Different Particle Sizes

The graph in Figure 35 also illustrates this change in heat content as a function of particle size for the different assigned temperatures. As the temperature increases for all particle sizes, the heat content increases with a big jump when the temperature hits 300 ^{o}C, and the biggest spike in heat content occurring with the 2.5mm particle size. Notice from the graph that for the 2.5mm particle size increasing the temperature from 200 ^{o}C to 300 ^{o}C, the heat content increase from 18.7kJ/g to almost 23kJ/g. On the other hand, for the 0.71mm and 0.3mm sizes, the increase in heat content recorded lower values of 18.5kJ/g to 20.9kJ/g and 18.6kJ/g to 21.8kJ/g, respectively, with increase in temperature from 200 ^{o}C to 300 ^{o}C.

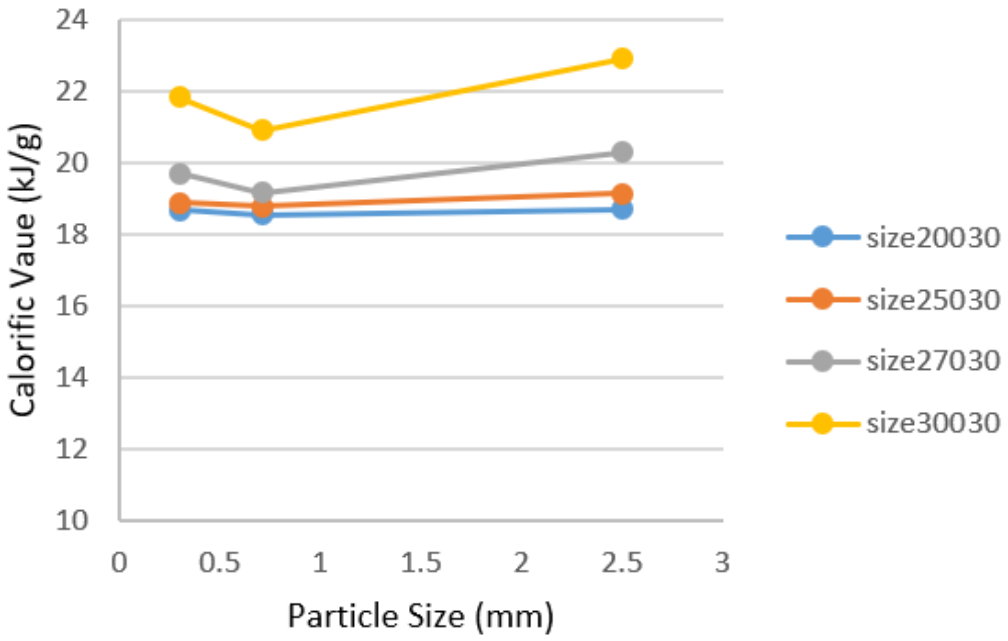

Figure 35 Heat Content as a Function of Particle Size for Different Temperatures

Checking the effect of residence time for the 2.5mm size at 270 °C, shows that the heat content exhibits an increasing trend as residence time increases as depicted in the graph of Figure 36. The graph also shows the highest values for heat content to be when the RT was 45mins and 120mins with 23.8kJ/g and 23.6 kJ/g, respectively. This is interesting as the same heat content was gained with almost 1/3 of the residence time put in.

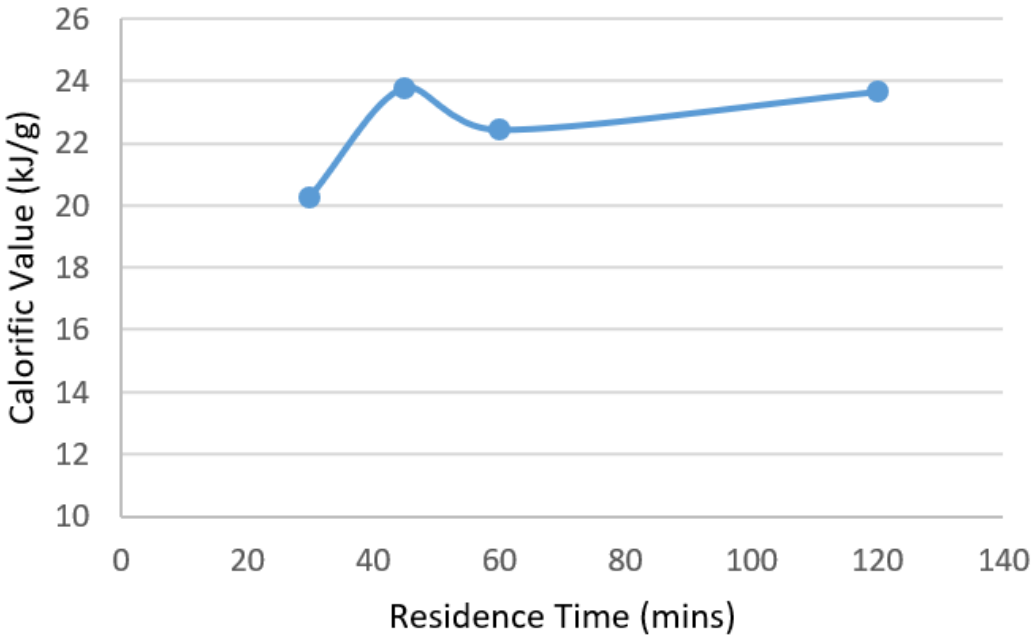

Figure 36 Heat Content as a Function of Residence Time for 2.5mm at 270 °C

Based on previous analyses so far, 2.5mm is the favourable size option and still the investigation of its 270°C temperature condition sets with several residence times is proving to be fertile. Just by looking at the heat content, one can well say that the best is 270°C for 45mins among its range. But it doesn't settle here as this conclusion needs more solidification since there are several factors at play. The energy yield column of Table 9

for 2.5mm at 270ºC as a function of residence time is plotted in Figure 37. The trend is obviously increasing with increasing residence time with again a noticeable peak at 45mins recording 128.5%. the second highest value of energy yield was 127.6% recorded at 120mins. This behaviour is like that of Figure 36 as the energy yield directly resemble the heat content and its change with residence time.

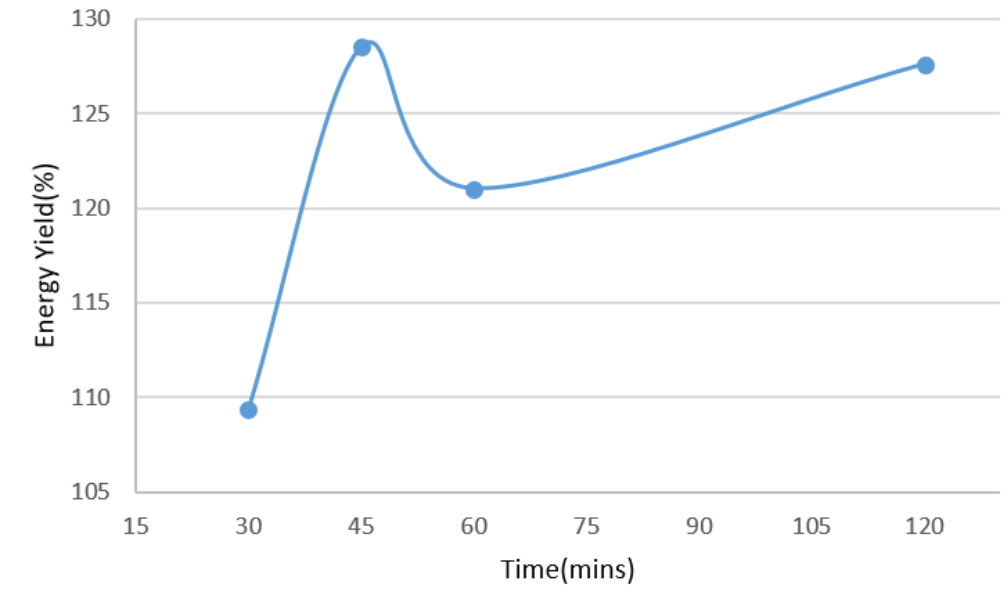

c

Figure 37 Energy Yield as a Function of Residence Time for 2.5mm at 270C

Although this can be conclusive as to which residence time is favourable for highest heat content and energy yield, but the fact that there is a trade-off relationship between those two and the SY can't be ignored. So, it is not limited to which condition sets the highest score in value because something is being lost along the way; sample mass.

Now, looking at the EDR in the last column of Table 9, another trend seems to impose itself. EDR serves as a simple numerical relation to evaluate how optimal is the trade-off between SY and EY for the different residence times and is plotted in Figure 38.

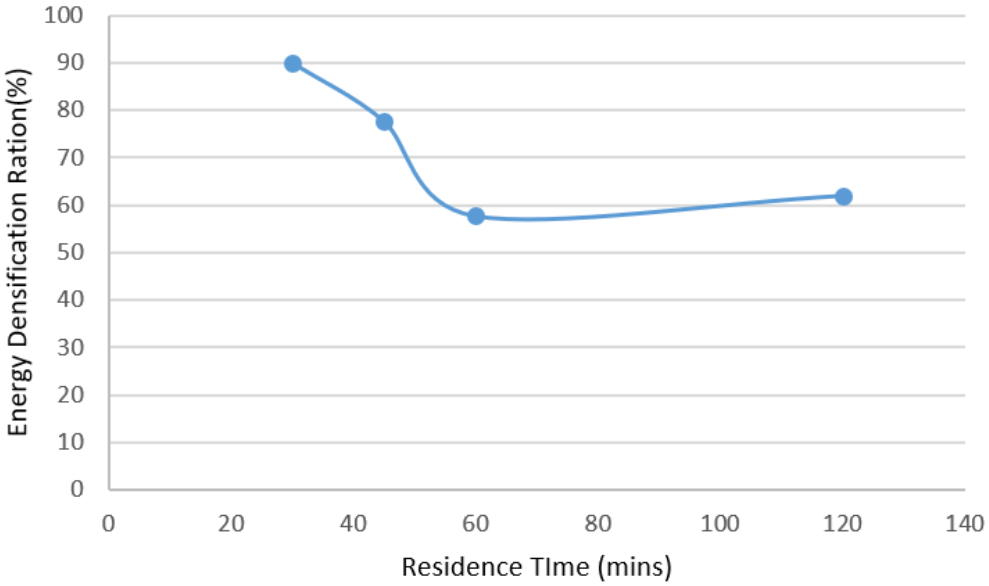

Figure 38 Energy Densification Ratio as a Function of Residence Time for 2.5mm at 270C

As the residence time increases, the EDR for 2.5mm 270^{o}C shows a decreasing trend. The lowest point was recorded for 60mins while the highest, contrary to what seemed optimal, was for 30mins and not 45mins. This depicts that the most efficient trade-off of mass loss to energy gain is for torrefied sample at 270^{o}C for 30mins.

Another numerical analysis to deal with this trade-off was used to identify the optimal residence time by evaluating the loss and gain percentages of SY and EY and

their ratio, GLR. The loss is simply the percentage of mass loss during the torrefaction process and the gain is the percentage of energy gained by this sample after this loss. The gain, loss, and GLR were calculated using the following formulas.

$$Loss\ (\%) = 100 - SY(\%)$$

$$Gain(\%) = EY(\%) - 100$$

$$GLR(\%) = \frac{Gain(\%)}{Loss(\%)} \times 100$$

The values are shown in the last column of Table 10 with the highest GLR of 72.2% recorded by the 45mins residence time, going back to it as the optimal, unlike what was indicated by the EDR.

Table 10 Heat Content, Energy Yields, EDR, and GLR for Selected Samples

Avg. particle size (mm)	Temp. (ºC)	Res. time (min)	Solid yield (wt%)	Heat Content (kJ/g)	Raw OS Heat Content (kJ/g)	Energy Yield (%)	EDR (%)	GLR (%)
2.5	270	30	82.3	20.266	18.528	109.4	90.02007	52.9
2.5	270	45	60.5	23.81	18.528	128.5	77.74746	72.2
2.5	270	60	47.66	22.426	18.528	121.03	57.68691	40.2
2.5	270	120	48.54	23.6448	18.528	127.6	61.94509	53.6

Figure 39 shows the GLR plotted against residence time with clear peak at 45mins.

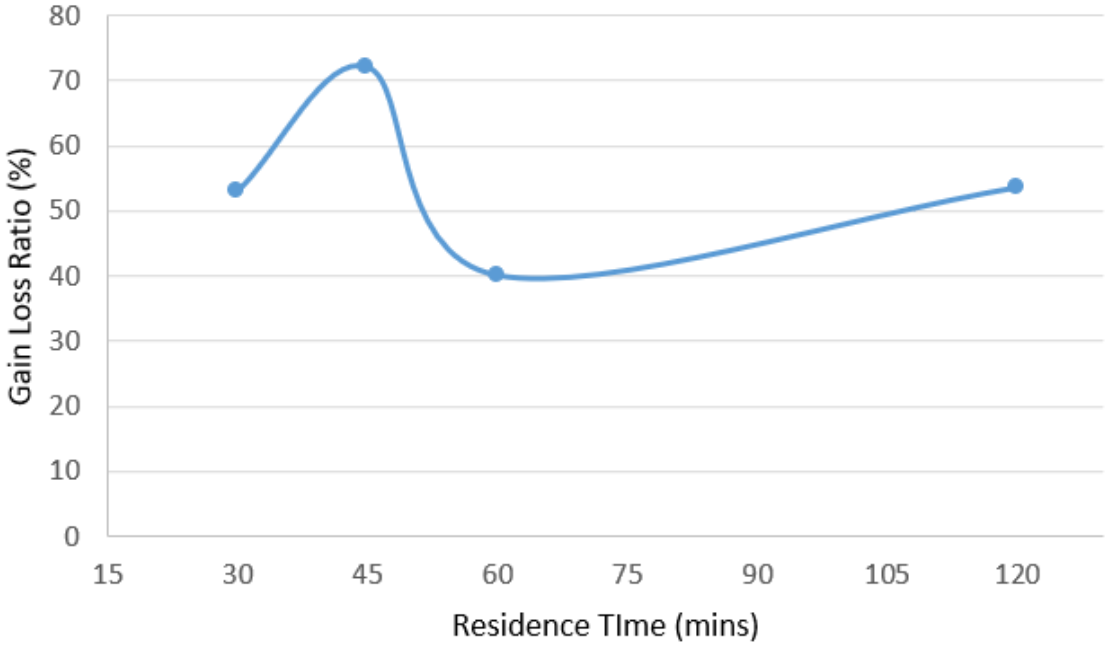

Figure 39 Gain Loss Ratio as a Function of Residence Time for 2.5mm at 270C

Nevertheless, it should not be forgotten that this analysis is based on discrete values caused by the discretized conditions sets of parameters, focusing on time here. Only selected times were tried and studied with relatively "huge" gaps in between ruling out a great deal of possible outcomes, whether peaks or dips.

To solve this issue further and check what is the optimal condition set, a proposed method by Lee and Lee (2014) was used. It is conducted by plotting the normalized heat content and SY against T and RT, whereby the intersection of the curves labels the

optimal [70, 145]. This method does a better job at including ruled out possibilities as it gives a sense of continuity to outcomes of different condition sets.

Normalization can be conducted using the following equation [70]:

$$NormalizedValue = \frac{x_i}{\sqrt{\sum_{i=1}^{i=n} \frac{x_i^2}{(n-1)}}}$$

With n being the number of parameter points and x_i the parameter value.

The sort of plots was performed for the 2.5mm size as a function of temperature as shown in Figure 40. Now, by observing the intersection of the heat content curve with the SY curves in the graph, a simple projection can be performed on the temperature axis to find the optimal temperature. The optimal temperature was proximal to 268^{o}C.

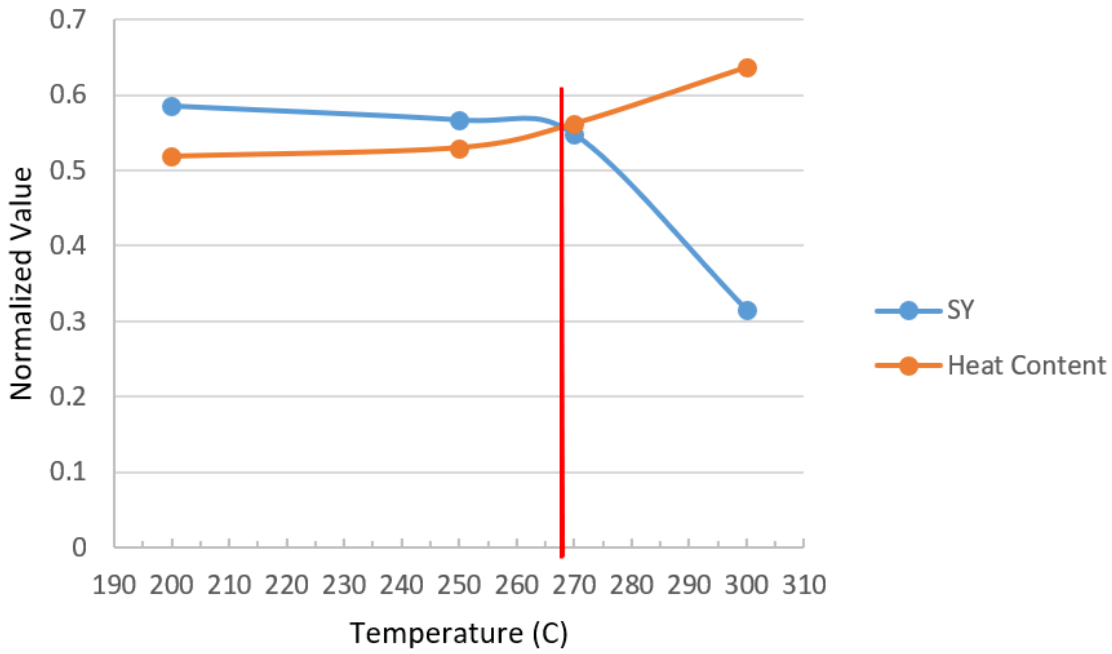

Figure 40 Normalized Heat Content and Solid Yield vs. Temperature for 2.5mm Size

The same can be performed to determine the optimal time for this temperature. Figure 41 shows the heat content curve and the SY curves plotted against residence time for 270°C. Projecting the intersection to the time axis gives an optimal residence time of approximately 40mins which is rather between 30mins and 45mins, neither nor, but not included in the condition sets.

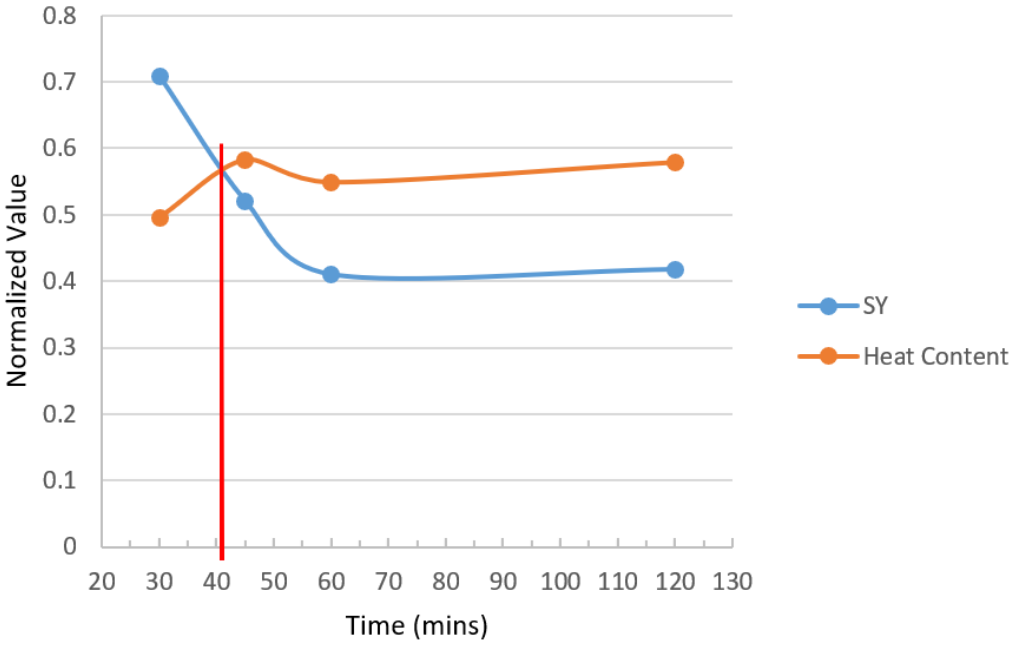

Figure 41 Normalized Heat Content and Solid Yield vs. Time for 2.5mm and 270 °C

The optimal torrefaction temperature (268°C) and residence time (40mins) found were very close to the used conditions of 270°C and 45mins, and in proximate agreement with the optimum conditions of 280°C and 30mins reported by Cellatuglo et al. (2015) but for solid olive mill residue [123]. Felfli et al. (2005) recommended torrefaction temperatures between 250-270°C and long enough RT [146]. Furthermore, it was reported that torrefaction temperatures above 300°C are not advisable as the process enters pyrolysis limits, allowing substantial devolatilization, hence high LY and low SY [122]; not what is intended. The range of torrefaction RT of 10-60mins was aforementioned to be the most effective [122, 136] also backs up our optimal RT finding here.

Other similar-application fuels were tested for heat content and compared to the selected optimal as represented by Figure 42. For this comparison wood and coals from three sources (local, Irish, and Sudanese) were used along with the raw OS (Pan). The

treated OS at the optimal torrefaction conditions with 23.8kJ/g heat content almost equated one of the coal sources, specifically the Irish which recorded 24kJ/g in heat content. It was higher than wood and local coal, but lower than Sudanese with heat contents of 18.7kJ/g, 21.3kJ/g, and 29.2kJ/g, respectively.

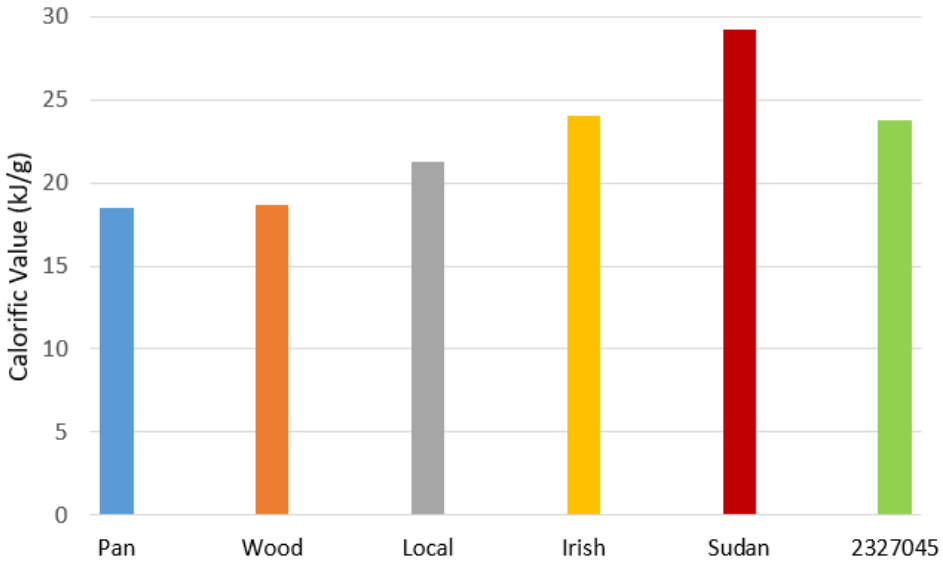

Figure 42 Where Does our Best Option Fit in?

F. Mixing with Coal

Torrefied OS can either be used for whatever burning application either alone or with other fuels mainly coal. To see whether there is a synergetic effect in terms of heat content of the latter, torrefied OS in this study was mixed with coal and tested. Figure 43 shows a graphical presentation of heat content against OS fraction in OS-coal mixtures; 25%, 50%, 75%. The plot shows a decrease in the heat content as the OS fraction mixed with SC increases, particularly from 27kJ/g with 25% OS fraction to 24.5kJ/g with 75% OS fraction. When mixed with IC, which is calorifically almost the same as the OS mixed in, the heat content change was negligible as OS fraction increased. On the other hand, when OS was mixed with the LC, the heat content increased from 21.5kJ/g to 22.62kJ/g as the OS fraction increased from 25% to 75%, respectively. The behaviour of the mixture was similar in all three cases whereby the heat content was dictated by the influence of each component fraction, i.e. weighted average, without any signs of synergy. Nevertheless, it is still important to use OS-coal mixtures when firing as it reduces coal consumption, dependence, and emissions.

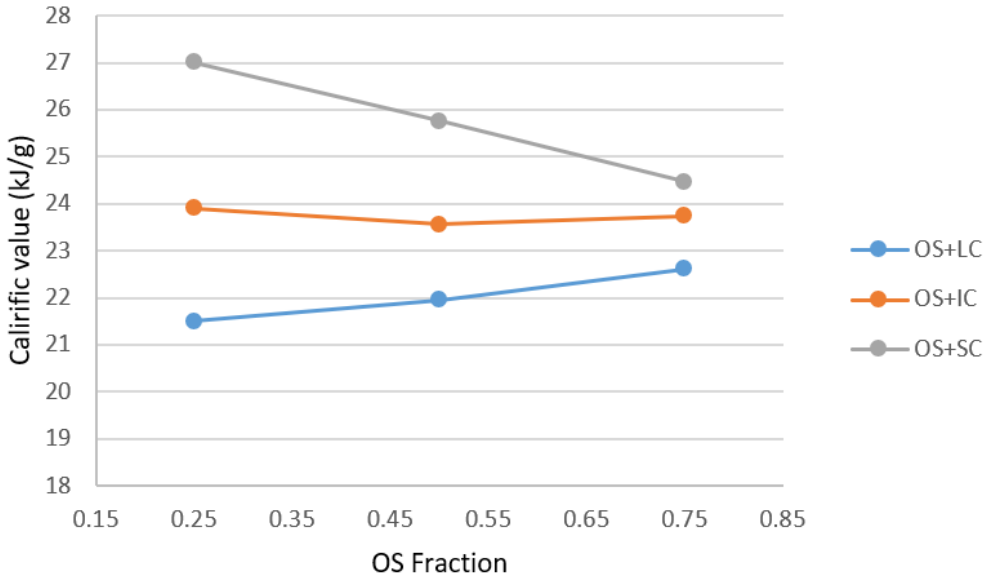

Figure 43 Optimal Mixed with Several Coal Sources

G. Compositional Analysis

Proximate and ultimate was performed to see how the composition of OS changes under different torrefaction conditions. The proximate analysis included the moisture content (MC), volatile matter (VM), ash, and fixed carbon (FC) with the results presented in Table 11.

Table 11 Proximate Analysis

Sample ID	Proximate Analysis			
	Moisture (%)	**Volatiles (%)**	**Ash (%)**	**Fixed Carbon (%)**
Raw	15.30	77.00	0.79	6.91
2320030	5.90	77.00	0.48	16.62
2325030	1.90	76.00	0.42	21.68
23250120	1.60	70.00	0.60	27.80
2327030	2.45	74.00	0.50	23.05
2327045	1.30	57.00	1.30	40.40
2327060	1.30	61.00	0.76	36.94
23270120	1.00	56.00	0.73	42.27
2330030	1.40	60.00	0.69	37.91
42520030	4.10	76.50	0.49	18.91
42525030	3.65	75.00	0.68	20.67
42527030	2.10	74.00	0.51	23.39
42530030	1.58	71.80	0.25	26.37
1820030	4.10	77.00	0.61	18.29
1825030	1.59	75.30	1.00	22.11
1827030	3.45	73.10	1.35	22.10
1830030	2.15	58.10	1.73	38.02

Compared to the raw OS, all torrefaction conditions succeeded in lowering the MC and raising the FC, significantly. For instance, focusing here on the 2.5mm particle size, the mildest torrefaction temperature and time of 200^{o}C and 30mins lowered the MC from 15.3% to 5.9% and raised the FC from 6.91% to 16.62%. When it comes for the VM, mild torrefaction conditions didn't have that huge of an impact, but the VM decrease was very noticeable as the temperature and residence time increased. Not much of a change was seen for the ash portion, and there isn't a functional pattern with torrefaction conditions. This might be attributed to the fact that the studied temperature and residence time are relatively not harsh enough to have an effect on the ash content of the biomass [91, 125, 147].

As for the ultimate analysis, C, H, O, N, S, and Cl contents were determined. As seen in Table 12, it is clear that for as torrefaction temperature and residence time increase, the C% increases while the H% and O% decrease, with the latter to a greater extent. For example, looking at the 2.5mm size, the change in C going from raw OS to torrefied at 300^{o}C and 30mins, was a increase by 33.5% while that for H and O was a decrease by 12.1% and 31.4%, respectively. It can be said here that oxygen and some oxygen containing compounds are the most volatile, while carbon and carbon containing compounds the least. The other elements, N, S, and Cl don't show any significant change over the changes in torrefaction conditions, and their content portion, in the first place, is quite low.

Table 12 Ultimate Analysis

Sample ID	Ultimate Analysis					
	C(wt.%)	**H(wt.%)**	**O(wt.%)**	**N(wt.%)**	**S(wt.%)**	**Cl(wt.%)**
Raw	46.00	5.80	47.18	0.20	0.03	0.010
2320030	47.90	5.70	45.81	0.10	0.01	0.019
2325030	51.00	5.70	42.76	0.10	0.02	0.024
23250120	51.30	5.60	40.88	1.60	0.02	0.028
2327030	51.85	5.70	41.83	0.10	0.02	0.027
2327045	64.50	5.50	28.38	0.30	0.02	0.030
2327060	61.20	5.30	32.62	0.10	0.02	0.030
23270120	64.86	5.30	28.29	0.80	0.02	0.025
2330030	61.40	5.10	32.39	0.40	0.02	0.024
42520030	48.80	5.90	43.89	0.90	0.02	0.023
42525030	50.30	6.00	41.50	1.50	0.02	0.044
42527030	52.00	6.00	41.07	0.40	0.02	0.027
42530030	63.50	5.55	30.08	0.60	0.02	0.026
1820030	48.20	5.80	45.27	0.10	0.02	0.027
1825030	49.80	5.70	41.58	1.90	0.02	0.035
1827030	51.87	5.80	39.15	1.80	0.03	0.042
1830030	62.90	5.40	29.24	0.70	0.03	0.025

A graphical method was established by chemical engineer and scientist Dirk Willem van Krevelen, incorporating a plot of H/C ratio against O/C ratio, in the study of coal structure and reactions in 1950 [148, 149]. Since this method helps in gaining an insight on the processes taking place during coalification, it is relevant and helpful to be used with torrefaction (mild coalification of biomass). A Van Krevelen plot for this study is shown in Figure 44 for all the torrefaction condition points including coal for comparison.

Two noticeable clusters are present in the diagram, the first one in the lower area of O/C≈1 and H/C≈0.35, and the second in the higher area of O/C≈1.4 and H/C≈0.65. Mainly the samples of the higher area are, for all sizes, those of 30mins and up to 270^{o}C with the exception of 250^{o}C at 120mins. The samples whereby temperatures hit 300^{o}C for all sizes were located in the, "more coal", lower region on the Van Krevelen diagram, with the addition to the samples of 270^{o}C at 45mins, 60mins, and 120mins. More severe torrefaction conditions of temperature and time drives the OS to a more "coal like" nature with lower H and O content and higher C content.

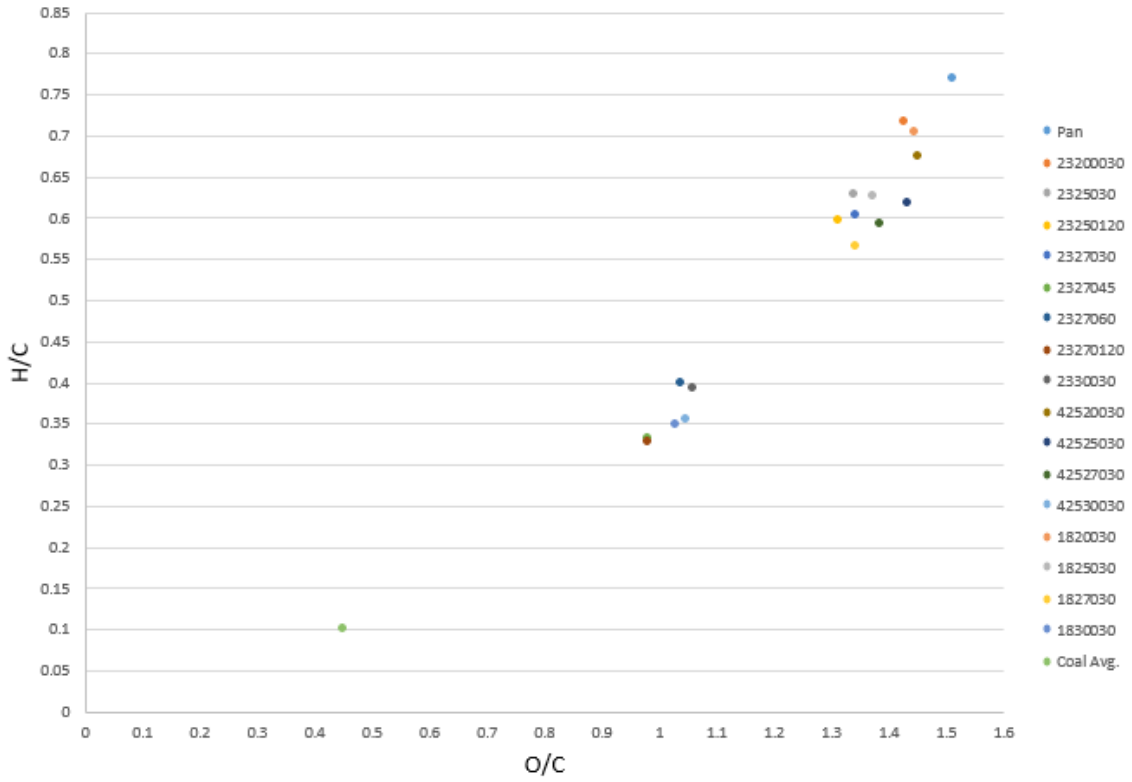

Figure 44 Van Krevelen Diagram for all Torrefaction Condition Points

Another representation of the Van Krevelen diagram in terms of the effect of particle size, temperature, and time is shown in Figure 45. The clusters are the same as the original, but here categorized based on particle size for clarity. Following the trend lines, as the particle size increases an upward shift in points occurs which is an increase in H content. The 2.5mm particle size points has the most profound shift, whereas for 0.71mm and 0.3mm it's not that definite, but what is definite is that both of their points are lower than those of the 2.5mm on the H/C scale. Now, going from the higher cluster up on the H/C and the O/C scale towards lower cluster, goes along the increase in torrefaction temperature and time.

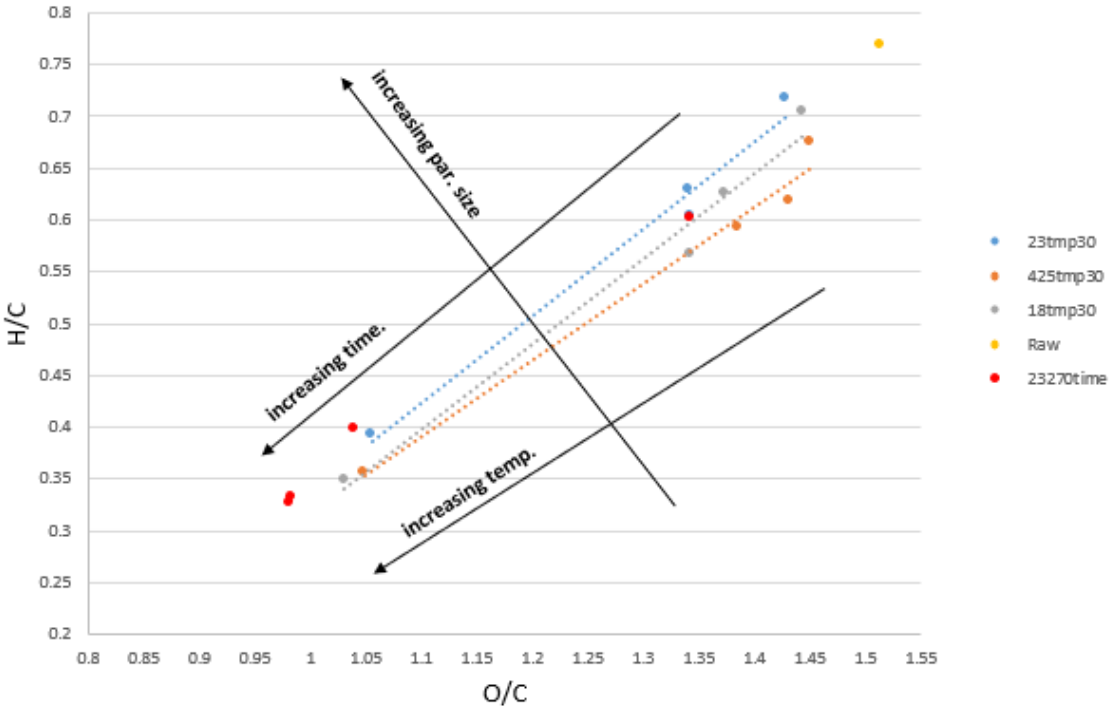

Figure 45 Representation of the Van Krevelen

H. Analysis of the Oxidative TGA Curves

The curves presented in this section are only those for the 2.5mm particle size to prevent excessive graph listing; the TGA curves for 0.71mm and 0.3mm can be found in backup. Nevertheless, it can be seen from Figure 46 and Figure 47, for different temperatures at 30mins, that there are three mass changes segments, the first one resembles moisture loss, the middle resembles generally volatile matter loss, and the last resembles char loss.

As the torrefaction temperature increases from 200^{o}C to 300^{o}C, the TGA curves show decrease in moisture loss and volatile matter loss indicating that more of each was being lost during torrefaction with increase in temperature. For example, by observing Figure 46(a) and Figure 47(b), the moisture and volatile matter loss decreased from 3% to 1.7% and from 53.4% to 31.2%, respectively. Meanwhile, the char loss was increasing in the TGA curves of the samples as the torrefaction temperature was increasing. This increased from a loss of 37.6% to 60.9%. This indicates that during torrefaction, the increase in temperature increases carbonization of the OS.

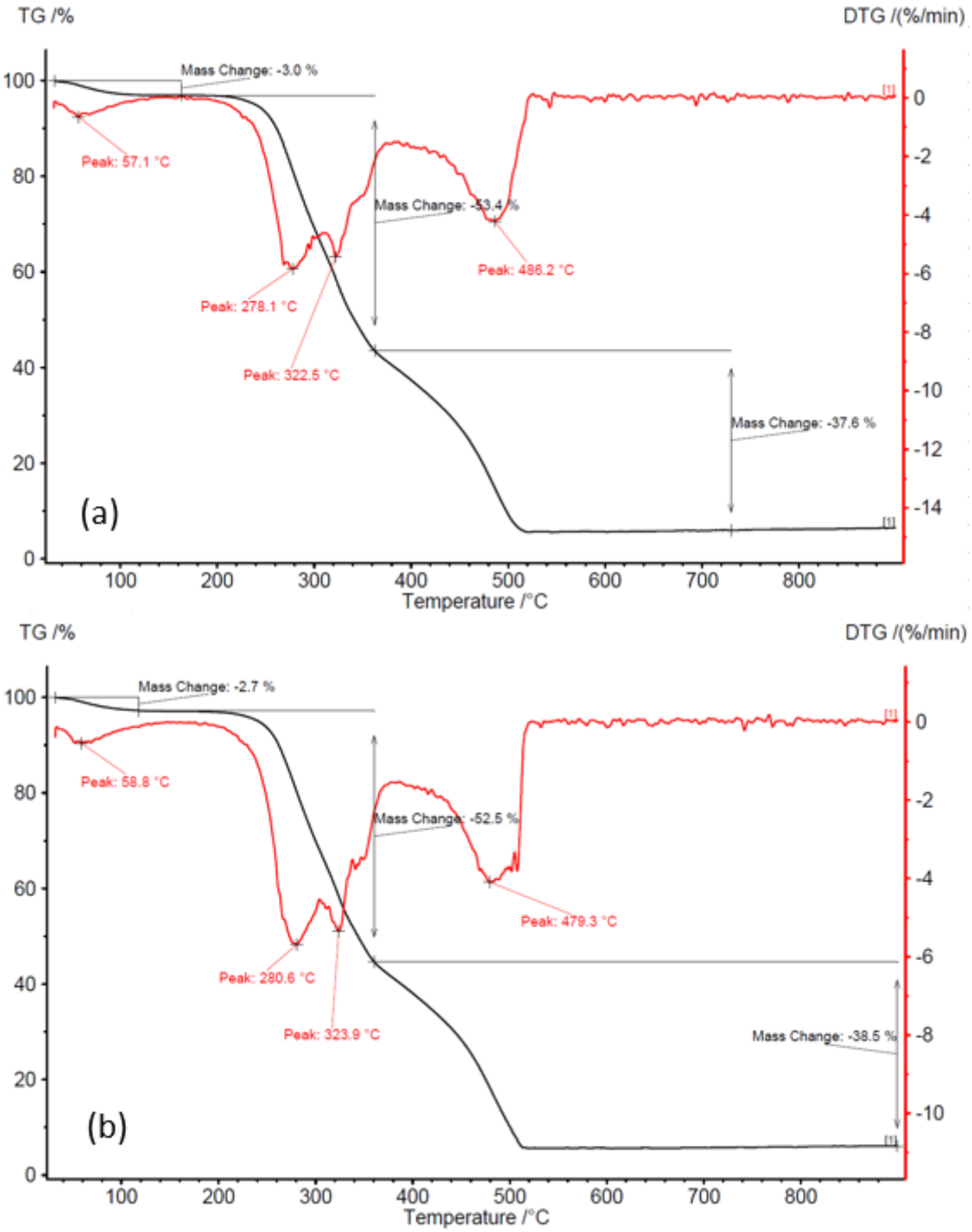

Figure 46 TGA (a)2.5mm for 200°C at 30mins (b)2.5mm for 250°C at 30mins

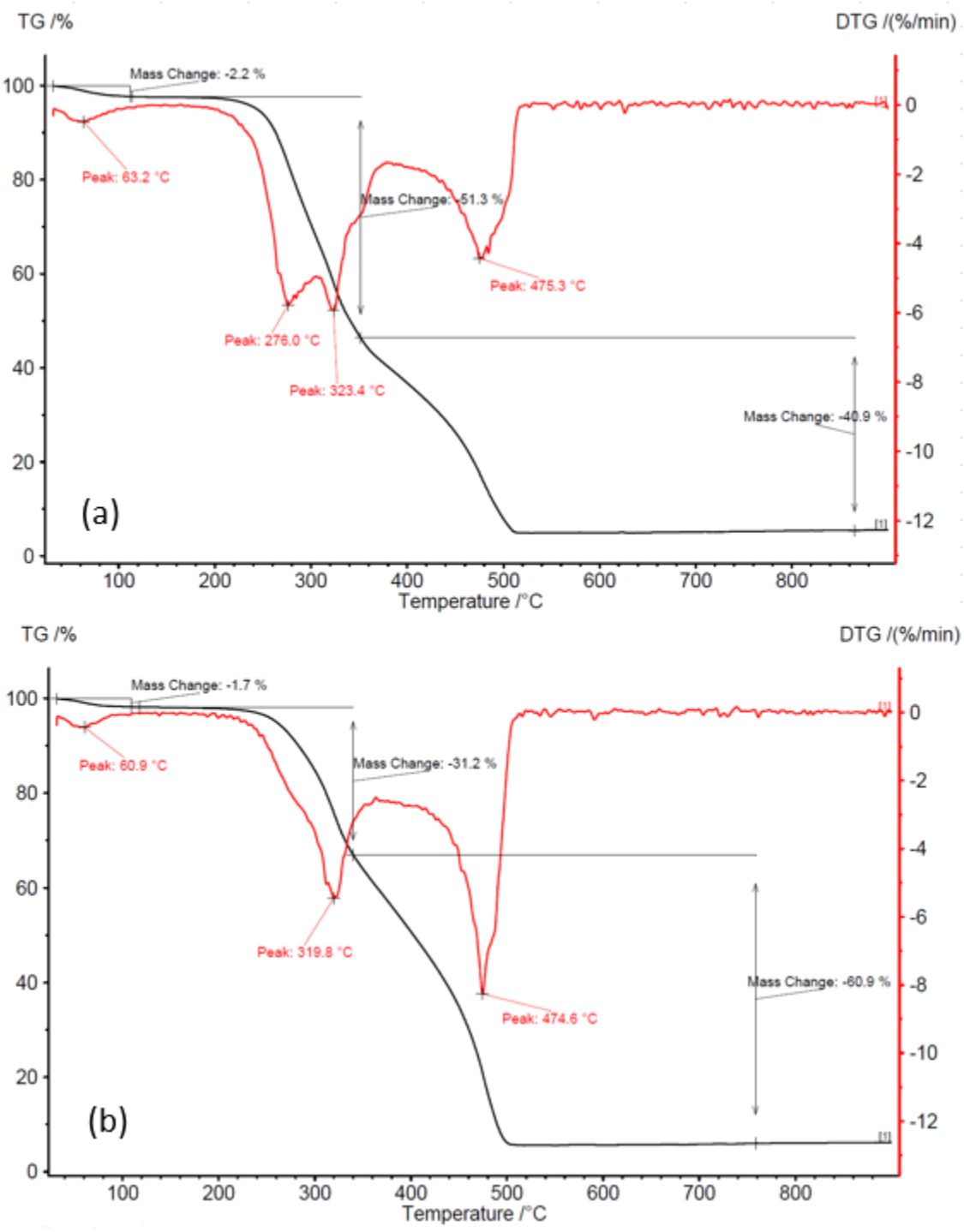

Figure 47 TGA (a)2.5mm for 270°C at 30mins (b)2.5mm for 300°C at 30mins

Figure 48 and Figure 49 show the TGA curves for samples at 270^{o}C and different residence times. The effect was similar to that of temperature in which here, from Figure 48(a) to Figure 49(b), the moisture loss and volatile matter loss decreased from 2.2% and 51.3% to 1.8% and 22.6%, respectively. The char loss increased from 40.9% to 68.4%. Here again, as the residence time of the torrefaction process increased, more moisture and volatile matter was being lost, and char was becoming more carbon-rich.

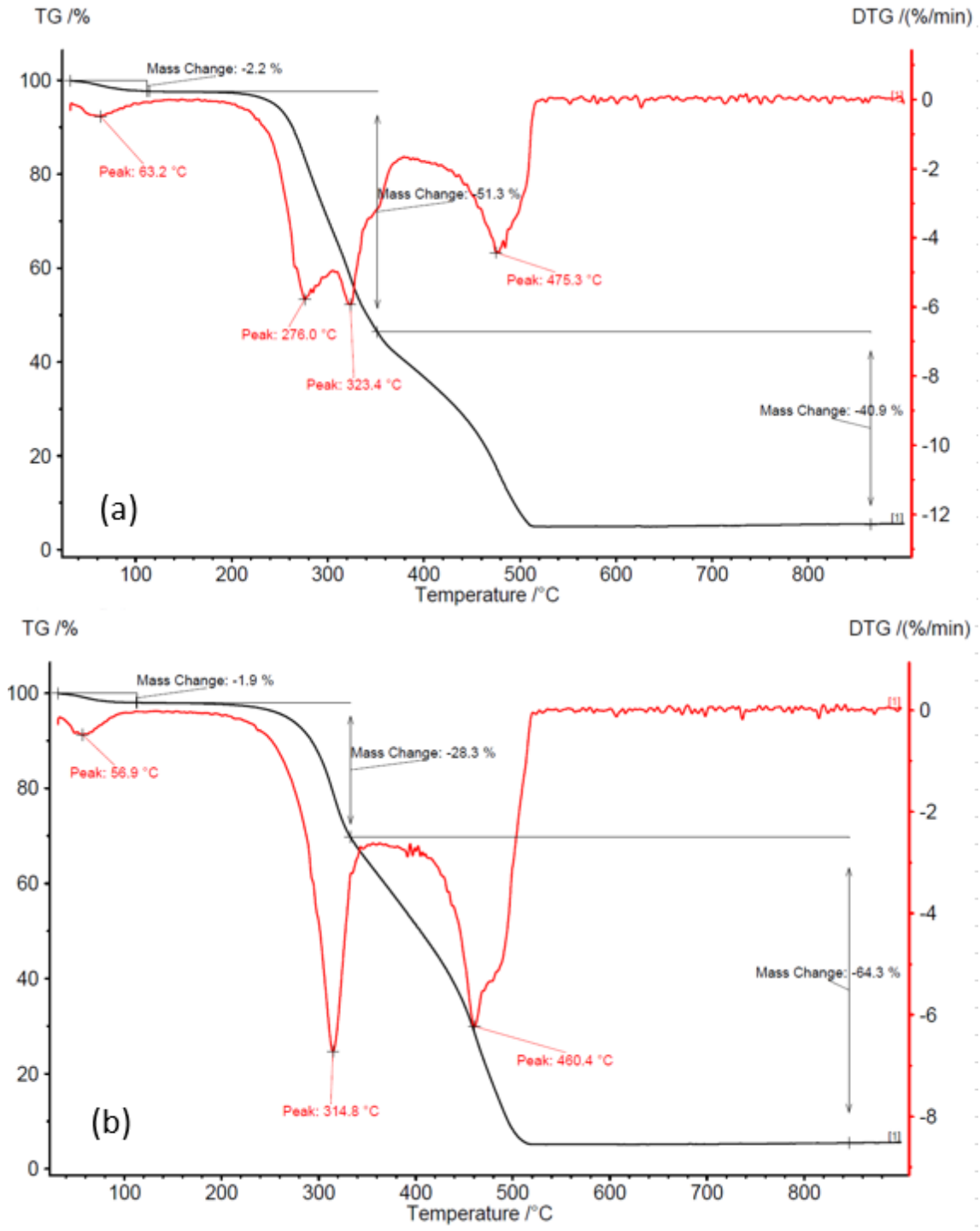

Figure 48 TGA (a)2.5mm for 270°C at 30mins (b)2.5mm for 270°C at 45mins

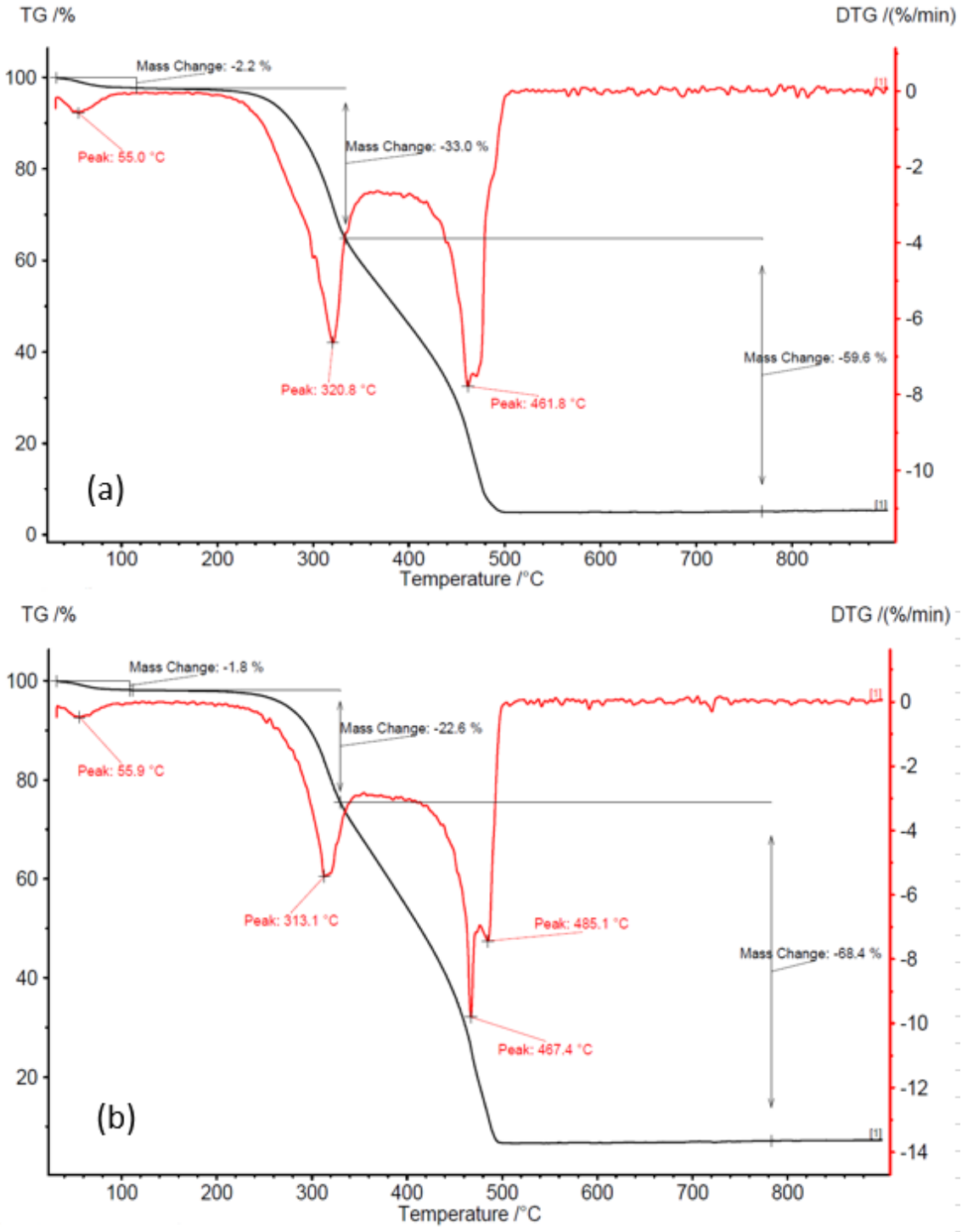

Figure 49 TGA (a)2.5mm for 270ºC at 60mins (b)2.5mm for 270ºC at 120mins

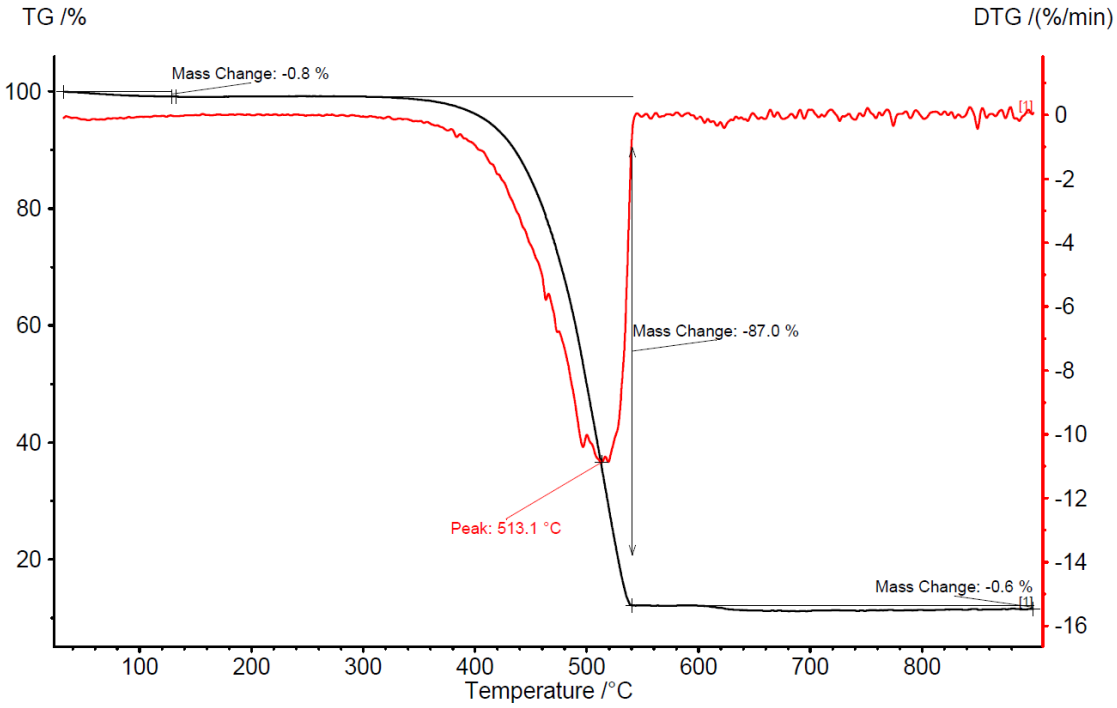

Figure 50 TGA of Sudan Coal

I. Surface and Gaseous FTIR Analysis

Surface FTIR helps in better identifying what functional groups, hence compounds, lost during torrefaction. Again here, the presented FTIR spectrums are for 25mm particle size at 30mins, with different temperatures, and another set of spectrums for 2.5mm size at 270^{o}C for different residence times. It can be observed from Figure 51 and Figure 52that as the temperature increases, the intensity at 1200-1300 cm^{-1} decreases, especially at 300^{o}C. This indicates deformation of -OH, C-O, and CH-, probably referring to water, cellulose, hemicellulose, and some lignin [150-154]. The range of 1300-1450 cm^{-1}, also shows decrease in intensity as the temperature increases, especially at 300^{o}C. This indicates mostly CH- groups from cellulose, hemicellulose, and some lignin degradation [150-156]. Going to the 1500-1740 cm^{-1} range, two distinct peaks at approximately 1600 cm^{-1} and 1700 cm^{-1} decrease with the increase in temperature. The 1600 cm^{-1} peak indicates O-H and C-O referring to adsorbed water and conjugated cellulose and lignin, while the 1700 cm^{-1} peak mostly indicates C=O groups referring to esters, ketones, and aldehydes of hemicellulose, and this peak disappears at 300^{o}C [150-154, 156, 157]. Finally, in the 3200-3400 cm^{-1} range the intensity decreases as the temperature reaches 300^{o}C, indicating the breakage of hydrogen bonds probably water or hydroxyl compounds [151, 152].

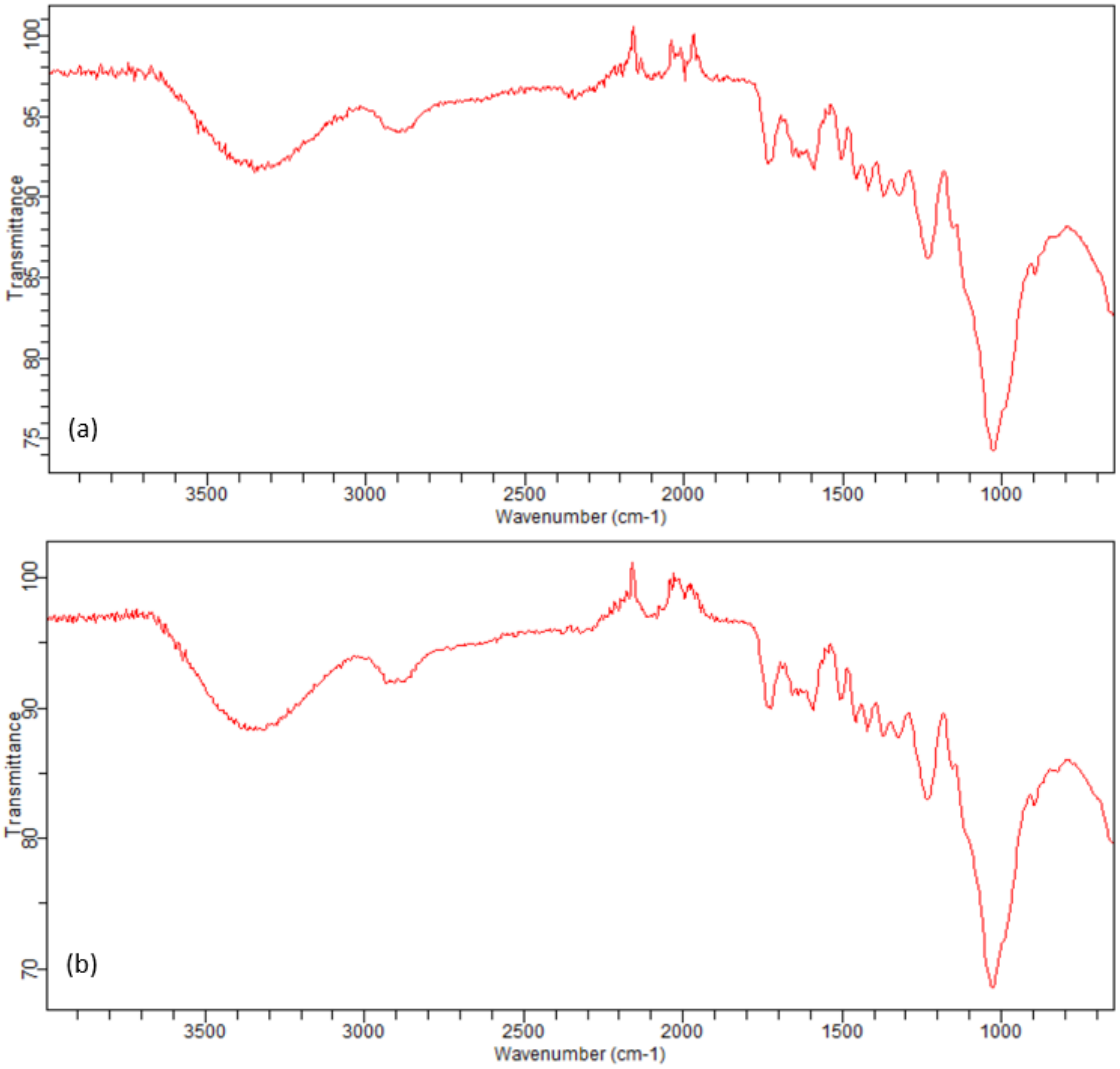

Figure 51 FTIR (a)2.5mm for 200oC at 30mins (b)2.5mm for 250oC at 30mins

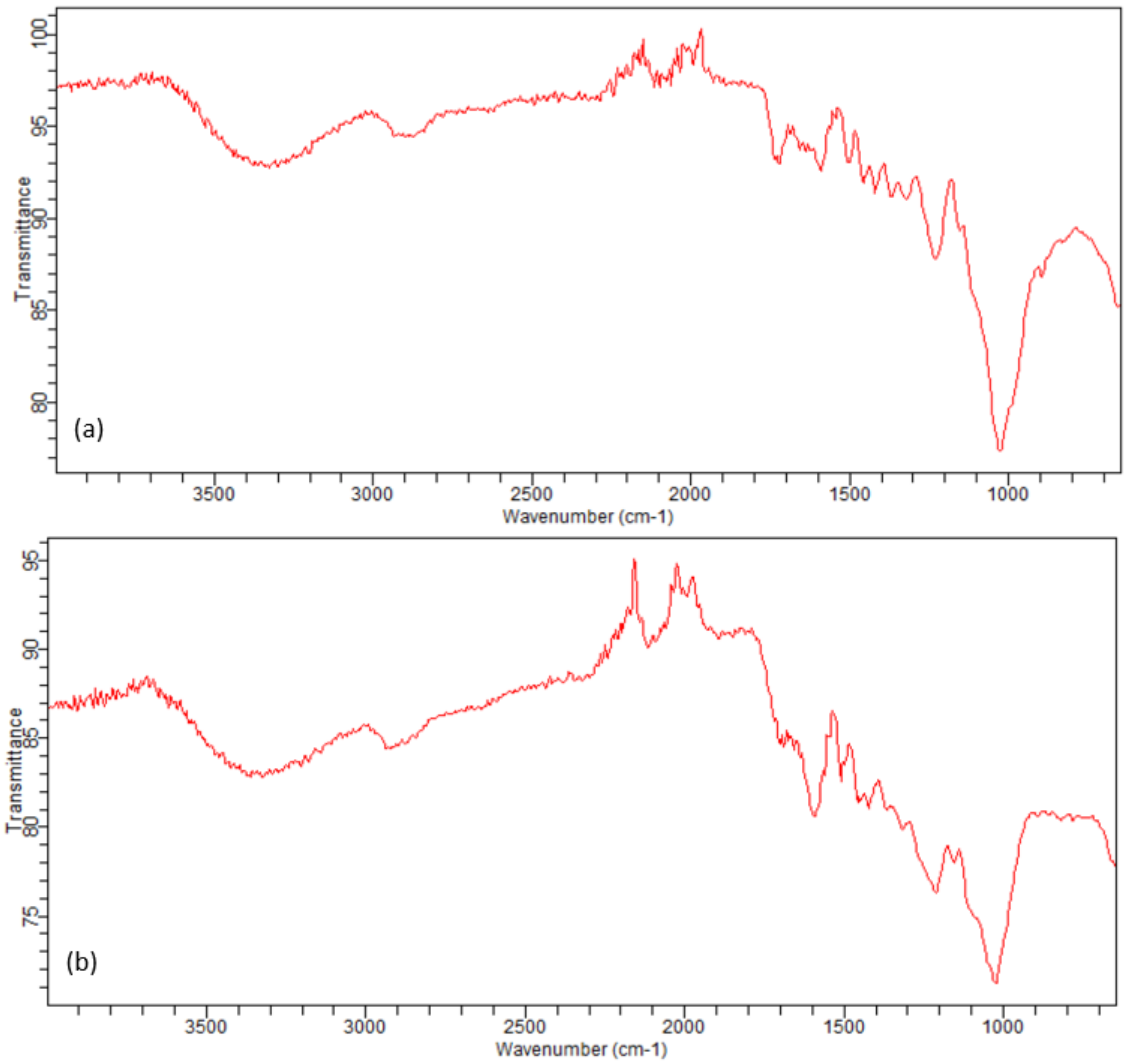

Figure 52 FTIR (a)2.5mm for 270oC at 30mins (b)2.5mm for 300oC at 30mins

Similar observation and analysis can be performed on Figure 53 and Figure 54 which show how residence times affect the available functional groups, hence compounds. For all the discussed peaks at the different wavelengths, the same appear here but with even a greater drop in intensities as the time increases, especially at 120mins.

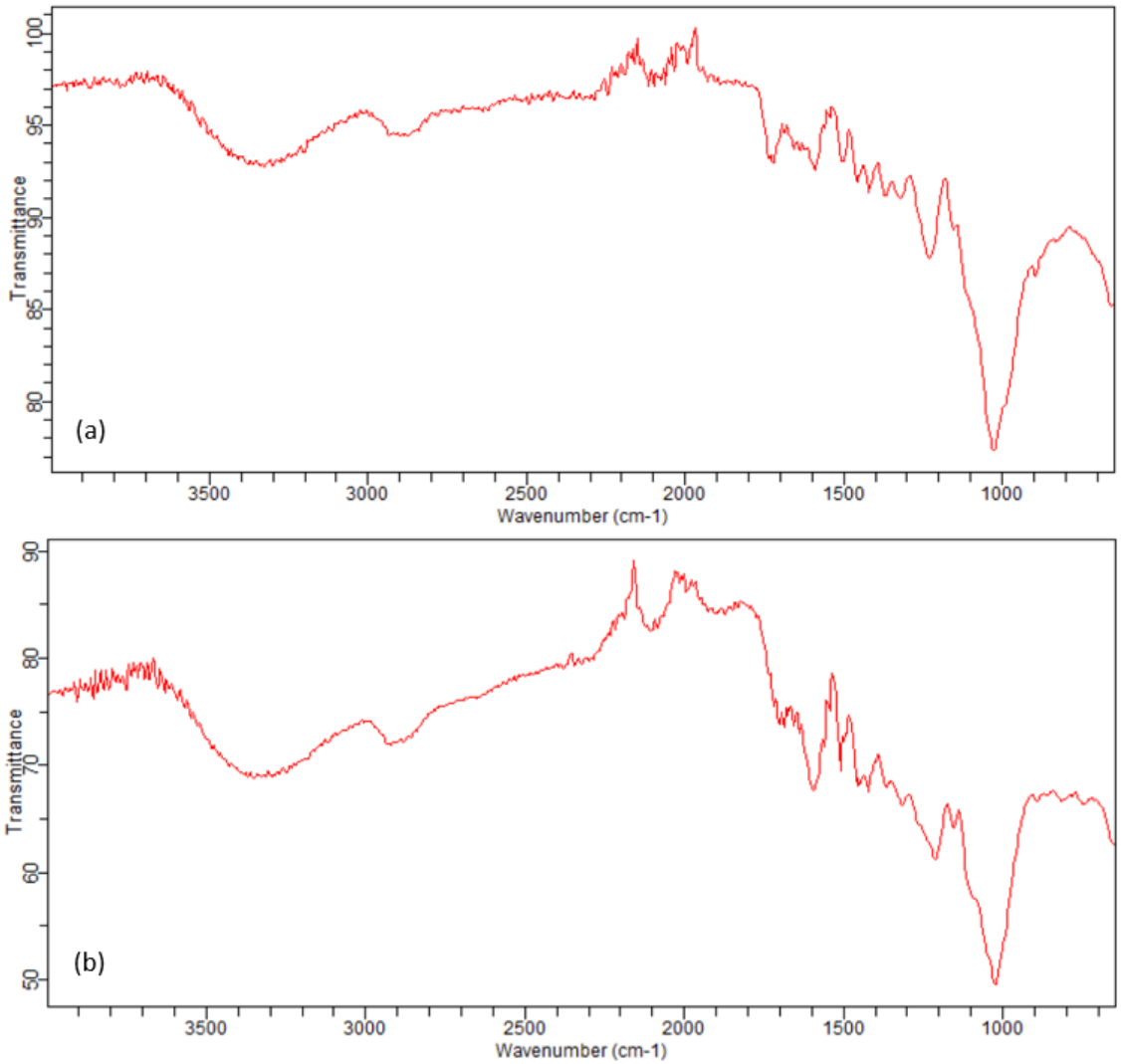

Figure 53 FTIR (a)2.5mm for 270oC at 30mins (b)2.5mm for 270oC at 45mins

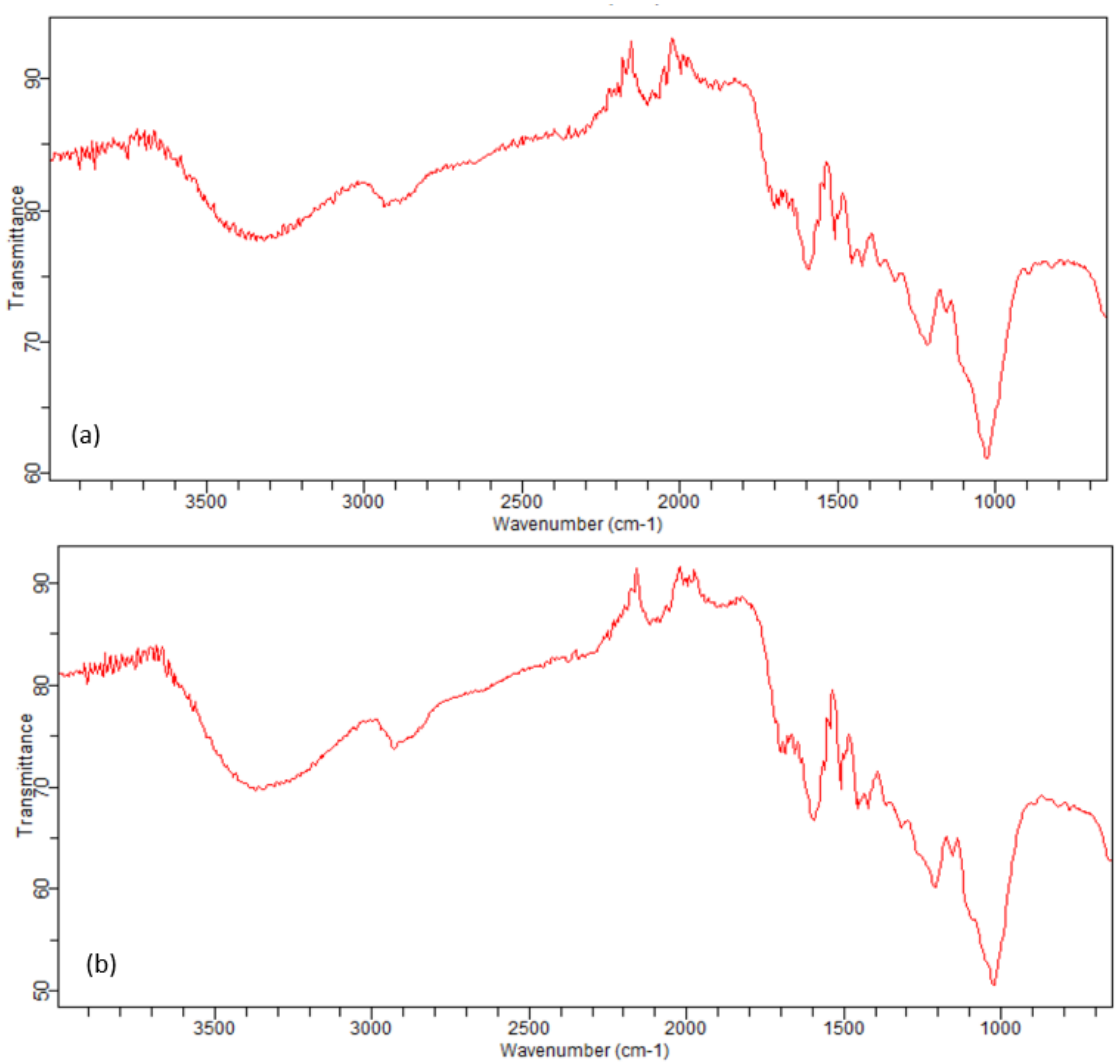

Figure 54 FTIR (a)2.5mm for 270oC at 60mins (b)2.5mm for 270oC at 120mins

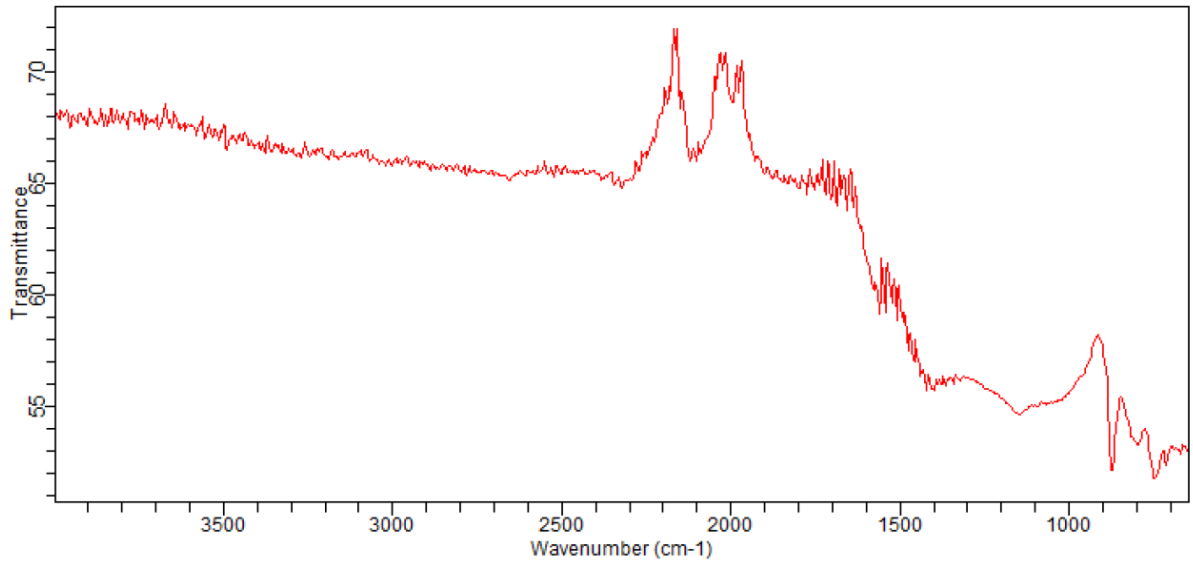

Figure 55 FTIR of Sudan Coal

The FTIR curves presented next are those of the released gases during the TGA runs of the samples. Each curve represents a mass loss peak at a specific temperature, but as before, not to overcrowd the section, the curves were categorized as being from the "devolatilization" stage from 150°C to 390°C or the "char burning stage" from 400°C to 530°C. Only curves for 2.5mm at 30mins and different temperatures, and 2.5mm at 270°C at different residence times are exhibited here.

The most prominent gas species detected in all the curves is CO_2 with a very distinct peak at around 2350cm^{-1}. However, the intensity of this peak in the "char burning" region, and out of those the highest were for torrefied samples at 300°C. The other peaks are in the ranges of 1050-1200cm^{-1}, 1660-1820cm^{-1}, and 3550-4000cm^{-1} referring probably to -OH group of some formic acid and methanol, C=O group of

ketones/aldehydes/esters, and water, respectively [158]. The source of the formic acid and methanol are probably the decomposed methoxyl groups from cellulose and lignin, and xylans of hemicellulose and lignin [158]. As shown in Figure 56 to Figure 59, these peaks are clear in the "devolatilization" region and non-existent in the "char burning" region. So, taking the "devolatilization" region alone, the FTIR peaks, which are actually small, of the gases released from the torrefied samples decreased with the increase in torrefaction temperature. The sharpest decrease was in the case of 300^{o}C torrefaction temperature samples. In any case these results indicate the success of the process in eliminating most volatiles, decomposing and deforming cellulose, hemicellulose, and lignin and carbonizing the OS.

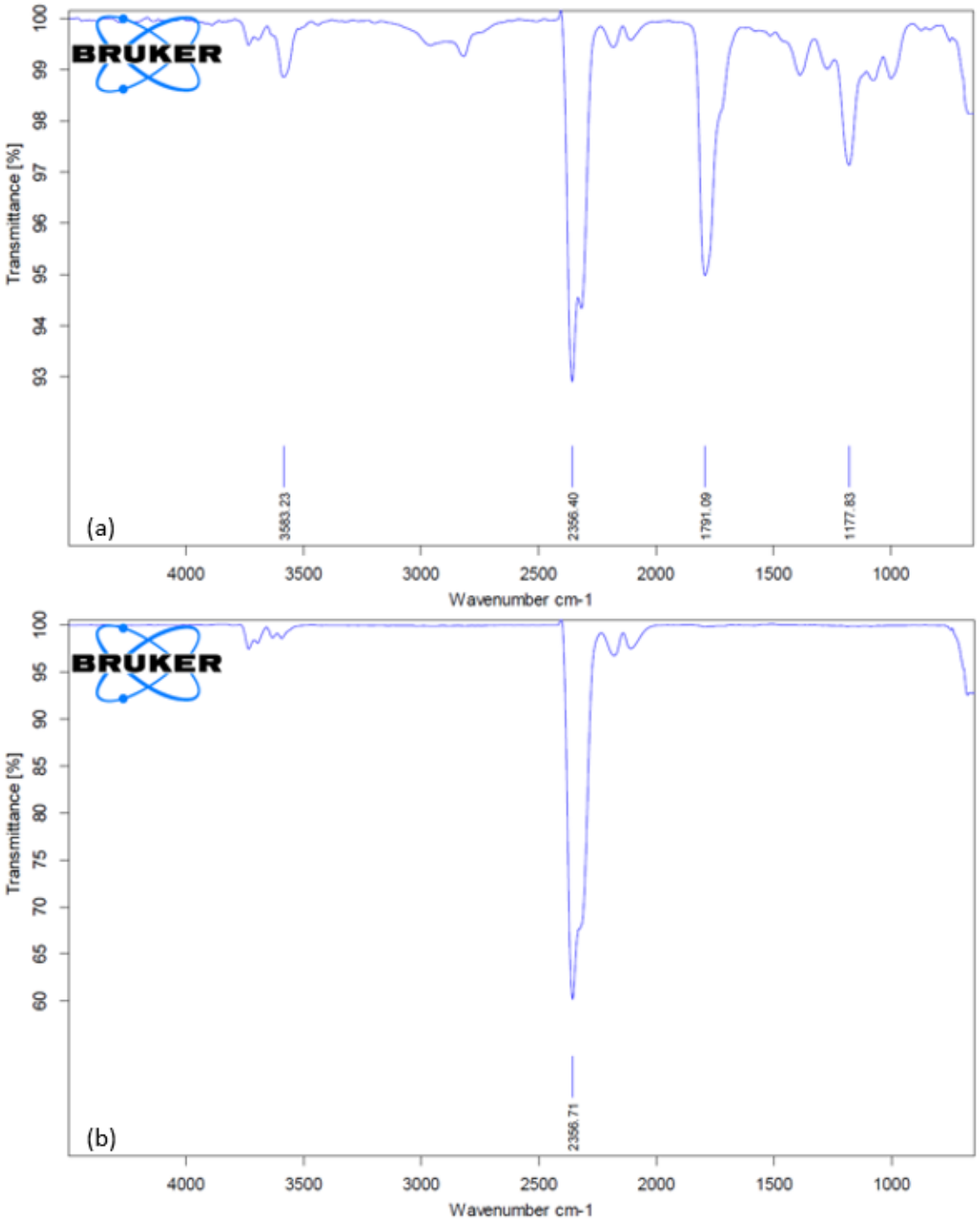

Figure 56 Gaseous FTIR 2.5mm for 200oC at 30mins (a) Devolatilization (b) Char Burning

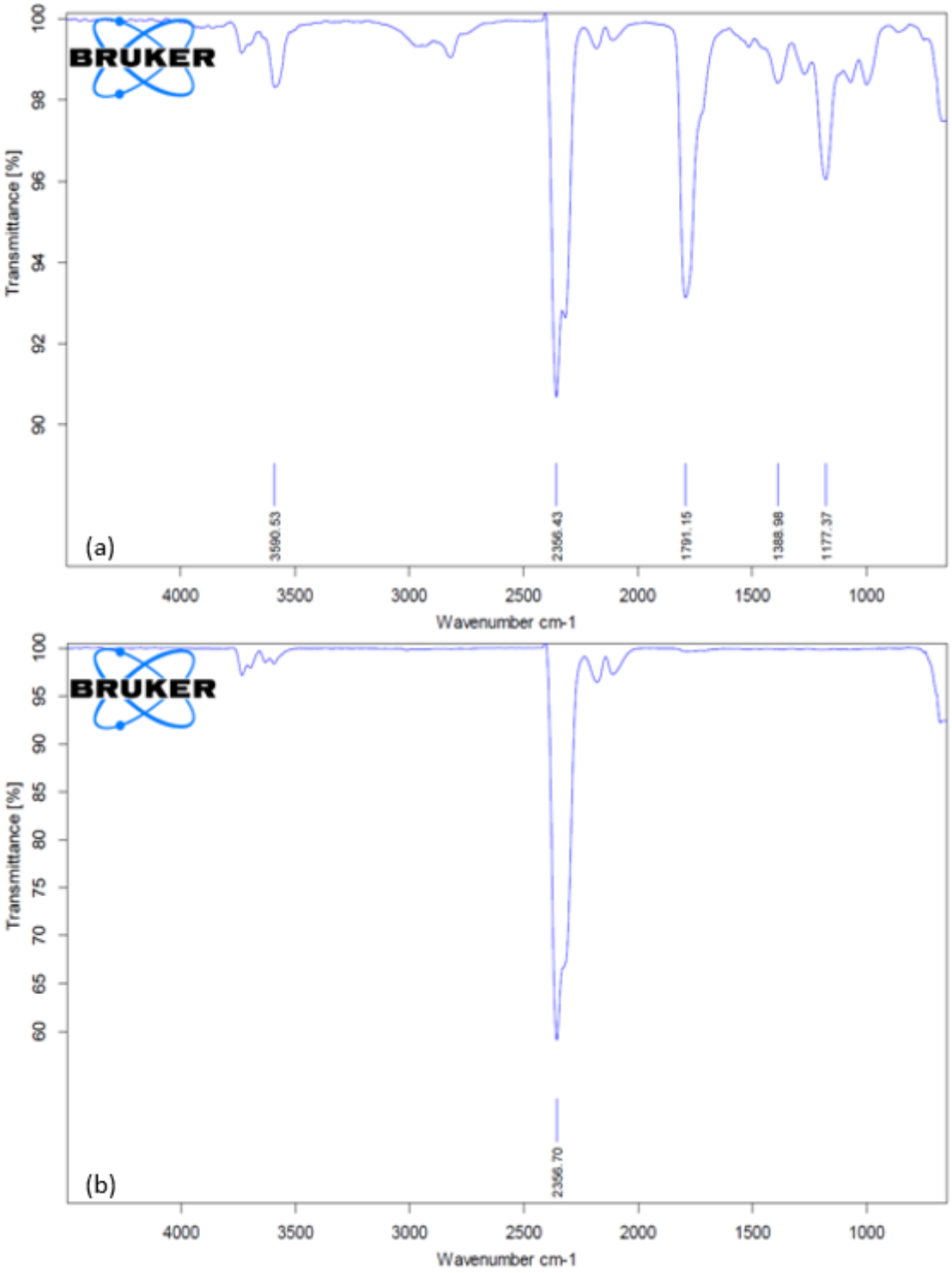

Figure 57 Gaseous FTIR 2.5mm for 250oC at 30mins (a) Devolatilization (b) Char Burning

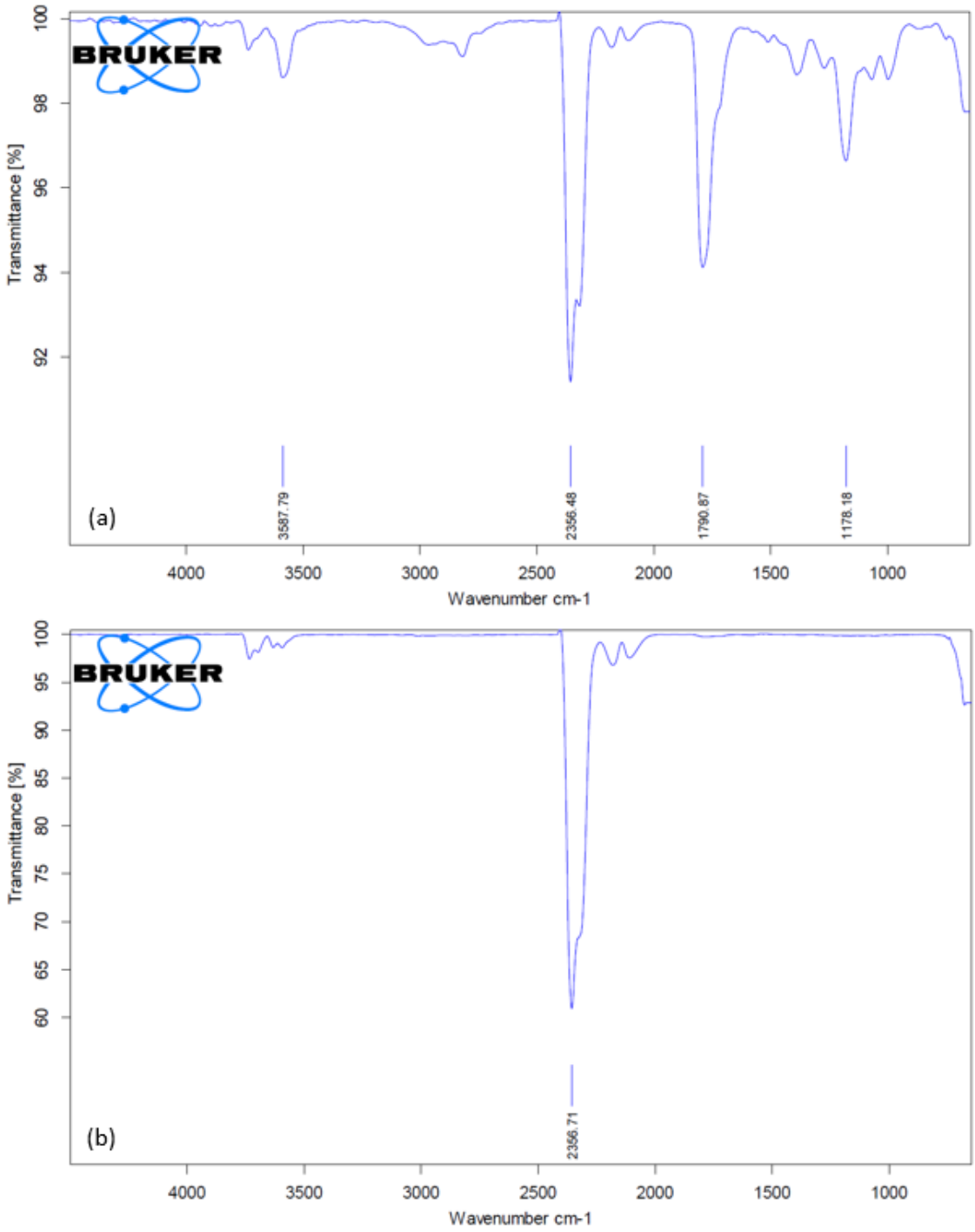

Figure 58 Gaseous FTIR 2.5mm for 270oC at 30mins (a) Devolatilization (b) Char Burning

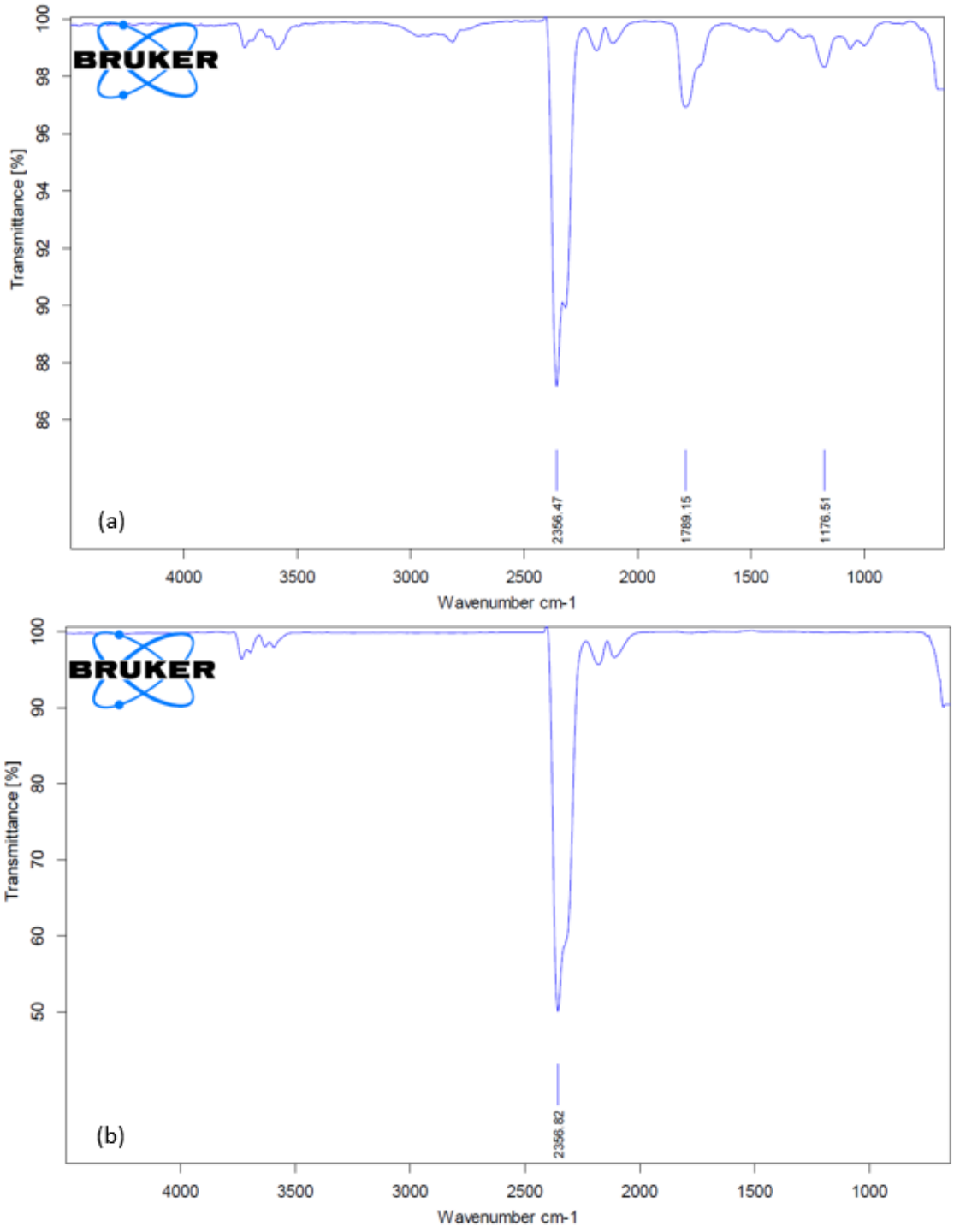

Figure 59 Gaseous FTIR 2.5mm for 300oC at 30mins (a) Devolatilization (b) Char Burning

Figure 60 to Figure 63 show the FTIR curves of the gas released during TGA of 2.5mm samples torrefied at 270^{o}C for different residence times. Similar analyses can be conducted here with the peaks of CO_2 at 2350cm^{-1}, -OH group at 1050-1200cm^{-1}, C=O group at 1660-1820cm^{-1}, and water at 3550-4000cm^{-1}. Less gases of the "devolatilization" region are detected and none but CO_2 in the "char burning region". Moreover, as the residence time increases, the intensity of detected gasses decreases to a negligible amount when hitting 120mins, 60mins, and even 45mins.

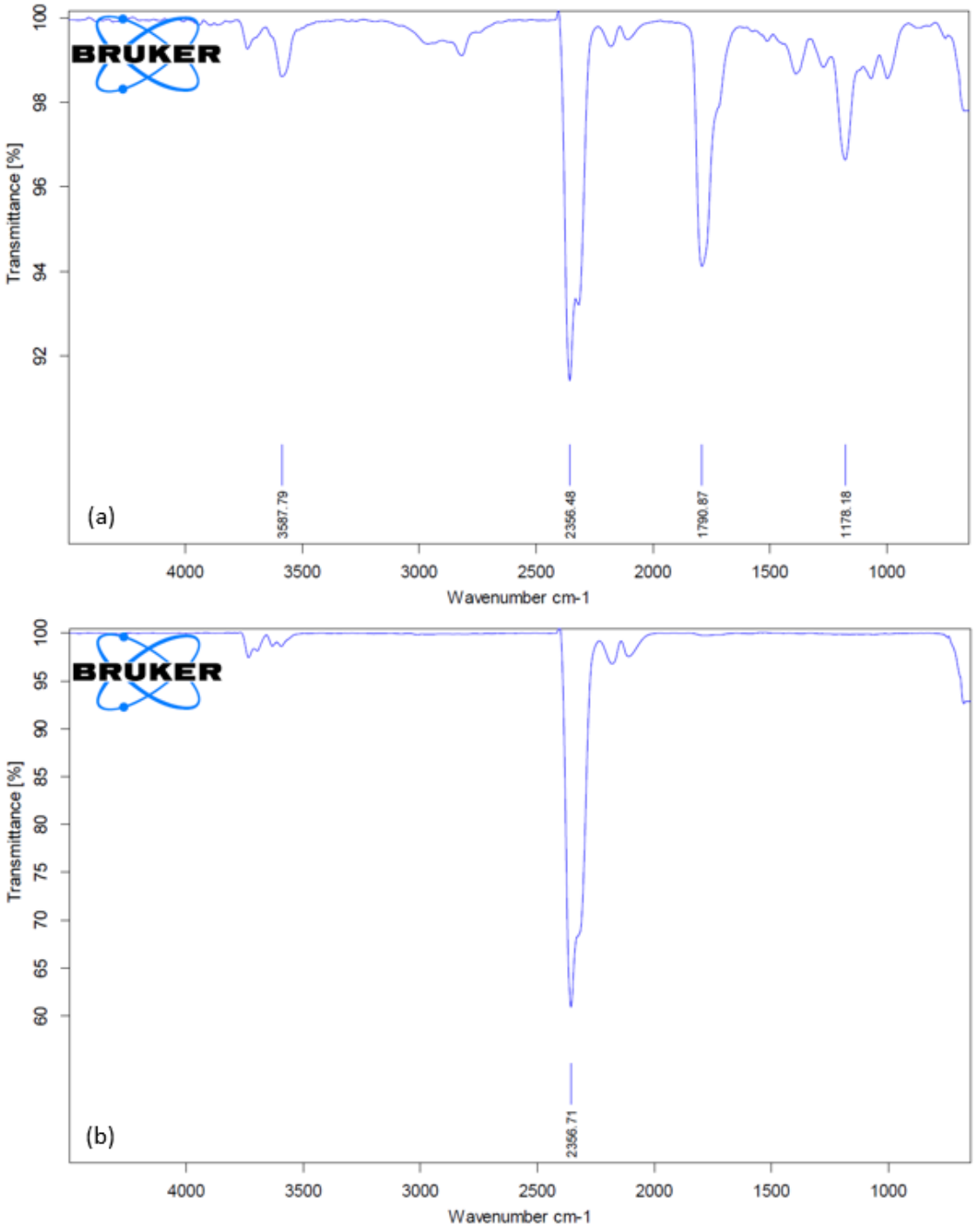

Figure 60 Gaseous FTIR 2.5mm for 270oC at 30mins (a) Devolatilization (b) Char Burning

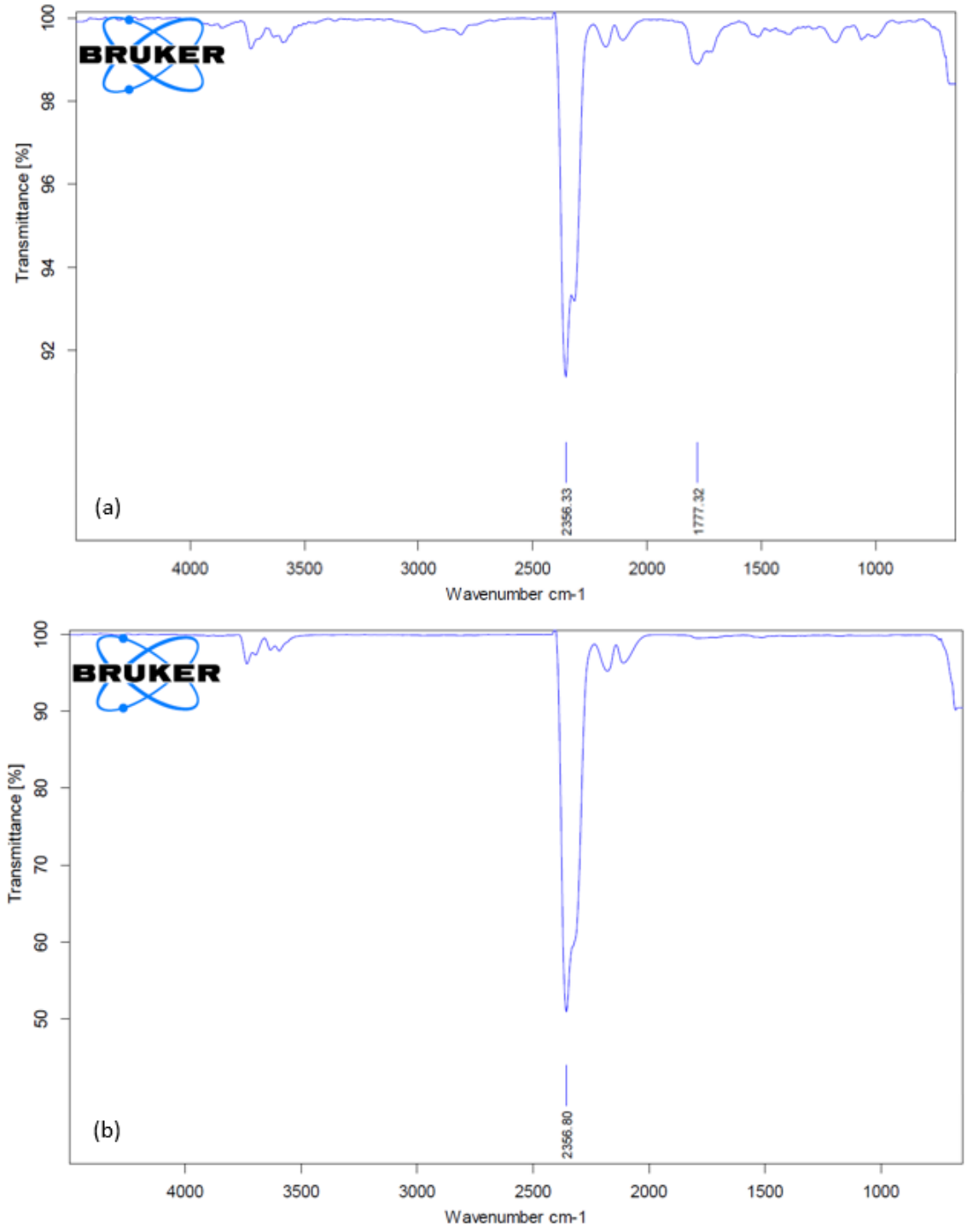

Figure 61 Gaseous FTIR 2.5mm for 270oC at 45mins (a) Devolatilization (b) Char Burning

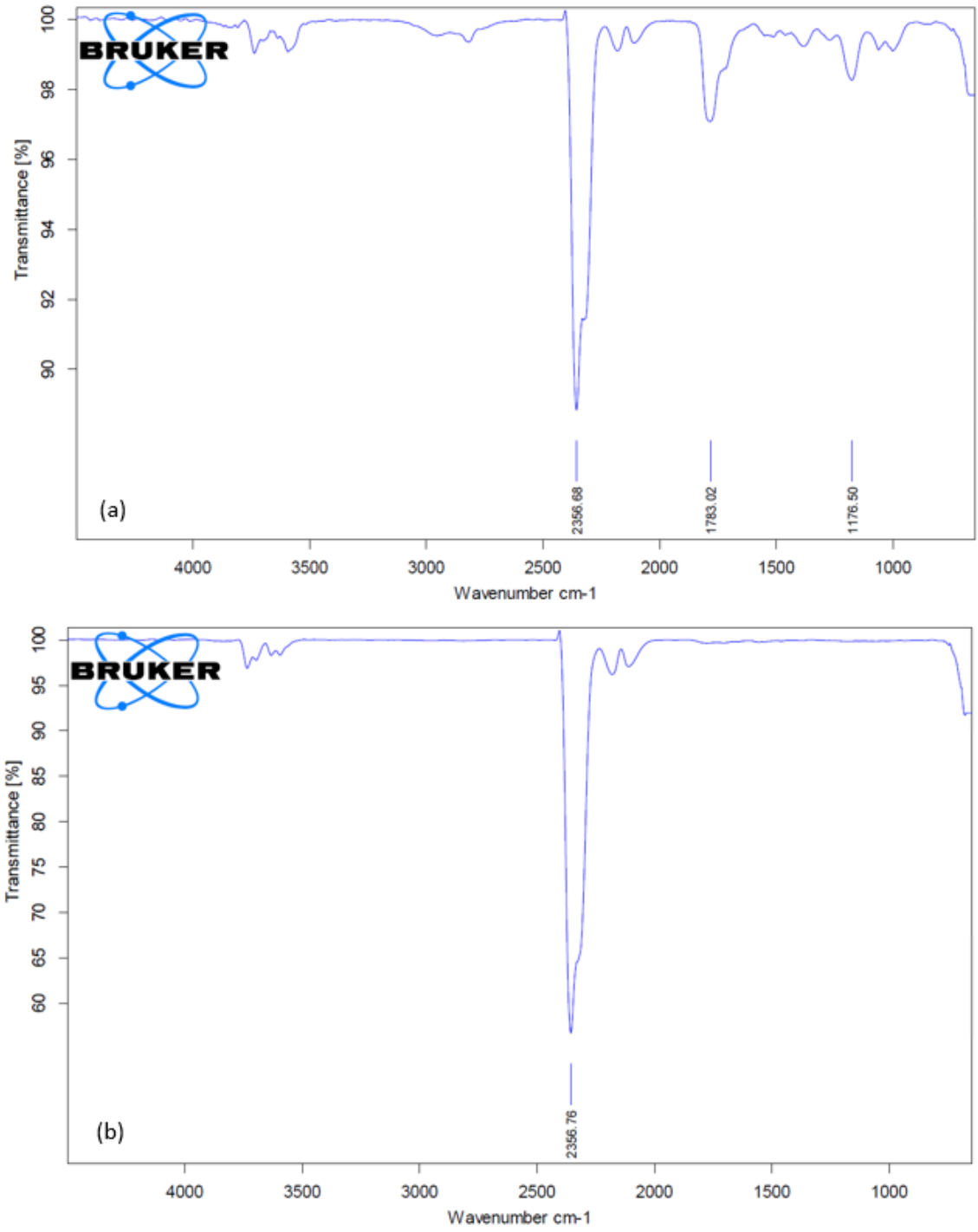

Figure 62 Gaseous FTIR 2.5mm for 270oC at 60mins (a) Devolatilization (b) Char Burning

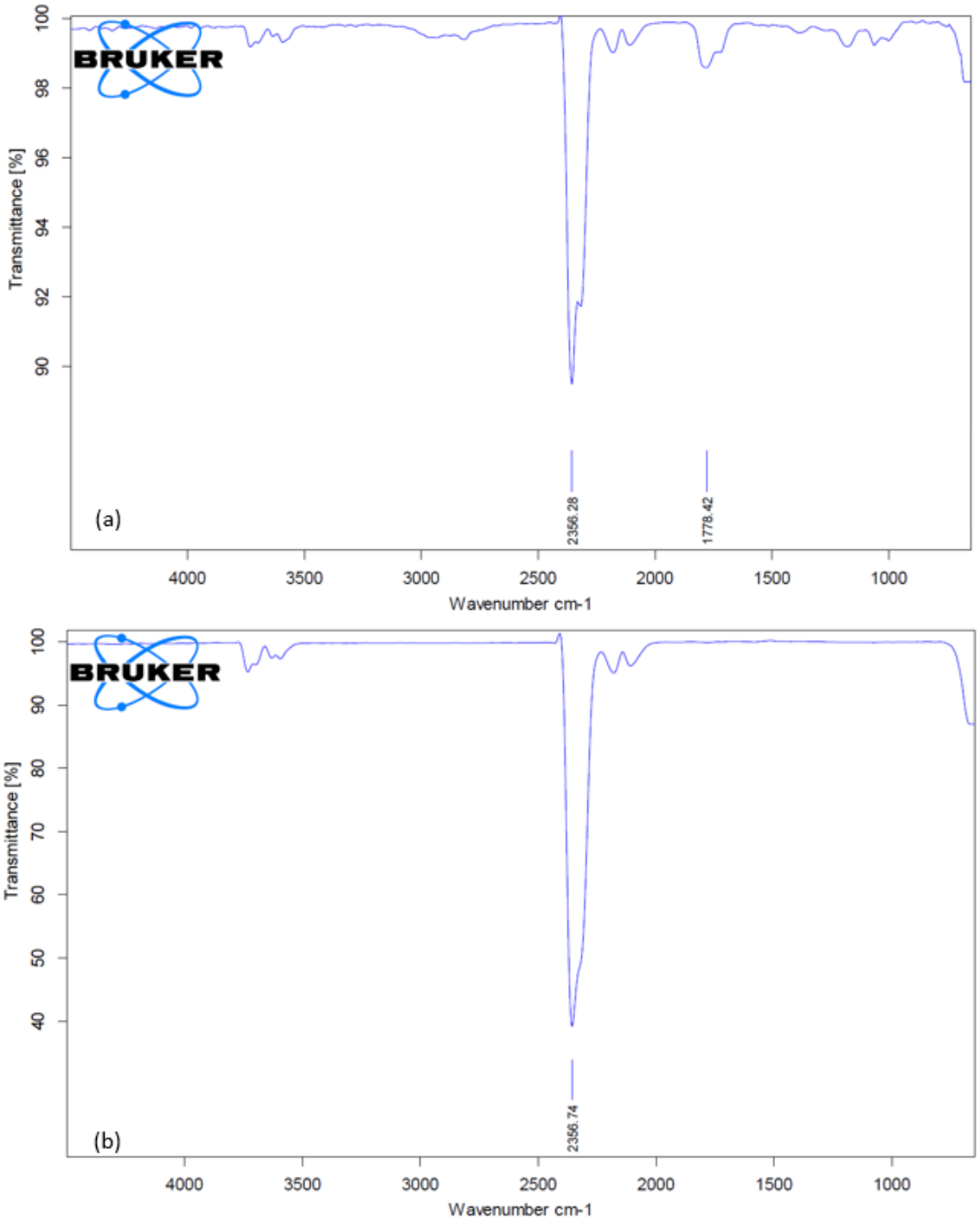

Figure 63 Gaseous FTIR 2.5mm for 270oC at 120mins (a) Devolatilization (b) Char Burning

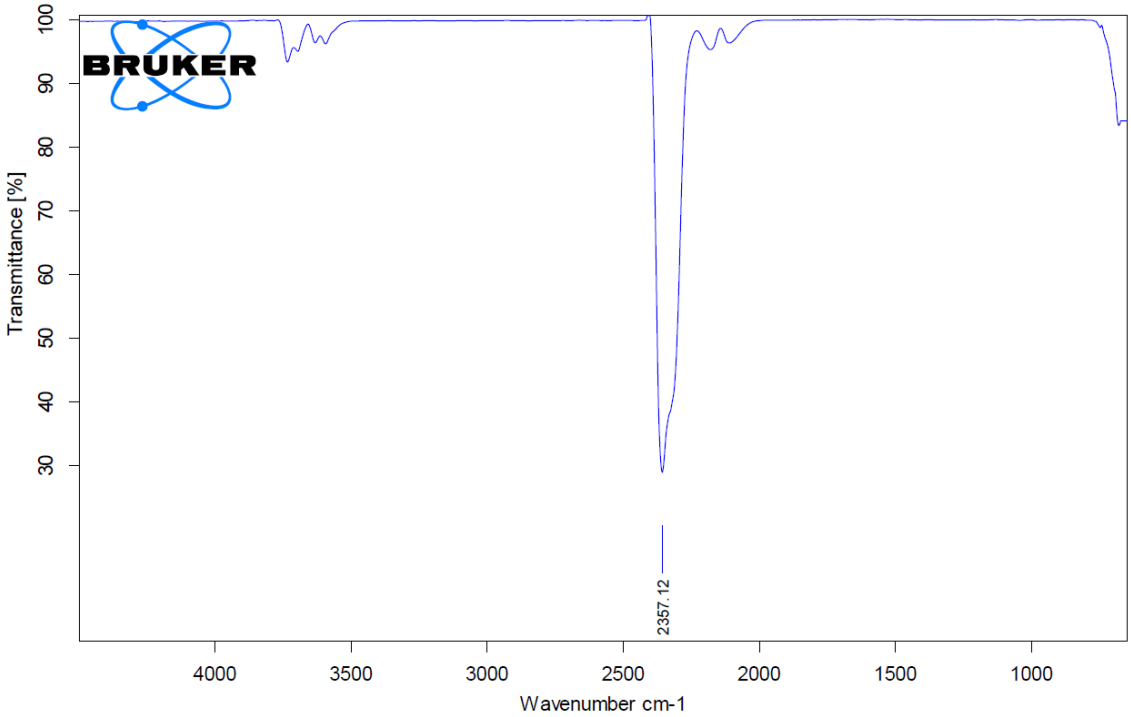

Figure 64 Gaseous FTIR of Sudan Coal

J. Morphological Analysis

To visualize the changes in morphology of the torrefied OS, SEM imaging was used. In Figure 65, the raw OS stone presents a tight structure with no pores or gaps to be found. It consists of dense form of endocarp with some grooves and tiny superficial nanopores [76], visible in Figure 65(b).

On the other hand, Figure 66 presents the surface structure of a torrefied OS sample. Pores of different sizes (5-20μm) emerge spread about the area and the compaction of the material seems to have lost integrity.

This damaged structure of the torrefied samples is attributed to the shrinkage and degradation of the components holding the dense OS structure. The dehydration and devolatilization during the breakdown of cellulose and hemicellulose gives rise to the formation of cracks and hence pores, evidently at elevated torrefaction temperature and residence time.

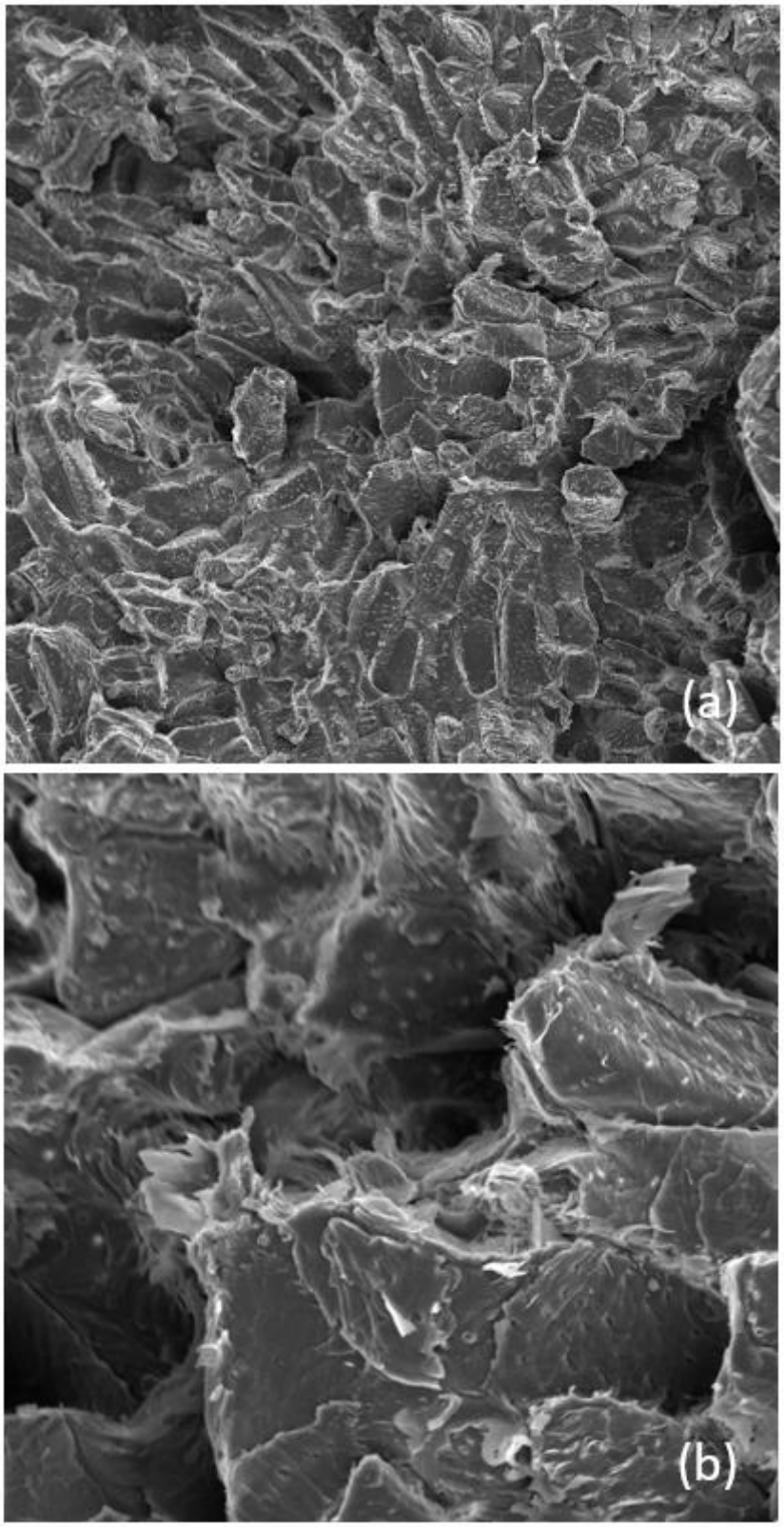

Figure 65 SEM Image of Raw OS (a) 100µm scale (b) 20µm scale

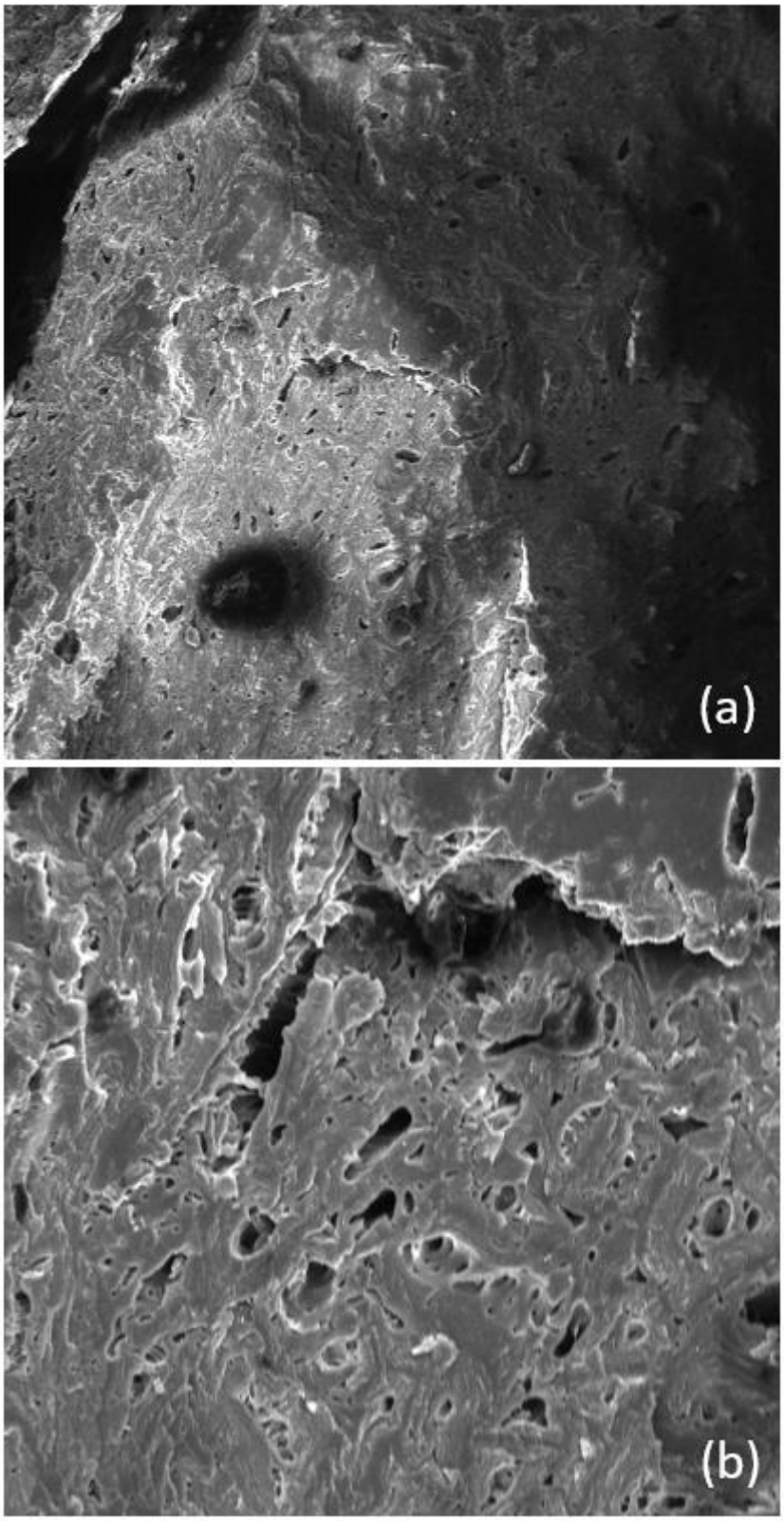

Figure 66 SEM Image of Torrefied OS (a) 100µm scale (b) 20µm scale

K. Hydrophobicity

For a complete qualitative and quantitative assessment of the hydrophobicity/hydrophilicity of a material, water droplets contact angle measurements are normally used. After numerous trials on doing so, the water droplet was either being rapidly absorbed into the OS sample or rolling away on it for several samples. This wasn't good enough for a clear comparison and analysis. The alternative was to conventionally weigh the samples then thoroughly dry them using a vacuum oven at -0.5bar and 85℃ for 60hrs and calculate the weight difference after. The samples were then left in open air for at least 24hrs to see how they perform in affinity to water, and then weighed again. The graph in Figure 67 shows the water gain trends of all the particle sizes torrefied for 30mins at different temperatures. Collectively for all cases, the water gain (%) decreased as the torrefaction temperature increased.

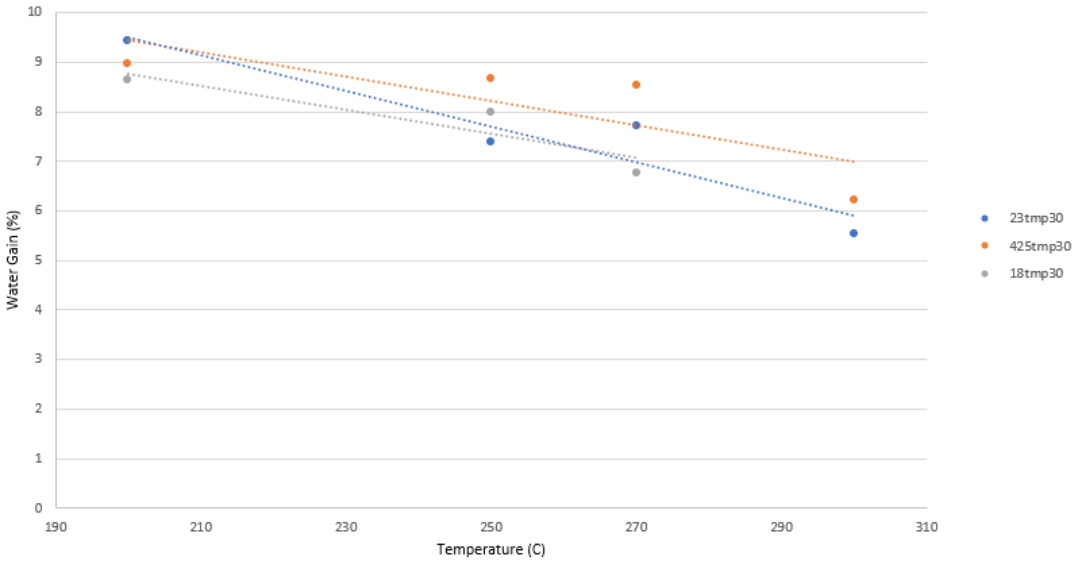

Figure 67 Water Gain as a Function of Torrefaction Temperature for all Particle Sizes

For the sake of assurance, the initial undried sample mass was recorded and compared to the resulting sample mass open to air for 24 hours after drying. The bar graph in Figure 68 shows that the weight initially and after were almost equal confirming the accuracy of the performance.

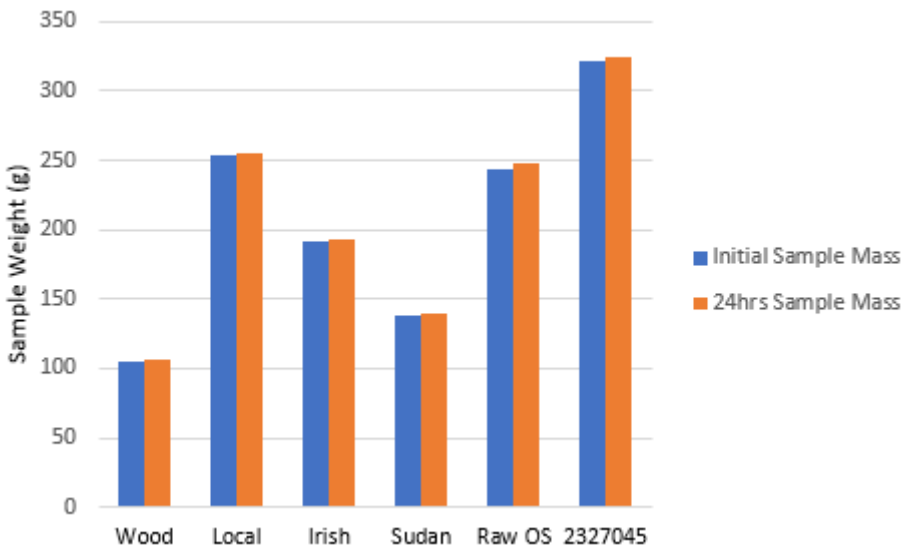

Figure 68 Initial and 24hrs Exposed Sample Mass Comparison

Where does our best option stand among comparable materials? Figure 69 presents the water retention (%) of raw OS, wood, local coal, Irish coal, and Sudanese coal, and OS at optimal conditions. Wood and raw OS exhibited the highest with almost 7% while our optimal was very similar to the Sudanese, highest coal grade, with around 4.5%.

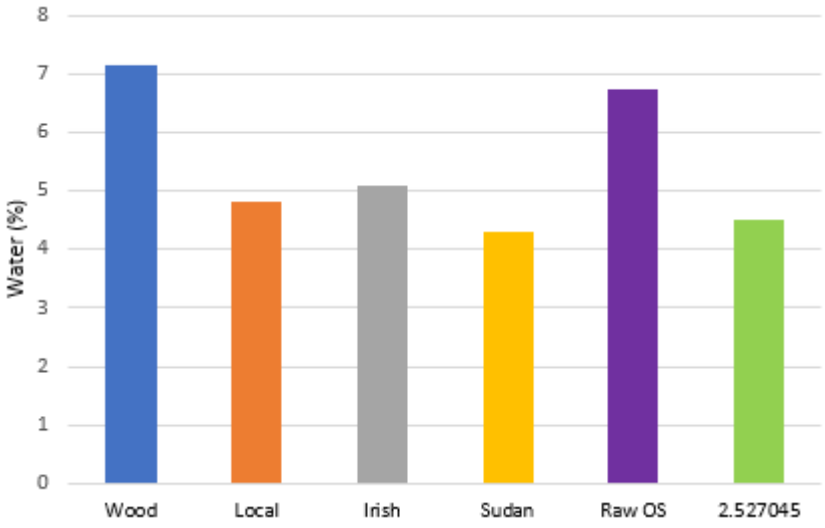

Figure 69 Where does our best option stand among comparable materials?

CHAPTER V
YIELDS PREDICTIVE MODEL

Artificial neural network modelling along with advanced optimization techniques like Genetic Algoritth and Nelder-Mead optimization are providing new modern prediction capabilities for complex chemical and biochemical systems [142, 159-163] . Due to multiple complex mechanisms occurring simultaneously in torrefaction of solid material it has been always challenging to predict the yields of the process using mechanistic models. This study implements an empirical model that couples artificial neural network with ordinary kriging interpolation to predict the solid, liquid and gas yields in the torrefaction of OS based on the OS size, reaction temperature and time. This model will provide the tool for predicting the yields and optimizing the process by the changing the material and process parameters accordingly.

Artificial neural network is implemented in this work to model the reaction yields (solid, liquid and gas) in terms of the process and material parameters (average olive stone particle size, reaction temperature, and reaction time). The experimental runs and conditions presented in Table 13 were used to develop the model.

Table 13 Torrefaction Parameters and Yields

Experiment number	Avg. particle size (mm)	Temp. (^{o}C)	Res. time (min)	Solid yield (wt%)	Liquid yield (wt%)	Gas yield (wt%)
1	2.5	200	30	87.9	8.2	3.9
2	2.5	200	60	87.2	12.5	0.3
3	2.5	200	120	86.2	13.4	0.3
4	2.5	250	30	85.1	13.3	1.6
5	2.5	250	60	80.3	17.7	1.98
6	2.5	250	120	62.9	16.03	21.1
7	2.5	300	30	47.2	41.6	11.2
8	2.5	300	60	40.2	49.1	10.7
9	2.5	300	120	38.8	50.03	11.1
10	0.71	200	30	89.5	7.1	3.4
11	0.71	200	60	86.8	12.1	1.1
12	0.71	200	120	85.9	13.7	0.42
13	0.71	250	30	88.7	10.4	0.84
14	0.71	250	60	79.4	18.75	1.8
15	0.71	250	120	70.8	25.1	4.05
16	0.71	300	30	74.1	21.7	4.2
17	0.71	300	60	37.1	50.9	12.02
18	0.71	300	120	37.2	50.5	12.3

19	0.3	200	30	91.1	8.5	0.37
20	0.3	200	60	87.7	12.1	0.16
21	0.3	200	120	86.5	12.6	0.96
22	0.3	250	30	86.7	11.5	1.8
23	0.3	250	60	81.4	16.9	1.7
24	0.3	250	120	68.2	26.6	5.2
25	0.3	300	30	70.3	24.8	4.8
26	0.3	300	60	39.4	48.6	11.9
27	0.3	300	120	38.4	50.4	11.2

ANN modelling is used for its efficiency in determining the optimum solution for complex processes like torrefaction. ANN is a modelling technique that is based on statistical optimization to relate certain inputs to certain outputs in an empirical form, it is usually used when it is difficult to find a mechanistic model for the process. ANN structure consists of three layers: input, hidden and output layer. The input layer consists of the parameters that are affecting the system, while the hidden layer is made of multiple layers that are made of a number of linear and nonlinear neurons (nodes) and that relates the input layer with the output layer (outer layer), the outer layer is the layer where the output responses are predicted from the ANN model. The ANN prediction accuracy depends mainly on the number of layers and nodes used, type of activation functions used for each node, and the number of data points used in training and validating the model; with the latter one being also important in optimizing the model structure.

A variety of activation functions (linear and nonlinear) have been used for optimizing the ANN structure and prediction. However simple linear models are always preferred from a practical point of view [164] because they are easy to implement for process control and design applications. Non-linear functions used in modelling has more mathematical flexibility which gives better fitting of the model, but more complex to solve in dynamic control applications. Therefore, in optimizing the ANN structure, non-linear nodes were only used in extreme cases where linear nodes failed to predict.

Heuristic approach is needed in order to find the optimum structure of the ANN for processes. In this model, 2/3 of the data points were used for training and 1/3 for validation, a K-fold approach was used in model optimization. JMP Pro 14 statistical analysis software was used for building and optimizing the ANN models.

A. Kriging Interpolation

Kriging interpolation is a data driven interpolation that is based on predicting new data points in the neighbourhoods of the initial points used. The technique was initially developed by Krige in 1952 [165], then Matheron [166] continued in deriving the formulas.

Ordinary kriging interpolation predicts the responses y_ks at the interpolated point x_ks based on the weighted sum of the observed responses (y_1,y_2…y_n) where there corresponding sampling points (x_1,x_2,x_3…x_n) falls in the neighbourhood of x_ks [167], as in the following equation.

$$y_k \equiv f(x_k) = \sum_{i=1}^{n} w_i f(x_i)$$

Where w_i being the weighted sum (kriging weights) that depends on the Euclidian distance h and $f(x_i)$ is the observed response of sample point x_i. The Euclidian distance h is calculated as in the equation:

$$h = \|x_i - x_j\|$$

This means that in determining the interpolated response $f(x_k)$ at the interpolated sample point x_k, the observed responses y_is for there corresponding x_is that falls nearer to x_k have more weight in predicting the response $f(x_k)$. Also, the higher number of x_is that falls in the neighbourhood of x_k, $f(x_k)$ is predicted with more confidence.

In calculating the kriging weights of the interpolated points, first the suitable variogram is derived, where the variogram is a statistical description of the dataset (exponential, Gaussian, cubic, etc.). The variogram γ depends on the Euclidian distance h, at each variance difference of the observations in the neighbourhood of x_k, and given as:

$$\gamma(h) = \frac{1}{2}[var(y_i - y_j)]$$

Then the covariance at each h is calculated by the equation:

$$Cov(h) = \sigma_{max}^2 - \gamma(h)$$

Where, σ_{max}^2 is the maximum variance of the variogram.

Finally, the calculated covariance is used to calculate the kriging weight at each interpolated point by solving the following system.

$$\begin{bmatrix} Cov(d_{1,1}) & \dots & Cov(d_{1,N}) & 1 \\ \vdots & \ddots & \vdots & \vdots \\ Cov(d_{N,1}) & \dots & Cov(d_{N,N}) & 1 \\ 1 & \dots & 1 & 0 \end{bmatrix} \times \begin{bmatrix} w_1 \\ \vdots \\ w_N \\ \lambda \end{bmatrix} = \begin{bmatrix} Cov(d_{1,k}) \\ \vdots \\ Cov(d_{N,k}) \\ 1 \end{bmatrix}$$

where $Cov(d_{i,j})$ and $Cov(d_{i,k})$ is the covariance of the distance $d_{i,j}$ and $d_{i,k}$ between sampling points x_i - x_j and x_i - x_k (interpolated point).

For improving the ANN models, ordinary kriging interpolation was implemented to interpolate the yields (solid, liquid and gas) at new process parameters (average particle size, temperature and time) points. A three-dimensional kriging interpolation was conducted at 20 new points in each dimension in which 9261 points were obtained. The interpolated ordinary kriging data were used to improve the empirical ANN model prediction compared to using just experimental data.

B. Coupling Kriging with ANN

In this model, Kriging interpolation was coupled with artificial neural network to overcome a major problem that ANN has, that is a low accuracy of prediction and validation using a small experimental data set. By using kriging interpolation new data points are generated at a good confidence interval based on nearest neighbourhood prediction, these data are then used to derive the ANN model with a better prediction accuracy.

The yields of the solid, liquid and gas were first collected from the experimental runs based on the design of experiments (DoE) set. Then kriging interpolation was conducted in the range of the process parameters (average particle size, temperature and time) for 20 steps in each dimension. Finally, the interpolated data points are then feed to train and validate the artificial neural network models to get a better prediction accuracy than the model that is built using only the experimental data as shown in Figure 70, this coupling of ordinary kriging with ANN is expected to stabilise the training and validation phases of the ANN and gives better prediction accuracy.

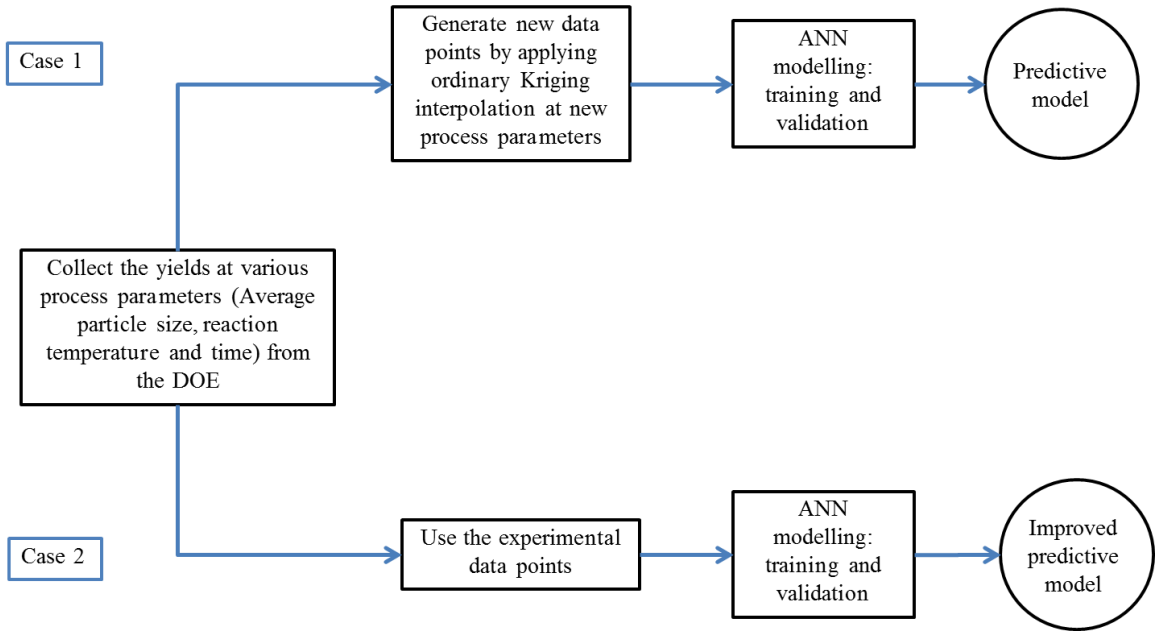

Figure 70 Schematic representation of the modelling methodology developed for coupling kriging interpolation – ANN.

C. Kriging-ANN Topology

For building the ANN model certain number of linear and nonlinear nodes is used with a certain number of hidden layers. Training and validating the ANN model also depends on the number of data points used, the higher number of data points used the more accurate and stable the model is. Thus, Kriging interpolation is used to increase the number of data points used for training and validating in order to get an accurate model with the least number of nodes.

Ordinary Kriging interpolation was optimized with a stable modified Gaussian variogram of the form of the following equation.

$$G = a * (1 - exp^{-\frac{h^b}{c^b}})$$

where a, b, and c are parameters to be calculated after the fitting of the experimental and theoretical variogram, and h is the lag distance of the experimental variogram.

The optimum step size used was 0.1100 mm for the average particle size, 5^{o}C for the reaction temperature and 4.5 min for the reaction time. A three-dimensional input parameter mesh with 20 points to interpolate for in each dimension was created, thus 9261 points where interpolated between the 27 experimental. Kriging interpolation was done on Matlab R2018b. The interpolated points that are done on different average particle size, time and temperatures steps are used for training and validating the ANN model.

ANN modelling was done using the original and interpolated data and both models were compared. Linear nodes where used when possible to make the model simple and compatible for further process control purposes in the future. The optimum ANN structure for predicting the solid and liquid yields was made of 4 linear nodes, two

in the first hidden layer and two in the second hidden layer, and for predicting the gas yield 3 linear nodes with 1 tanh node were used in two hidden layers as shown in Figure 71.

Linear node of the form:

$$F = ax + b$$

Tanh node of the form:

$$F = \frac{e^{2x} - 1}{e^{2x} + 1}$$

where F is the activation function, and x refers to the linear combination of input parameters.

For training the ANN models 2/3 of the data were used for training and 1/3 for validation. The optimum ANN model is obtained by minimizing the error between measured and predicted data points in validation and training phases, where an absolute minimum is obtained for an accurate ANN model. Therefore, a multi-start approach was used, in which the fitting parameters are estimated by various initial points [164, 168].

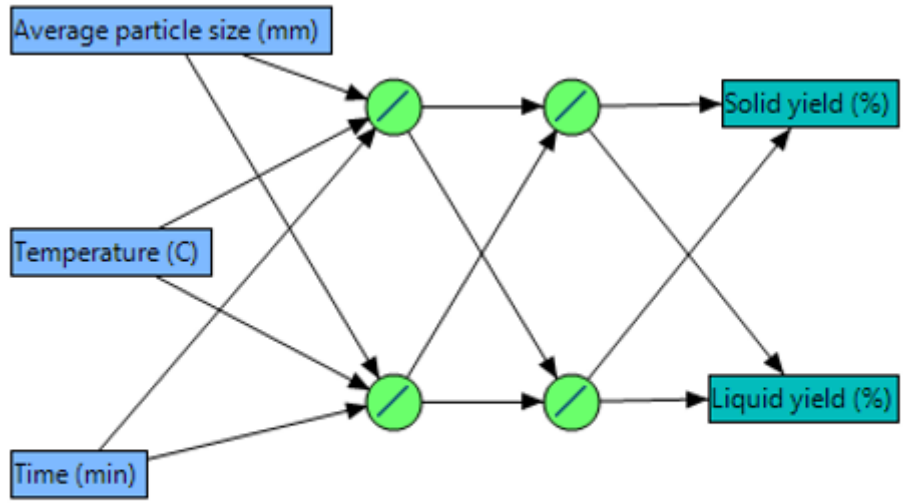

(a)

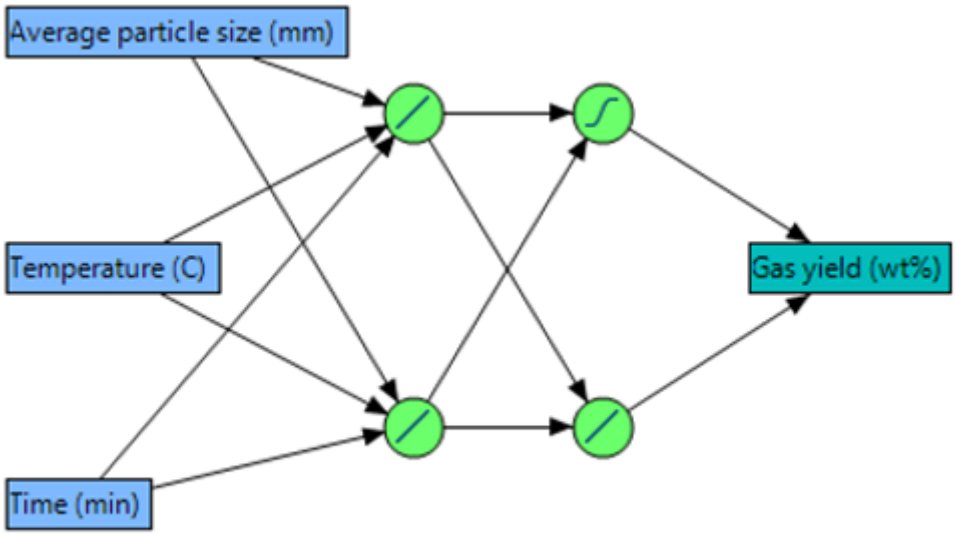

(b)

Figure 71 (a) ANN structure for predicting solid and liquid yields, (b) ANN structure for predicting gas yield

D. Models Training and Validation

The ANN models are calibrated in training and validation phases to obtain the weights and empirical parameters by minimizing the squared error between the experimental and predicted yields. The ANN models predict the solid, liquid and gas yields in terms of the average particle size, reaction temperature and time. The original experimental data and the interpolated data are fed in two separate ANN models and the obtained models are compared in Table 14 which shows the optimized ANN models prediction yields accuracy before and after kriging in training and validation phases. Where for the solid yield the prediction accuracy (R^2) improved by 11.1% and 27.27% in training and validation, respectively. Similarly, the liquid yield prediction accuracy increased by 13.54% and 8.45% in the training and validation, respectively, and the gas yield accuracy increased by 1% and 14.77% in training and validation.

Table 14 Optimized ANN models prediction yields accuracy before and after Kriging in training and validation phases

Phase yields	Measures	Training original exp. data	Validating original exp. data	Training interpolated data	Validating interpolated data
Solid yield	R^2	0.8138	0.71493	0.9041	0.9099
	RMSE	8.6599	11.0336	5.559	5.4037
	Mean Abs Dev	7.7475	10.4076	4.4402	4.4294
	-LogLikehood	64.3977	34.3790	2783.332	1375.971
	SSE	1349.913	1095.6756	27442.889	12935.74
	Sum Frequency	18	9	888	443
Liquid yield	R^2	0.7823	0.8026	0.8882	0.8704
	RMSE	7.4383	6.5564	4.841	4.8042
	Mean Abs Dev	6.4440	5.7369	3.9316	3.9695
	-LogLikehood	61.6605	29.6944	2660.587	1323.87
	SSE	995.919	386.882	20814.491	10224.72
	Sum Frequency	18	9	888	443
Gas yield	R^2	0.9020	0.7733	0.9091	0.8875
	RMSE	1.6344	3.0492	1.3539	1.4843
	Mean Abs Dev	0.9577	2.1286	0.9013	1.0465
	-LogLikehood	27.8114	22.8046	1529.126	803.5511
	SSE	23.1654	83.683	1627.9425	976.00
	Sum Frequency	18	9	888	443

This huge improvement in the ANN model prediction is mainly due to the increase in the number of the interpolated points after applying Kriging interpolation. The Kriging interpolation gave more weight to the points falling in the neighbourhood of the concentrated experimental points and less weight to the outlier experimental points. The Kriging interpolation improved the resolution of the experimental points. Also, the improvement of the prediction stability of the ANN model after applying the interpolation can be seen with the decrease of the mean absolute deviation of the model prediction, where the solid, liquid and gas yields' mean absolute deviation improved by 42.69%, 38.99%, and 5.89%, respectively in training and 57.44%, 30.81% and 50.84%, respectively in validation. This improvement in the model stability is mainly due to the improvement of the trend representation after using Kriging interpolation.

Similarly, Figure 72 shows the yields' data points used and model prediction before and kriging interpolation, where Figure 73 shows the improvement in defining the yields' trend after Kriging. The comparisons confirm that Kriging interpolation is a powerful tool in improving the ANN model prediction of the solid, liquid and gas yields. Given that the torrefaction process is a complex process on a mechanistic level, the developed ANN model is useful in understanding the effect of different process parameters on the reaction yields.

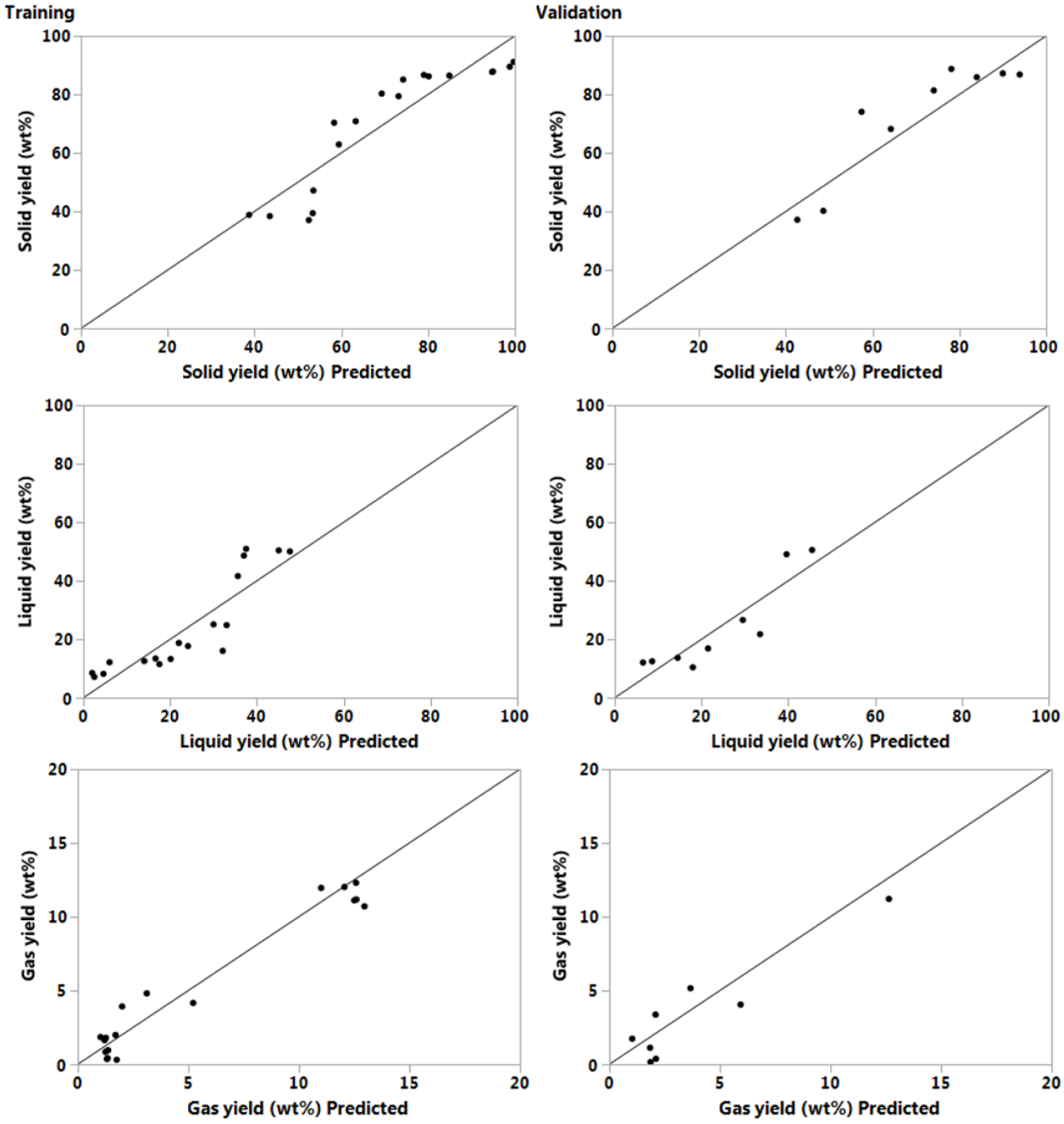

Figure 72 Yields' data points used and model prediction before Kriging interpolation.

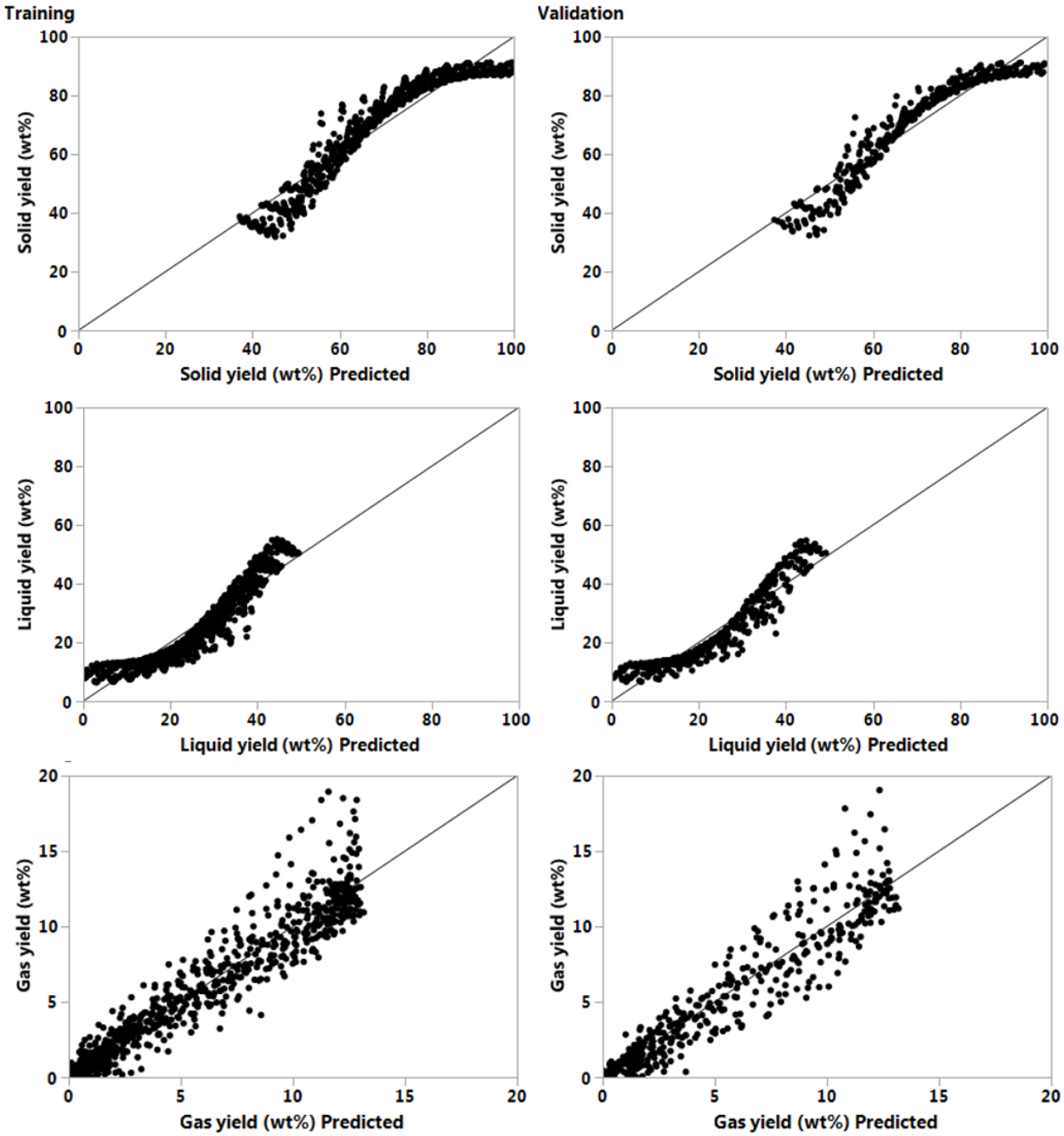

Figure 73 Yields' data points used and model prediction after Kriging interpolation.

E. Optimal Profiles

The developed ANN model after kriging interpolation is represented by a system of linear and non-linear equations that predicts the solid, liquid and gas yields in terms of the average olive stone particle size(mm), reaction temperature(^{o}C) and reaction time (min) according to the following relations.

$$\alpha = 207.0 - 0.4833\theta - 0.1946\mu - 0.6619\varepsilon$$

$$\beta = 0.3784\theta - 0.6932\varepsilon + 0.1291\mu - 79.36$$

$$\gamma = 11.29tanh(0.2479\varepsilon + 0.02316\theta + 0.01803\mu - 7.814) - 0.06607\theta - 0.06055\mu - 0.2088\varepsilon + 28.98$$

Where α, β, and γ are the predicted solid, liquid and gas yields in wt% respectively, and ε, θ, and μ are the average olive stone particle size (mm), reaction temperature (^{o}C) and reaction time (min), respectively.

These profiles show that the average OS particles size has the smallest effect on all the yields, while the reaction temperature and time are the ones with the major effect.

CONCLUSION

Amid the on-going air-polluting emissions in a fossil fuel ruled energy realm, there is an opposing persistence to mitigate this through research, development, and implementation of all kinds of renewable energy solutions. This study aimed on the use of biomass as a source of renewable energy, specifically the torrefaction of olive stones for co-firing applications. Torrefaction temperature, residence time, and particle size were the parameters investigated to finally find the optimal at 2.5mm PS, 268^{o}C T, and 40mins RT. During this treatment method, the target was the solid char product and finding the best sweet spot possible between solid yield and energy yield. Throughout torrefaction of OS, moisture and other volatiles are lost thus decreasing the oxygen and hydrogen percentages leading to higher carbon content by ratio. Consequently, the energy content and density of the OS increases, its solid-to-energy ratio rises, and its hydrophobicity enhances, factors making it excellent as a coal fuel alternative, safer to store, easier to handle/process, and inexpensive to transport [45, 169-171].

For further study, some interesting recommendations include:

- Extensive effect of particle size and involved heat and mass transfers, with the aid of CFD (or any finite computational tool).
- Include as much as possible temperatures and residence times in experimental studies.
- Investigation and optimization of torrefaction reactor designs including the biomass feed fill factor.
- Economic analysis; at what scale and using what biomass is it feasible?

- Feasibility of net thermal efficiency of the process; energy output-to-energy input ratio.
- Further study on liquid product and assessments of its uses.
- Heat integration within the torrefaction setup/process using the gas product.
- Investigation of using solar energy as heat input to the torrefaction process.

REFERENCES

[1] United Nations Framework Convention on Climate Change, "Paris Agreement," 2015.

[2] M. Howells *et al.*, "Integrated analysis of climate change, land-use, energy and water strategies," *Nature Climate Change,* vol. 3, pp. 621-626, 2013 2013.

[3] D. Gielen, F. Boshell, D. Saygin, M. Bazilian, N. Wagner, and R. Gorini, "The role of renewable energy in the global energy transformation," *Energy Strategy Reviews,* vol. 24, pp. 38-50, 2019.

[4] R. K. Pachauri and L. A. Meyer, "Climate Change 2014: Synthesis Report. Contribution of Working Groups I, II and III to the Fifth Assessment Report of the Intergovernmental Panel on Climate Change," Intergovernmental Panel on Climate Cahnge (IPCC), Geneva, Switzerland;2014, Available: https://www.ipcc.ch/report/ar5/syr/.

[5] International Renewable Energy Agency (IRENA), "Global Renewables Outlook: Energy Transformation 2050," International Renewable Energy Agency, Abu Dhabi.2020.

[6] R. Cherif, F. Hasanov, and A. Pande, "Riding the Energy Transition: Oil Beyond 2040," International Monetary Fund, 2017.

[7] M. Grayson, "On a global scale, reducing fossil-fuel dependent is more than just a technology change," *Nature,* vol. 551, no. 7682, 2017.

[8] F. Mey and M. Diesendorf, "Who owns an energy transition? Strategic action fields and community wind energy in Denmark," *Energy Research & Social Science,* vol. 35, pp. 108-117, 2018.

[9] B. K. Sovacool, "How long will it take? Conceptualizing the temporal dynamics of energy transitions," *Energy Research & Social Science,* vol. 13, pp. 202-215, 2016.

[10] International Renewable Energy Agency (IRENA), "The Power to Change: Solar and Wind Cost Reduction Potential to 2025," Abu Dhabi, 2016.

[11] International Renewable Energy Agency (IRENA), "Renewable Capacity Statistics," IRENA, Abu Dhabi, 2017.

[12] International Energy Agency (IEA), "IEA Finds CO2 Emissions Flat for Third Straight Year Even as Global Economy Grew in 2016," IEA, Paris, 2017.

[13] International Energy Agency (IEA), "The Role of Energy Efficiency in the Clean Energy Transition," IEA, Paris, 2018.

[14] International Renewable Energy Agency (IRENA) and International Energy Agency (IEA), "Perspectives for the Energy Transition – Investment Needs for a Low-Carbon Energy System," IRENA and IEA, Abu Dhabi and Paris, 2017.

[15] International Renewable Energy Agency (IRENA), "Global Energy Transformation: A Roadmap to 2050," IRENA, Abu Dhabi, 2018.

[16] International Renewable Energy Agency (IRENA), "Electric Vehicles: Technology Brief," IRENA, Abu Dhabi, 2017.

[17] International Energy Agency (IEA), "Global EV Outlook," OECD/IEA, Paris, 2017.

[18] International Renewable Energy Agency (IRENA), "REmap: Roadmap for a Renewable Energy Future," IRENA, Abu Dhabi, 2016.

[19] Eueopean Commission. (2019). *Reneable Energy: Moving towards a Low Carbon Economy*.

[20] R. Ortwin and J. Paul Marshall, "Coal, nuclear and renewable energy policies in Germany: From the 1950s to the “Energiewende”," *Energy Policy,* vol. 99, pp. 224-232, 2016.

[21] C. Morris and A. Jungjohann, "Energize the People to Effect Policy Change," *Nature,* vol. 551, pp. 138-140, 2017.

[22] C. Kemfert, "Germany must go back to its low-carbon future," *Nature,* vol. 549, pp. 26-27, 2017.

[23] D. Drysdale, B. Vad Mathiesen, and S. Paardekooper, "Transitioning to a 100% renewable energy system in Denmark by 2050: assessing the impact from expanding the building stock at the same time," *Energy Efficiency,* vol. 12, pp. 37-55, 2019.

[24] B. V. Mathiesen *et al.*, "IDA’s energy vision 2050—technical data and methods," Aalborg University, Copenhagen, Denmark, 2015.

[25] International Renewable Energy Agency (IRENA), "30 Years of Policies for Wind Energy: Lessons from 12 Wind Energy Markets," IRENA, Abu Dhabi, 2013.

[26] Ministry of New and Renewable Energy, "Tentative State-wise break-up of Renewable Power target to be achieved by the year 2022 so that cumulative achievement is 175,000 MW," Government of India MNRE, Delhi, .

[27] Energy Information Administration, "Renewable Energy Explained," U.S. EIA, Washington DC, 2019.

[28] L. C. Stokes and H. L. Breetz, "Politics in the U.S. energy transition: Case studies of solar, wind, biofuels and electric vehicles policy," *Energy Policy,* pp. 76-86, 2018.

[29] D. Meyer, I. Mytelka, R. Press, E. L. DallOglio, P. T. de Sousa Jr, and A. Grubler, "Brazilian ethanol: unpacking a success story of energy technology innovation," in *Energy Technology Innovation: Learning from Historical Successes and Failures,* A. Grubler, Ed., 2014.

[30] International Energy Agency (IEA), "Market Report Series: Renewables 2018," OECD/IEA, Paris, 2018.

[31] National Development and Reform Commission, "The 13th Five-Year Plan for Energy Development," NDRC, Beijing, 2016.

[32] International Renewable Energy Agency (IRENA), "Renewable Energy Prospects for the Russian Federation," IRENA, Abu Dhabi, 2017.

[33] Power Technology, "Is Russia Finally Ready to Embrace Renewable Energy?," 2018.

[34] D. Saygin, M. Hoffman, and P. Gordon, "How Turkey Can Ensure A Successful Energy Transition," Center for American Progress, Washington DC, 2018.

[35] International Renewable Energy Agency (IRENA), "Accelerating the Energy Transition through Innovation," IRENA, Abu Dhabi, 2017.

[36] D. Saygin, M. K. Patel, E. Worrell, C. Tam, and D. Gielen, "Potential of best practice technology to improve energy efficiency in the global chemical and petrochemical sector," *Energy,* pp. 5779-5790, 2011.

[37] E. Palm, L. J. Nilsson, and M. Ahman, "Electricity-based plastics and their potential demand for electricity and carbon dioxide," *Journal of Cleaner Production,* pp. 548-555, 2016.

[38] J. H. Wesseling, S. Lechtenbohmer, M. Ahman, L. J. Nilsson, E. Worrell, and L. Coenen, "The transition of energy intensive processing industries towards deep

decarbonization: Characteristics and implications for future research," vol. 79, pp. 1303-1313, 2017.

[39] International Renewable Energy Agency (IRENA), "Innovation Priorities to Transform the Energy System: An Overview for Policy Makers," IRENA, Abu Dhabi, 2018.

[40] Oak Ridge National Laboratory, ORNL, Oak Ridge, Tennesse, USA, 2016.

[41] D. Saygin, D. Gielen, M. Draeck, E. Worrell, and M. K. Patel, "Assessment of the technical and economic potentials of biomass use for the production of steam, chemicals and polymers," *Renewable and Sustainable Energy Reviews,* vol. 40, pp. 1153-1167, 2014.

[42] International Renewable Energy Agency (IRENA), "Biofuels for Aviation: Technology Brief," IRENA, Abu Dhabi, 2017.

[43] International Renewable Energy Agency (IRENA), "Biogas for Road Vehicles: Technology Brief," IRENA, Abu Dhabi, 2017.

[44] V. Benavente and A. Fullana, "Torrefaction of olive mill waste," *Biomass and Bioenergy,* vol. 73, pp. 186-194, 2015.

[45] I. Iáñez-Rodríguez, M. Á. Martín-Lara, G. Blázquez, A. Pérez, and M. Calero, "Effect of torrefaction conditions on greenhouse crop residue: Optimization of conditions to upgrade solid characteristics," *Bioresource Technology,* vol. 244, pp. 741-749, 2017.

[46] A. J. Callejon-Ferre, B. Velazquez-Marti, J. A. Lopez-Martinez, and F. Manzano-Agugliaro, "Greenhouse crop residues: Energy potential and models for the prediction of their higher heating value," *Renewable and Sustainable Energy Reviews,* vol. 15, no. 2, pp. 948-955, 2011.

[47] D. Boskou, "Olive oil: chemistry and technology ", D. Boskou, Ed. Library of congress Cataloging – in – Publication Data.

[48] P. Bartocci, M. D'Amico, N. Moriconi, G. Bidini, and F. Fantozzi, "Pyrolysis of olive stone for energy purposes," *Energy Procedia,* vol. 82, pp. 374-380, 2015.

[49] B. D'Alessandro, P. Bartocci, and F. Fantozzi, "Gas turbines CHP for bioethanol and biodiesel production without waste streams," in *Proceedings of the ASME Turbo Expo*, Vancouver, BC, Canada, 2011, vol. 1, pp. 691-700.

[50] F. Fantozzi, B. D'Alessandro, P. Bartocci, U. Desideri, and G. Bidini, " Assessment of the energy conversion of whole oil fruits with

a pyrolysis and gas turbine process, ," in *Proceedings of the ASME Turbo Expo*, Glasgow, United Kingdom, , 2010, vol. 1, pp. 685-693.

[51] F. Fantozzi, B. D'Alessandro, P. Bartocci, U. Desideri, and G. Bidini, "Performance evaluation of the IPRP technology when

fuelled with biomass residuals and waste feedstocks, ," in *Proceedings of the ASME Turbo Expo*, Orlando, FL; United States, , 2009, vol. 1, pp. 449-458.

[52] F. Fantozzi and C. Buratti, "Anaerobic digestion of mechanically treated OFMSW: Experimental data on biogas/methane production and residues characterization," *Bioresource Technologies,* vol. 102, pp. 8885-8892, 2011.

[53] F. Fantozzi and C. Buratti, "Biogas production from different substrates in an experimental continuously stirred tank reactor anaerobic digester," *Bioresource Technologies,* vol. 100, pp. 5783-5789, 2009.

[54] F. Fantozzi, C. Buratti, C. Morlino, and S. Massoli, "Analysis of biogas yield and quality produced by anaerobic digestion of different combination of biomass

and inoculums," in *Proceedings of 16th Biomass Conference and Exhibition*, Valencia; Spain,, 2008.

[55] F. Fantozzi, V. Pistolesi, S. Massoli, A. Pugliese, and G. Bidini, " Anaerobic digestion of spoiled milk in batch reactors: technical and economic feasibility," in *69th Conference of the Italian Thermal Machines Engineering Association*, Milano; Italy, , 2014.

[56] N. Petrov, T. Budinova, M. Razvigorova, J. Parra, and P. Galiatsatou, "Conversion of olive wastes to volatiles and carbon adsorbents," *Biomass and Bioenergy,* vol. 32, pp. 1303-1310, 2008.

[57] B. Girgis, L. Khalil, and T. Tawfic, "Porosity development in carbon derived from olive oil mill residue under steam pyrolysis," *Journal of Porous Materials,* vol. 9, pp. 105-113, 2002.

[58] F. Fantozzi, "State of the art on the management of waste from mills," *Industrie Alimentari,* vol. 52, no. 534, pp. 74-80, 2013.

[59] B. P. Fantozzi F, Colantoni S, Desideri U,, "Rotary Kiln Slow Pyrolysis For Syngas And Char Production From Biomass And Waste - Part 1 Working Envelope Of The Reactor," *Journal Engineering for Gas Turbines Power,* vol. 129, no. 4, pp. 901-907, 2007.

[60] F. Fantozzi, P. Bartocci, S. Colantoni, and U. Desideri, "Rotary Kiln Slow Pyrolysis For Syngas And Char Production From Biomass And Waste - Part 2 Introducing Product Yields In The Energy Balance," *Journal of Engineering for Gas Turbines & Power,* vol. 129, no. 4, pp. 908-913, 2007.

[61] B. D'Alessandro, M. D'Amico, U. Desideri, and F. Fantozzi, "The IPRP (Integrated Pyrolysis Regenerated Plant) technology: From concept to

demonstration," *Applied Energy,* vol. 101, no. Special Issue on Sustainable Development of Energy, Water and Environmental Systems, pp. 423-431, 2013.

[62] A. Paethanom *et al.*, "A low-cost pyrogas cleaning system for power generation: Scaling up from lab to pilot," *Applied Energy,* vol. 111, pp. 1080-1088, 2013.

[63] N. Moriconi *et al.*, "Design and preliminary operation of gasification plant for micro-CHP with internal combustion engine and SOFC," in *69th Conference of the Italian Thermal Machines Engineering Association*, Milano; Italy, , 2014.

[64] Energy Information Administration, "Biomass Explained," EIA, Washington DC,2018.

[65] S. Zafar, "Biomass Energy in Middle East," EcoMENA, Doha, Qatar,2020.

[66] R. Singh, A. Shukla, S. Tiwari, and M. Srivastava, "A review on delignification of lignocellulosic biomass for enhancement of ethanol production potential," *Renewable and Sustainable Energy Reviews,* vol. 32, pp. 713-728, 2014.

[67] J. U. H. Beltrán, I. O. Hernandez De Lira, M. M. Cruz-Santos, and A. Saucedo-Luevanos, "Insight into Pretreatment Methods of Lignocellulosic Biomass to Increase Biogas Yield: Current State, Challenges, and Opportunities," *Applied Science,* 2019.

[68] P. Sharma, C. Bhandari, S. Kumar, B. Sharma, P. Bhadwal, and N. Agnihotr, "Dietary Fibers: A Way to a Healthy Microbiome," in *Handbook of Food Bioengineering: Diet, Microbiome and Health,* vol. 11, 2018, pp. 299-345.

[69] L. Du, Z. Wang, S. Li, W. Song, and W. Lin, "A Comparison of Monomeric Phenols Produced from Lignin by Fast Pyrolysis and Hydrothermal Conversions," *Journal of Chemical Reactor Engineering,* vol. 11, no. 1, pp. 135-145, 2013.

[70] I. Iáñez-Rodríguez, M. Ángeles Martín-Lara, G. Blázquez, A. Pérez, and M. Calero, "Effect of torrefaction conditions on greenhouse crop residue: Optimization of conditions to upgrade solid characteristics," *Bioresource Technology*, vol. 244, pp. 741-749, 2017 2017.

[71] E. Ruiz, J. Romero-Garcia, I. Romero, P. Manzanares, M. Negro, and E. Castro, "Olive-derived biomass as a source of energy and chemical," *Biofpr*, vol. 11, pp. 1077-1094, 2017 2017.

[72] E. Atallah, W. Kwapinski, M. N. Ahmad, J. J. Leahy, A. a. H. AL-Muhtaseb, and J. Zeaiter, "Hydrothermal carbonization of olive mill wastewater: Liquid phase product analysis," *Journal of Environmental Chemical Engineering*, 2019.

[73] E. Atallah, W. Kwapinski, M. N. Ahmad, J. Leahy, J.;, and J. Zeaiter, "Effect of water-sludge ratio and reaction time on the hydrothermal carbonization of olive oil mill wastewater treatment: Hydrochar characterization," *Journal of Water Process Engineering*, vol. 31, 2019.

[74] I. O. Council. (2007). Available: http://www.internationaloliveoil.org/

[75] G. Rodríguez, A. Lama, R. Rodríguez, A. Jiménez, R. Guillén, and J. Fernández-Bolaños, "Olive stone an attractive source of bioactive and valuable compounds," *Bioresource Technology*, vol. 99, pp. 5261-5269, 2007.

[76] P. Sangines, M. P. Dominguez, F. Sanchez, and G. San Miguel, "Slow pyrolysis of olive stones in a rotary kiln: Chemical and energy characterization of solid, gas, and condensable products," *Journal of Renewable and Sustainable Energy*, vol. 7, 2015.

[77] M. Volpe and L. Fiori, "From olive waste to solid biofuel through hydrothermal carbonisation: The role of temperature and solid load on secondary char

formation and hydrochar energy properties " *Journal of Analytical and Applied Pyrolysis,* vol. 124, pp. 63-72, 2017.

[78] S. Vitolo, L. Petarca, and B. Bresci, "Treatment of olive oil industry wastes," *Bioresource Technology,* vol. 67, pp. 129-137, 1998 1998.

[79] E. Atallah, W. Kwapinski, M. N. Ahmad, J. Leahy, J.;, A. a. H. AL-Muhtaseb, and J. Zeaiter, "Hydrothermal carbonization of olive mill wastewater: Liquid phase product analysis," *Journal of Environmental Chemical Engineering,* vol. 7, 2018.

[80] A. L. Feria, "The generated situation by the OMW in Andalusia " *Actas Proceeding Workshop Improlive Anexo,* p. 8, 2000.

[81] C. A. Garcia and G. Hodaifa, "Real olive oil mill wastewater treatment by photo-Fenton system using artificial unltraviolet light lamps," *Journal of Cleaner Production,* vol. 162, p. 10, 2017.

[82] M. Volpe *et al.*, "One stage olive mill waste streams valorisation via hydrothermal carbonisation," *Waste Management,* vol. 80, p. 10, 2018.

[83] G. Rodríguez-Gutiérrez, F. t. Rubio-Senent, A. Lama-Muñoz, A. n. García, and J. Fernández-Bolaños, "Properties of Lignin, Cellulose, and Hemicelluloses Isolated from Olive Cake and Olive Stones: Binding of Water, Oil, Bile Acids, and Glucose," *Journal of Agricultural and Food Chemistry,* vol. 62, pp. 8973-8981, 2014.

[84] R. Rodríguez, A. Jiménez, J. Fernández-Bolaños, R. Guillén, and A. Heredia, "Dietary fibre from vegetable products as source of functional ingredients," *Trends in Food Science and Technology,* vol. 17, no. 3-15, 2006.

[85] H. J. Kim and P. J. White, "In vitro bile-acid binding and fermentation of high, medium, and low molecular weight β-glucan," *Journal of Agricultural and Food Chemistry,* vol. 58, pp. 628-634, 2010.

[86] J. A. Story and D. Kritchevsky, "Comparison of the binding of various bile acids and bile salts in vitro by several types of fiber. J. Nutr. ," *Journal of Nutrition,* vol. 106, no. 1292-1294, 1976.

[87] M. E. Camire and M. P. Dougherty, "Raisin dietary fibre composition and in vitro bile acid bindig," *Journal of Agricultural and Food Chemistry,* vol. 51, pp. 834-837, 2003.

[88] J. A. Larrauri, I. Goñi, N. Martín-Carrón, P. Rupérez, and F. Saura-Calixto, "Measurement of health-promoting properties in fruit dietary fibres: antioxidant capacity, fermentability and glucose retardation index," *Journal of the Science of Food and Agriculture,* vol. 71, no. 515-519, 1996.

[89] M. Aguedo *et al.*, "Composition of by-products from cooked fruit processing and potential use in food products," *Journal of Food Composition and Analysis,* vol. 27, pp. 61-69, 2012.

[90] T. Miranda, A. Esteban, S. Rojas, I. Montero, and A. Ruiz, "Combustion Analysis of Different Olive Residues," *International Journal of Molecular Sciences,* vol. 9, pp. 512-525, 2008.

[91] A. Turbetskaya *et al.*, "Characterization of woodstove briquettes from torrefied biomass and coal," *Energy,* vol. 171, pp. 853-865, 2019.

[92] A. Heredia-Moreno, R. Guillén-Bejarano, J. Fernández-Bolaños, and M. Rivas-Moreno, "Olive stones as a source of fermentable sugars," *Biomass,* vol. 14, no. 2, pp. 143-148, 1987.

[93] G. Bianchi, "Lipids and phenols in table olives," *European Journal of Lipid Science and Technology,* vol. 105, pp. 229-242, 2003.

[94] F. Cruz-Perago´n, J. Palomar, and A. Ortega, "Ciclo energe´ tico integral del sector oleı´cola en la provincia de Jae´n (Espan˜ a)," *Grasas Aceites,* vol. 57, no. 2, pp. 19-28, 2006.

[95] F. Fiedler, "The state of the art of small-scale pellet-based heating systems and relevant regulations in Sweden, Austria and Germany. ," *Renewable Sustainable Energy Reviews,* vol. 8, no. 2, pp. 1-21, 2004.

[96] V. Skoulou, A. Swiderski, W. Yang, and A. Zabaniotou, "Process characteristics and products of olive kernel high temperature steam gasification (HTSG)," *Bioresource Technologies,* vol. 100, no. 24, pp. 44-51, 2009.

[97] G. Rodrı`guez, A. Lama, R. Rodrı`guez, A. Jime´nez, R. Guille´n, and J. Bolanos, "Olive stone an attractive source of bioactive and valuable compounds," *Bioresource Technologies,* vol. 99, pp. 5261-5269, 2008.

[98] C. Pattara, G. M. Cappelletti b, and A. Cichelli, "Recovery and use of olive stones: Commodity, environmental and economic assessment," *Renewable and Sustainable Energy Reviews,* vol. 14, pp. 1484-1489, 2010.

[99] M. Ragni, L. Melodia, F. Bozzo, M. Colonna, V. Megna, and F. Toteda, "Use of a destoned olive pomace in feed for heavy lamb production," *Italian Journal of Animal Science,* vol. 2, pp. 485-487, 2003.

[100] A. Cichelli and G. Cappelletti, "Valorization of olive residues by spreading on agricultural land: technical assets," presented at the VII international conference ‘‘Economie Europeana: present si perspective’’, Suceava, Romania, , 2007.

[101] A. El Asli and A.-I. Qatibi, "Ethanol production from olive cake biomass substrate," *Biotechnology and Bioprocess Engineering*, vol. 14, pp. 118-122, 2009.

[102] D. Montane´, J. Salvado´ , C. Torras, and X. Farriol, "High-temperature dilute-acid hydrolysis of olive stone for furfural production," *Biomass Bioenergy*, vol. 22, pp. 295-304, 2001.

[103] J. Tejeda-Ricardez, C. Vaca-Garcıa, and M. E. Borredon, "Design of a batch solvolytic liquefaction reactor for the vaporization of residues from the agricultural foodstuff," *Chemical Engineering Research and Design*, vol. 81, pp. 1066-1070, 2003.

[104] G. Siracusa, A. D. La Rosa, V. Siracusa, and M. Trovato, "Eco-Compatible use of olive huso as filler in thermoplastic composites," *Journal of Polymers and the Environment*, vol. 9, pp. 157-161, 2001.

[105] D. Dawson. (2006). Available: http://www.dennisdawson.com/industry.htm

[106] F. F. Mohammadi, J. T. Harrison, A. Czarnota, and C. Leonard, "Nonabrasive sensory exfoliating system," US Patent US 20050169868, 2005.

[107] G. Bla´zquez, F. Hernainz, M. Calero, and L. F. Ruiz-Nu´nez, "Removal of cadmium ions with olive stones: the effect of some parameters," *Process Biochemistry*, vol. 40, pp. 2649-2654, 2005.

[108] M. Calero, F. Herna´inz, G. Bla´zquez, and G. Tenorio, "Equilibrium modelling of removal of cadmium ions by olive stones," *Environmental Processes*, vol. 25, no. 261-266, 2006.

[109] N. Fiol, I. Villaescusa, M. Martınez, N. Miralles, J. Poch, and J. Serarols, "Sorption of Pb(II), Ni(II), Cu(II) and Cd(II) from aqueous solution by olive

stone waste " *Separation and Purification Technology,* vol. 50, pp. 132-140, 2006.

[110] R. S. Teixeira *et al.*, "Biomass pretreatment: a critical choice for biomass utilization via biotechnological routes," presented at the 5th Congress of the Brazilian Biotechnology Society (SBBIOTEC), Florianópolis, Brazil., 2014.

[111] P. Basu, *Biomass Gasification, Pyrolysis and Torrefaction*, 2nd ed. San Diego, CA, USA,: Elsevier Inc., 2013.

[112] H. Knoef, *Handbook Biomass Gasification*. Netherlads: BTG Biomass Technology Group, 2005.

[113] E. Atallah, J. Zeaiter, M. N. Ahmad, M. Kwapinska, J. J. Leahy, and W. Kwapinski, "The effect of temperature, residence time, and water-sludge ratio onhydrothermal carbonization of DAF dairy sludge," *Journal of Environmental Chemical Engineering,* vol. 8, 2020.

[114] P. C. A. Bergman, A. R. Boersma, Z. R.W.R;, and J. H. A. Kiel, "Torrefaction for biomass co-firing in existing coal-fired power station," ECN Biomass, Netherlands2005.

[115] A. Zabaniotou, G. Kalogiannis, E. Kappas, and A. Karabelas, "Olive residues (cuttings and kernels) rapid pyrolysis product yields and kinetics," *Biomass Bioenergy* vol. 18, pp. 411-420, 2000.

[116] M. L. Mart´ınez, M. M. Torres, C. A. Guzman, and D. M. Maestri, "Preparation and characteristics of activated carbon from olive stones and walnut shells," *Industrial Crops and Products,* vol. 23, pp. 23-28, 2006.

[117] M. N. Alaya, M. A. Hourieh, A. M. Youssef, and F. El-Sejariah, "Adsorption Properties of Activated Carbons Prepared from Olive Stones by Chemical and

Physical Activation," *Adsorption Science and Technology,* vol. 18, pp. 27-42, 2000.

[118] M. Lopez, C. Blanco, A. Martinez-Alonso, and J. Tascon, "Composition of gases released during olive stones pyrolysis," *Journal of Analytical and Applied Pyrolysis,* vol. 65, pp. 313-322, 2002.

[119] F. F. Costa, G. Wang, and M. r. Costa, "Combustion kinetics and particle fragmentation of raw and torrified pine shells and olive stones in a drop tube furnace," *Proceedingsof the Combustion Institute,* vol. 35, pp. 3591-3599, 2015.

[120] C. A. Luengo, F. Eliecer Fonseca Felfli, and G. Bezzon, "Capítulo X-Pirólise e Torrefação de Biomassa," *Biomass for Energy,* 2006.

[121] J. P. e. a. Bourgeois, "Torrefied wood from temperate and tropical species. Advantages and prospects," in *Proceedings of Conference 15e21 June 1984,* Goteborg, Sweden, , 1984, vol. III: Elsevier Applied Science Publishers.

[122] S. Negi, G. Jaswal, K. Dass, K. Mazumder, S. Elumalai, and J. K. Roy, "Torrefaction: a sustainable method for transforming of agriwastes to high energy density solids (biocoal)," *Reviews in Environmental Science and Biotechnology,* vol. 19, pp. 463-488, 2020.

[123] N. Cellatoglu and M. Ilkan, "Torrefaction of Solid Olive Mill Residue," *Bioresources,* vol. 10, no. 3, pp. 5876-5889, 2015.

[124] M. J. C. van der Stelt, H. Gerhauser, J. H. A. Kiel, and K. J. Ptasinski, "Biomass upgrading by torrefaction for the production of biofuels: A review," *Biomass and Bioenergy,* vol. 35, pp. 3748-3762, 2011.

[125] M. Strandberg, I. Olofsson, L. Pommer, S. Wiklund-Lindstrom, K. Aberg, and A. Nordin, "Effects of temperature and residence time on continuous torrefaction of spruce wood," *Fuel Processing Technology*, 2015.

[126] M. Kwapinska *et al.*, "Fluidized Bed Gasification of Torrefied and Raw Grassy Biomass (Miscanthus × gigantenus). The Effect of Operating Conditions on Process Performance," *Energy & Fuels*, vol. 29, p. 11, 2015 2015.

[127] A. Trubetskaya *et al.*, "Characterization of woodstove briquettes from torrefied Biomass and coal," *Energy*, vol. 171, pp. 853-865, 2019 2019.

[128] J. F. Gonza´lez *et al.*, "Combustion optimization of biomass residue pellets for domestic heating with a mural boiler " *Biomass and Bioenergy*, vol. 27, no. 2, pp. 145-154, 2004.

[129] *Standard Test Method for Moisture in the Analysis Sample of Coal and Coke*, ASTM, D3173/D3173M − 17a, 2020.

[130] *Standard Test Method for Volatile Matter in the Analysis Sample of Coal and Coke*, ASTM, D3175 − 20, 2020.

[131] *Standard Test Method for Ash in the Analysis Sample of Coal and Coke from Coal*, ASTM, D3174 − 12, 2018.

[132] *Standard Practice for Ultimate Analysis of Coal and Coke*, ASTM, D3176 − 15, 2015.

[133] F. Sánchez, K. Araus, M. P. Domínguez, and G. San Miguel, "Thermochemical transformation of residual avocado seeds: torrefaction and carbonization," *Waste Biomass Valor*, vol. 8, pp. 2495-2510, 2016.

[134] F. Sánchez and G. San Miguel, "Improved fuel properties of whole table olive stones via pyrolytic processing," *Biomass and Bioenergy*, vol. 92, pp. 1-11, 2016.

[135] S. Proskurina, J. Heinimö, F. Schipfer, and E. Vakkilainen, "Biomass for industrial applications: the role of torrefaction," *Renewable Energy*, vol. 111, pp. 265-274, 2017.

[136] D. R. Nhuchhen, P. Basu, and B. Acharya, "A Comprehensive Review on Biomass Torrefaction," *International Journal of Renewable Energy & Biofuels*, 2014.

[137] G. Toscano *et al.*, "Torrefaction of tomato industry residues," *Fuel*, vol. 143, pp. 89-97, 2015.

[138] D. Chen, K. Cen, X. Jing, J. Gao, C. Li, and Z. Ma, "An approach for upgrading biomass and pyrolysis product quality using a combination of aqueous phase bio-oil washing and torrefaction pretreatment," *Bioresource Technology*, vol. 233, pp. 150-158, 2017.

[139] D. Thrän *et al.*, "Moving torrefaction towards market introduction e Technical improvements and economic-environmental assessment along the overall torrefaction supply chain through the SECTOR project," *BIOMASS AND BIOENERGY* vol. 89, pp. 184-200, 2016.

[140] D. Ciolkosz and R. Wallace, "A review of torrefaction for bioenergy feedstock production," *Biofpr*, vol. 5, pp. 317-329, 2011.

[141] M. Nimlos, E. Brooking, M. Looker, and R. Evans, "Biomass torrefaction studies with a molecular beam mass spectrometer," *American Chemical Society Division of Fuel Chemistry*, vol. 48, pp. 590-591, 2003.

[142] D. Pandey, S;, P. Indranil, S. Das, J. Leahy, J.;, and W. Kwapinski, "Multi-gene genetic programming based predictive models for municipal solid waste gasification in a fluidized bed gasifier. ," *Bioresource Technology,* vol. 179, pp. 524-533, 2015.

[143] J. H. Peng, H. T. Bi, S. Sokhansanj, and J. C. Lim, "A Study of Particle Size Effect on Biomass Torrefaction and Densification," *Energy Fuels,* vol. 26, pp. 3826-3839, 2012.

[144] H. S. Lau, H. Kiat Ng, S. Gan, and S. A. Jourabchi, "Torrefaction of oil palm fronds for co-firing in coal power plants," *Energy Procedia,* vol. 144, pp. 75-81, 2018.

[145] S. M. Lee and J.-W. Lee, "Optimization of biomass torrefaction conditions by the Gain and Loss method and regression model analysis," *Bioresource Technology,* vol. 172, pp. 438-443, 2014.

[146] F. F. Felfli, C. A. Luengo, J. A. Suárez, and P. A. Beatón, "Wood briquette torrefaction," *Energy for Sustainable Development,* vol. IX, no. 3, 2005.

[147] L. Shang *et al.*, "Changes of chemical and mechanical behavior of torrefied wheat straw " *Biomass and Bioenergy,* vol. 40, pp. 63-70, 2012.

[148] M. Schnitzer and I. Hoffman, "Pyrolysis of Soil Organic Matter," *Soil Microbiology,* 1964.

[149] D. W. Van Krevelen, "Graphical statistical method for study of structure and reaction processes of coal," *Fuel,* vol. 29, pp. 269-284, 1950.

[150] M. Traore, J. Kaal, and A. Martinez Cortizas, "Application of FTIR spectroscopy to the characterization of archeological wood," *Spectrochimica Acta Part A: Molecular and Biomolecular Spectroscopy,* vol. 153, 2016.

[151] M. Schwanninger, J. C. Rodrigues, H. Pereira, and B. Hinterstoisser, "Effects of short-time vibratory ball milling on the shape of FT-IR spectra of wood and cellulose," *Vibrational Spectroscopy,* vol. 36, 2004.

[152] D. Fengel and M. Ludwig, *Das Papier,* vol. 45, no. 2, pp. 45-51, 1991.

[153] G. Muller, C. Schopper, H. Vos, A. Kharazipour, and A. Polle, " FTIR–ATR spectroscopic analyses of changes in wood properties during particle- and fibreboard production of hard- and softwood trees," *Bioresources,* vol. 4, pp. 49-71, 2009.

[154] C. M. Popescu, M. C. Popescu, G. Singurel, C. Vasile, D. S. Argyropoulos, and S. Willfor, " Spectral characterization of eucalyptus wood

" *Applied Spectroscopy,* vol. 61, pp. 1168–1177, 2007.

[155] H. Chen, C. Ferrari, M. Angiuli, J. Yao, C. Raspi, and E. Bramanti, "Qualitative and quantitative analysis of wood samples by Fourier transform infrared spectroscopy and multivariate analysis," *Carbohydrate Polymers,* no. 82, pp. 772-778, 2010.

[156] R. Herrera, X. Erdocia, R. Llano-Ponte, and J. Labidi, "Characterization of hydrothermally treated wood in relation to changes on its chemical composition and physical properties," *Journal of Analytical and Applied Pyrolysis,* vol. 107, pp. 256-266, 2014.

[157] Z. H. Li, N. Labbé, S. G. Driese, and H. D. Grissino-Mayer, "Micro-scale analysis of tree-ring δ18O and δ13C on α-cellulose spline reveals high-resolution intra-annual climate variability and tropical cyclone activity," *Chemical Geology,* vol. 284, pp. 138-147, 2011.

[158] E. Biagini, F. Barontini, and L. Tognotti, "Devolatilization of Biomass Fuels and Biomass Components Studied by TG/FTIR Technique," *Industrial & Engineering Chemistry Research,* vol. 45, pp. 4486-4493, 2006.

[159] H. Ismail, Y; *et al.*, "ANN-Kriging hybrid model for predicting carbon and inorganic phosphorus recovery in hydrothermal carbonization," *Waste Management* vol. 85, pp. 242-252, 2019.

[160] M. Pishnamazi, H. Ismail, Y;, S. Shirazian, J. Iqbal, G. Walker, M;, and N. Collins, "Application of lignin in controlled release : development of predictive model based on artificial neural network for API release," *Cellulose,* 2019.

[161] H. Ismail, Y; *et al.*, "Developing ANN-Kriging hybrid model based on process parameters for prediction of mean residence time distribution in twin-screw wet granulation," *Powder Technology,* vol. 343, pp. 568-577, 2019.

[162] S. Shirazian, H. Ismail, Y;, M. Singh, R. Shaikh, D. Crocker, M;, and G. Walker, M;, "Multi-dimensional population balance modelling of pharmaceutical formulations for continuous twin-screw wet granulation: Determination of liquid distribution," *International Journal of Pharmaceutics,* vol. 566, pp. 352-360, 2019.

[163] H. Ismail, Y;, S. Shirazian, M. Singh, D. Whitaker, A. Albadarin, B;, and G. Walker, M;, "Compartmental approach for modelling twin-screw granulation using population balances," *International Journal of Pharmaceutics,* 2019.

[164] S. Shirazian, M. Kuhs, S. Darwish, D. Croker, and G. M. Walker, "Artificial neural network modelling of continuous wet granulation using a twin-screw extruder," *International Journal of Pharmaceutics,* vol. 521, no. 1, pp. 102-109, 2017/04/15/ 2017.

[165] D. G. Krige, "A statistical approach to some basic mine valuation problems on the Witwatersrand," *Journal of the Southern African Institute of Mining and Metallurgy* vol. 52, no. 9, pp. 201-203, 1952.

[166] G. Matheron, "Principles of geostatistics," *Economic Geology,* vol. 58, no. 8, pp. 1246-1266, 1963.

[167] F. Boukouvala, F. J. Muzzio, and M. G. Ierapetritou, "Dynamic Data-Driven Modeling of Pharmaceutical Processes," *Industrial & Engineering Chemistry Research,* vol. 50, no. 11, pp. 6743-6754, 2011/06/01 2011.

[168] P. Kazemi *et al.*, "Computational intelligence modeling of granule size distribution for oscillating milling," *Powder Technology,* vol. 301, pp. 1252-1258, 2016/11/01/ 2016.

[169] M. A. Martin-Lara, A. Ronda, M. C. Zamora, and M. Calero, "Torrefaction of olive tree pruning: Effect of operating conditions on solid product properties," *Fuel,* vol. 202, pp. 109-117, 2017.

[170] B. Neminda Madanayake, S. Gan, C. Eastwick, and H. Kiat Ng, "Biomass as an energy source in coal co-firing and its feasibility enhancement via pre-treatment techniques," *Fuel Processing Technology,* vol. 159, pp. 287-305, 2017.

[171] E. Gucho, K. Shahzad, E. Bramer, N. Akhtar, and G. Brem, "Experimental Study on Dry Torrefaction of Beech Wood and Miscanthus," *Energies,* vol. 8, no. 5, pp. 3903-3923, 2015.